

# Supplementary Material of Land Surface Temperature Super-Resolution with a Scale-Invariance-Free Neural Approach: Application to MODIS

Romuald Ait-Bachir<sup>\*†</sup>, Carlos Granero-Belinchon<sup>\*†</sup>, Aurélie Michel<sup>‡</sup>, Julien Michel<sup>§</sup>, Xavier Briottet<sup>‡</sup> and Lucas Drumetz<sup>\*†</sup>

<sup>\*</sup>IMT Atlantique, Lab-STICC, UMR 6285, 29238, CNRS, Brest, France

<sup>†</sup>ODYSSEY Team-Project, INRIA Ifremer IMT-Atl., 35042, CNRS, Brest, France

<sup>‡</sup>ONERA-DOTA, University of Toulouse, F-31055 Toulouse, France

<sup>§</sup> CESBIO, University de Toulouse, CNES, CNRS, INRAE, IRD, UT3, 31401 Toulouse, France.

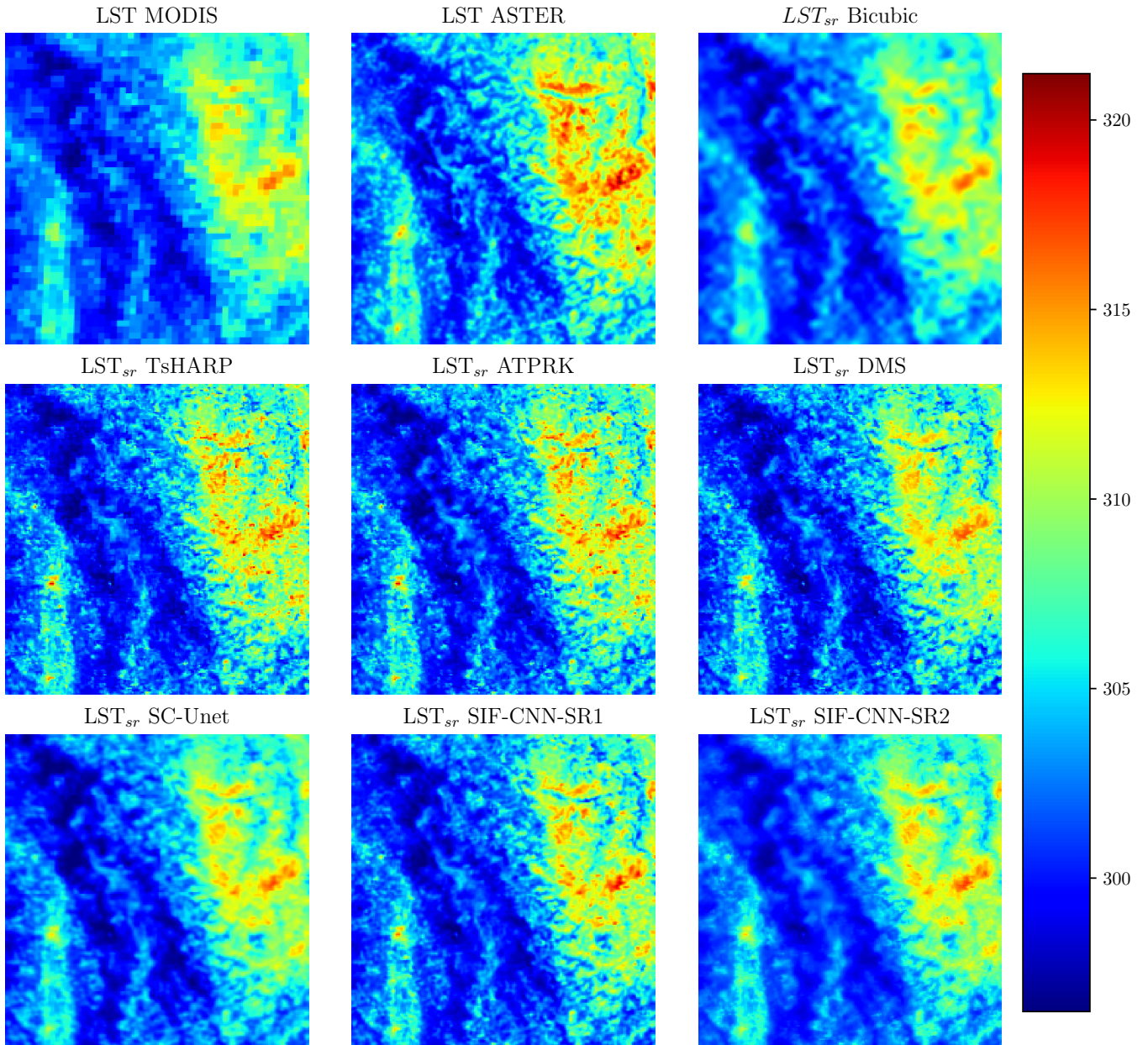


Fig. 1. Visualization of the LST of MODIS and ASTER respectively at 1km and 250m of spatial resolution alongside the super-resolution LST obtained with the different approaches.

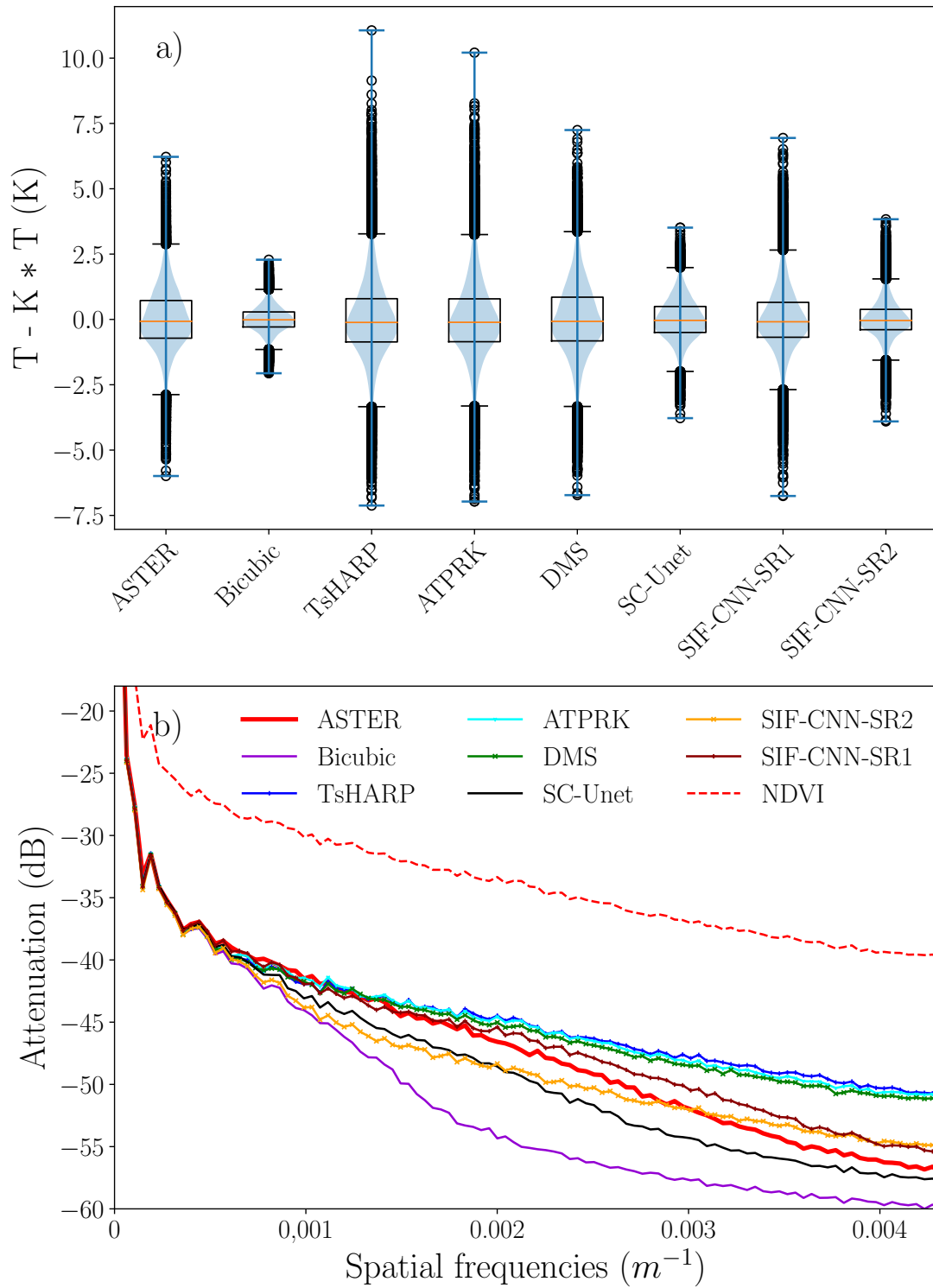


Fig. 2. Statistical analysis of the image visualized in figure 1. a) Boxplots and Violinplots representing the statistical distribution of the values of the high pass filtered LST of ASTER and obtained with the different super-resolution approaches. b) Attenuation spectra of the ASTER LST (red), LST obtained with statistical super-resolution methods TsHARP and ATPRK (blue), DMS (green), SC-Unet (black), SIF-CNN-SR1 (brown) and SIF-CNN-SR2 (orange). The attenuation spectra of the MODIS NDVI is also shown in dashed red.

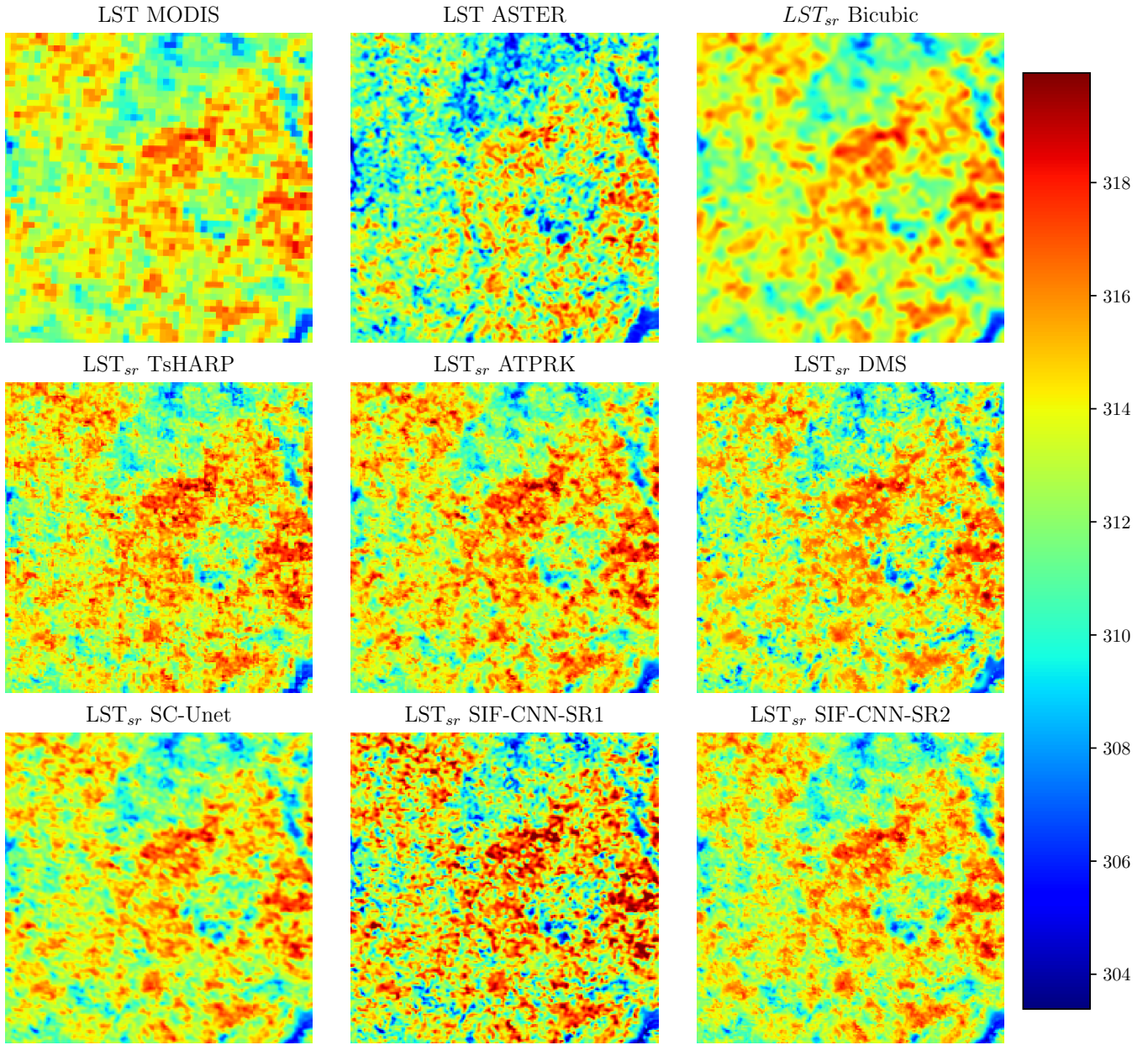


Fig. 3. Visualization of the LST of MODIS and ASTER respectively at 1km and 250m of spatial resolution alongside the super-resolution LST obtained with the different approaches.

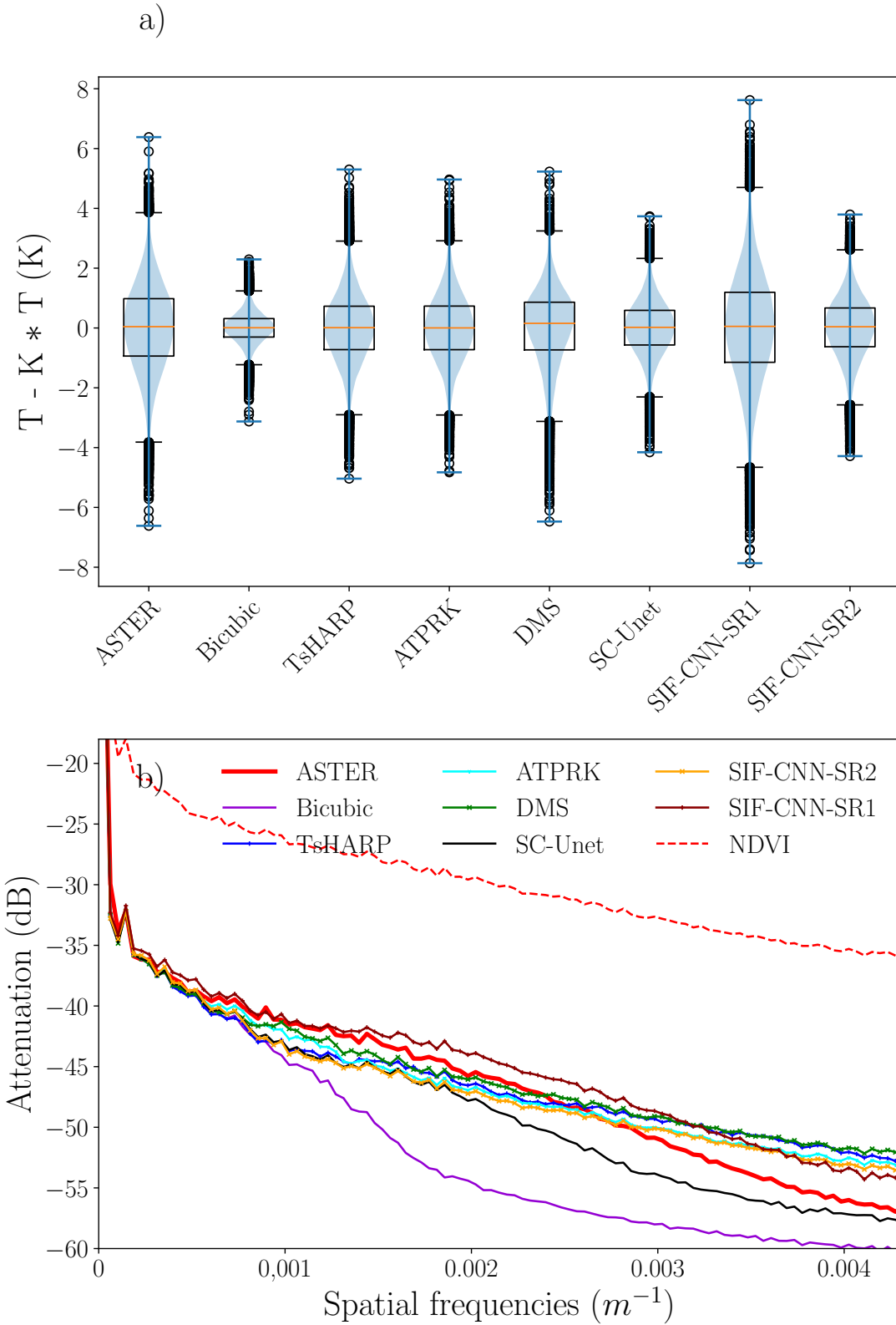


Fig. 4. Statistical analysis of the image visualized in figure 3. a) Boxplots and Violinplots representing the statistical distribution of the values of the high pass filtered LST of ASTER and obtained with the different super-resolution approaches. b) Attenuation spectra of the ASTER LST (red), LST obtained with statistical super-resolution methods TsHARP and ATPRK (blue), DMS (green), SC-Unet (black), SIF-CNN-SR1 (brown) and SIF-CNN-SR2 (orange). The attenuation spectra of the MODIS NDVI is also shown in dashed red.

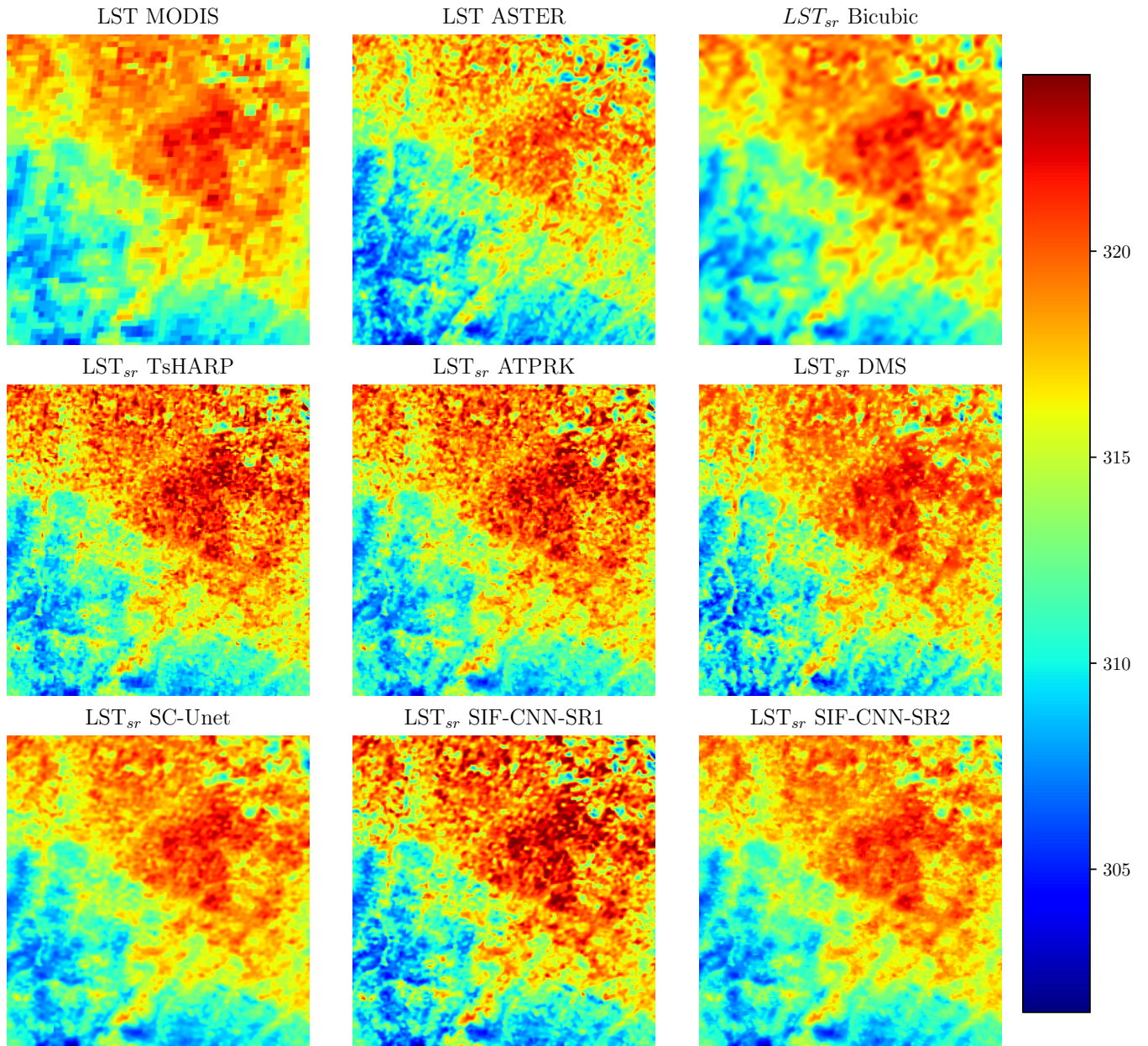


Fig. 5. Visualization of the LST of MODIS and ASTER respectively at 1km and 250m of spatial resolution alongside the super-resolution LST obtained with the different approaches.

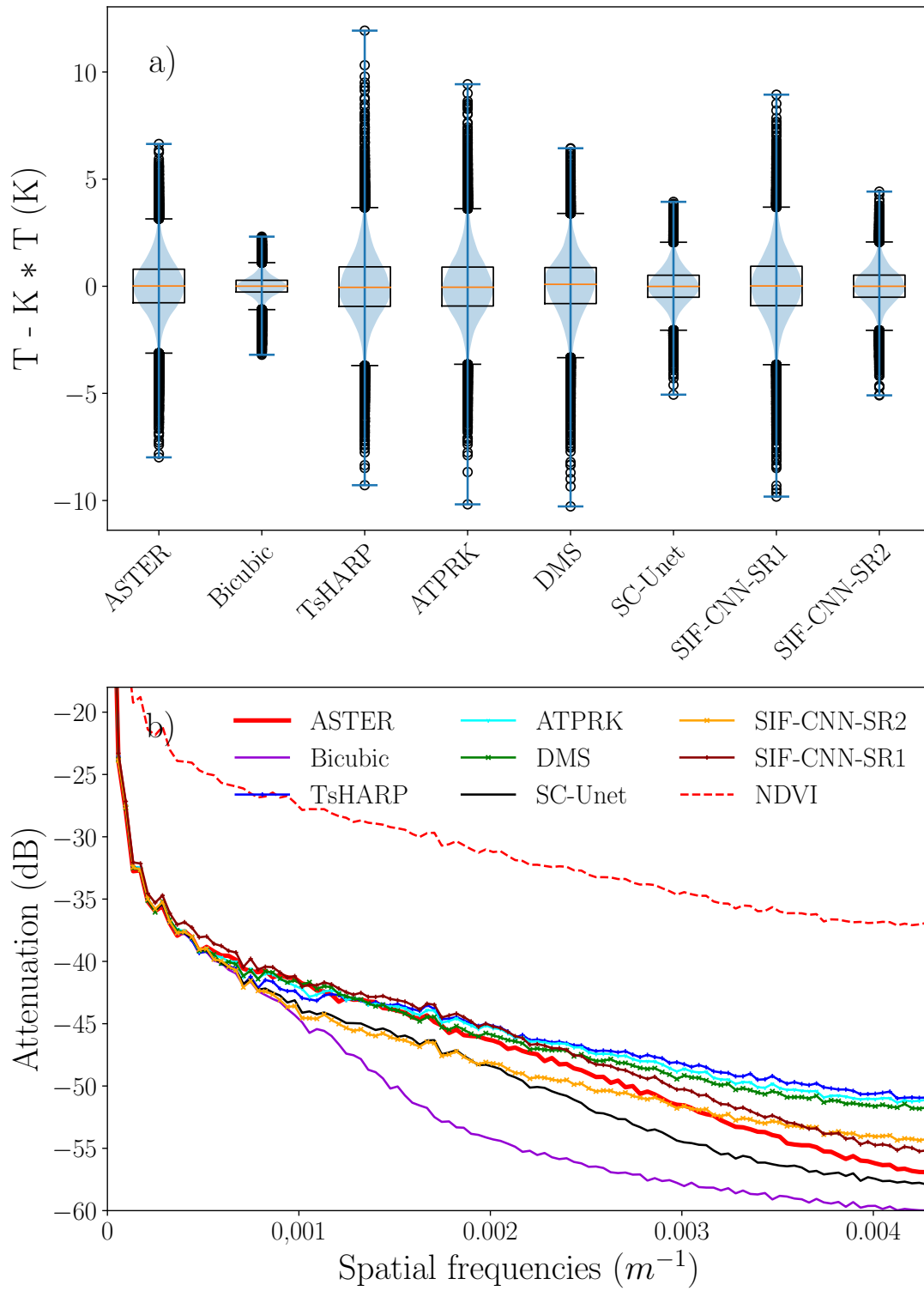


Fig. 6. Statistical analysis of the image visualized in figure 5. a) Boxplots and Violinplots representing the statistical distribution of the values of the high pass filtered LST of ASTER and obtained with the different super-resolution approaches. b) Attenuation spectra of the ASTER LST (red), LST obtained with statistical super-resolution methods TsHARP and ATPRK (blue), DMS (green), SC-Unet (black), SIF-CNN-SR1 (brown) and SIF-CNN-SR2 (orange). The attenuation spectra of the MODIS NDVI is also shown in dashed red.

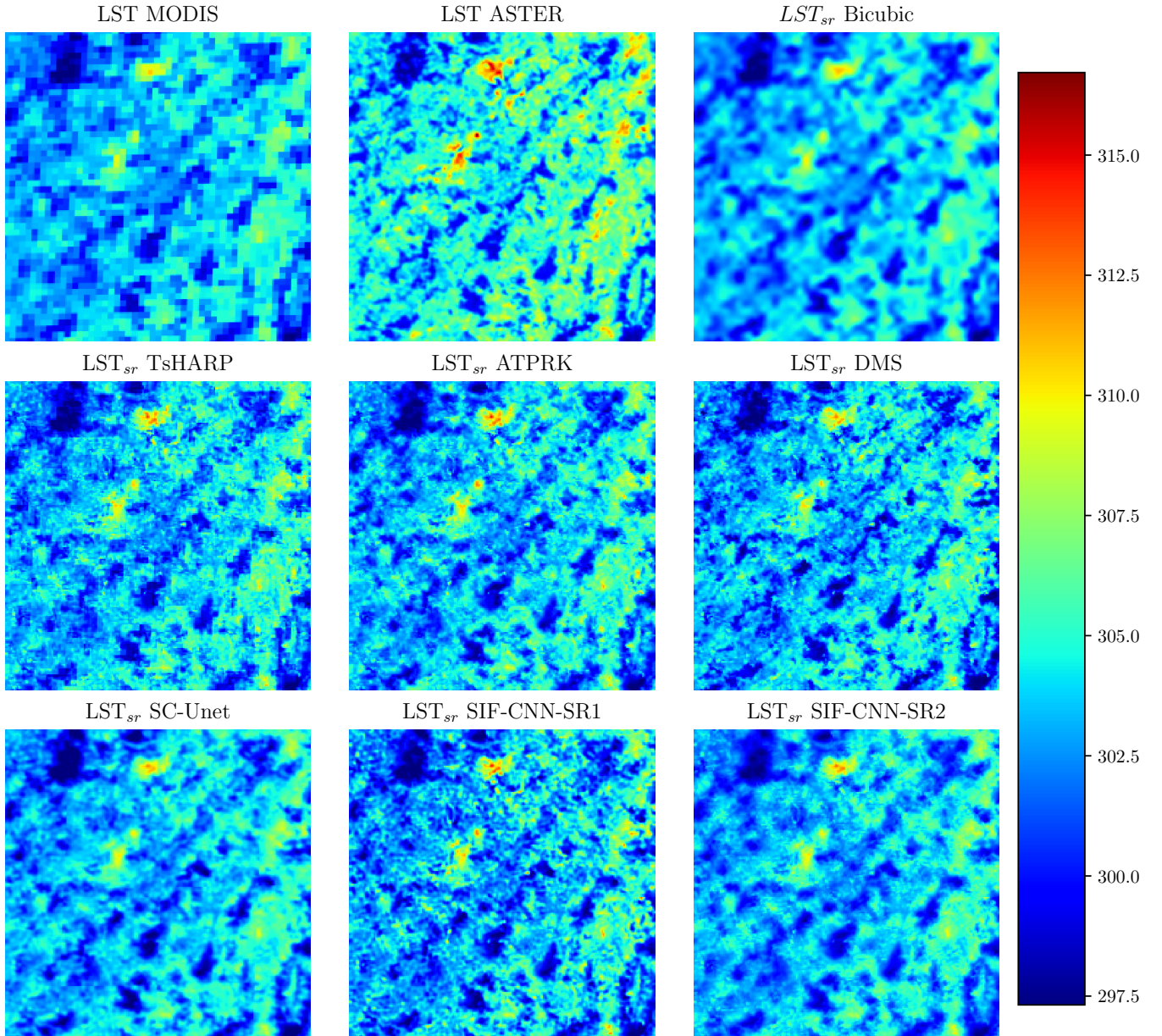


Fig. 7. Visualization of the LST of MODIS and ASTER respectively at 1km and 250m of spatial resolution alongside the super-resolution LST obtained with the different approaches.

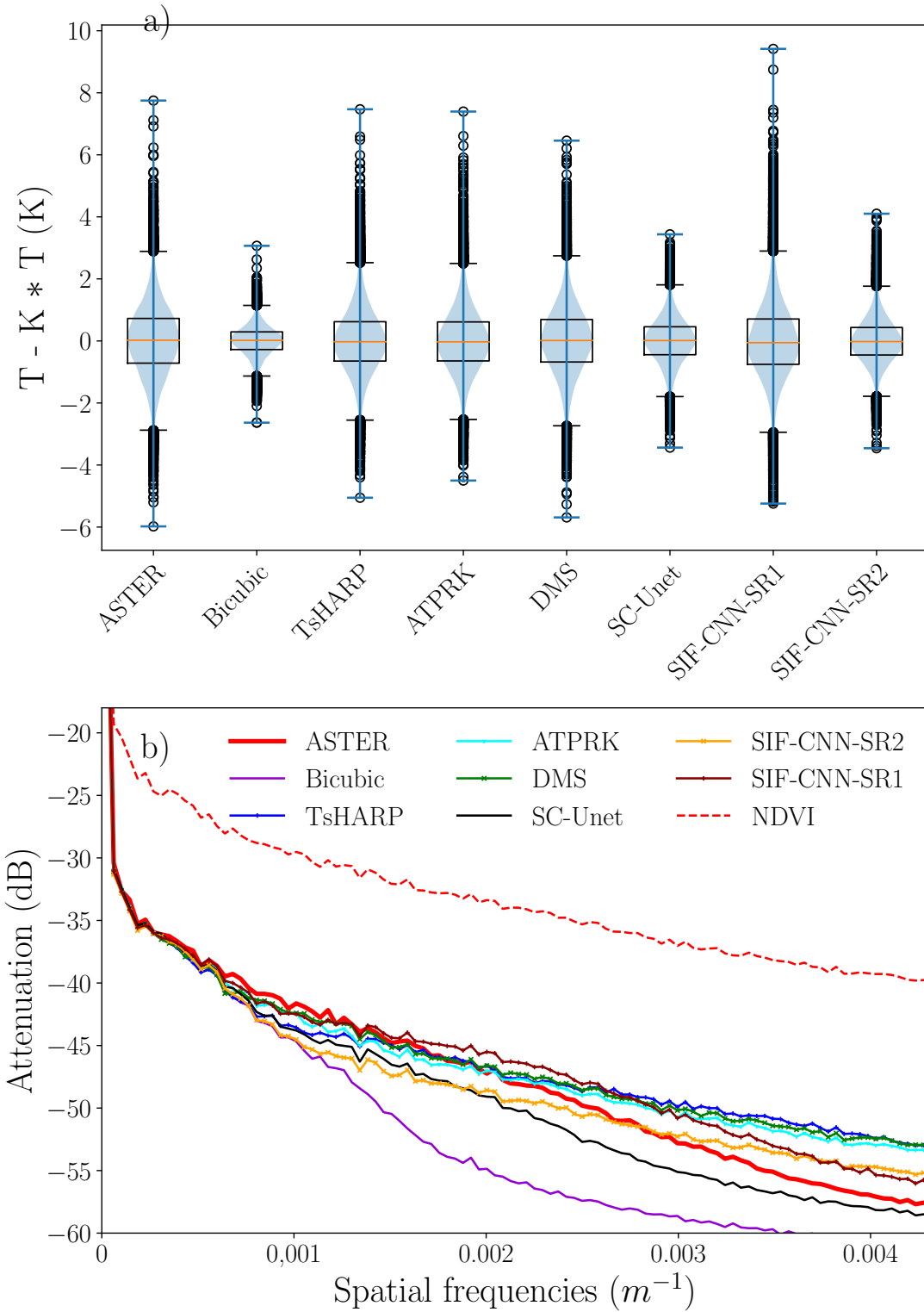


Fig. 8. Statistical analysis of the image visualized in figure 7. a) Boxplots and Violinplots representing the statistical distribution of the values of the high pass filtered LST of ASTER and obtained with the different super-resolution approaches. b) Attenuation spectra of the ASTER LST (red), LST obtained with statistical super-resolution methods TsHARP and ATPRK (blue), DMS (green), SC-Unet (black), SIF-CNN-SR1 (brown) and SIF-CNN-SR2 (orange). The attenuation spectra of the MODIS NDVI is also shown in dashed red.

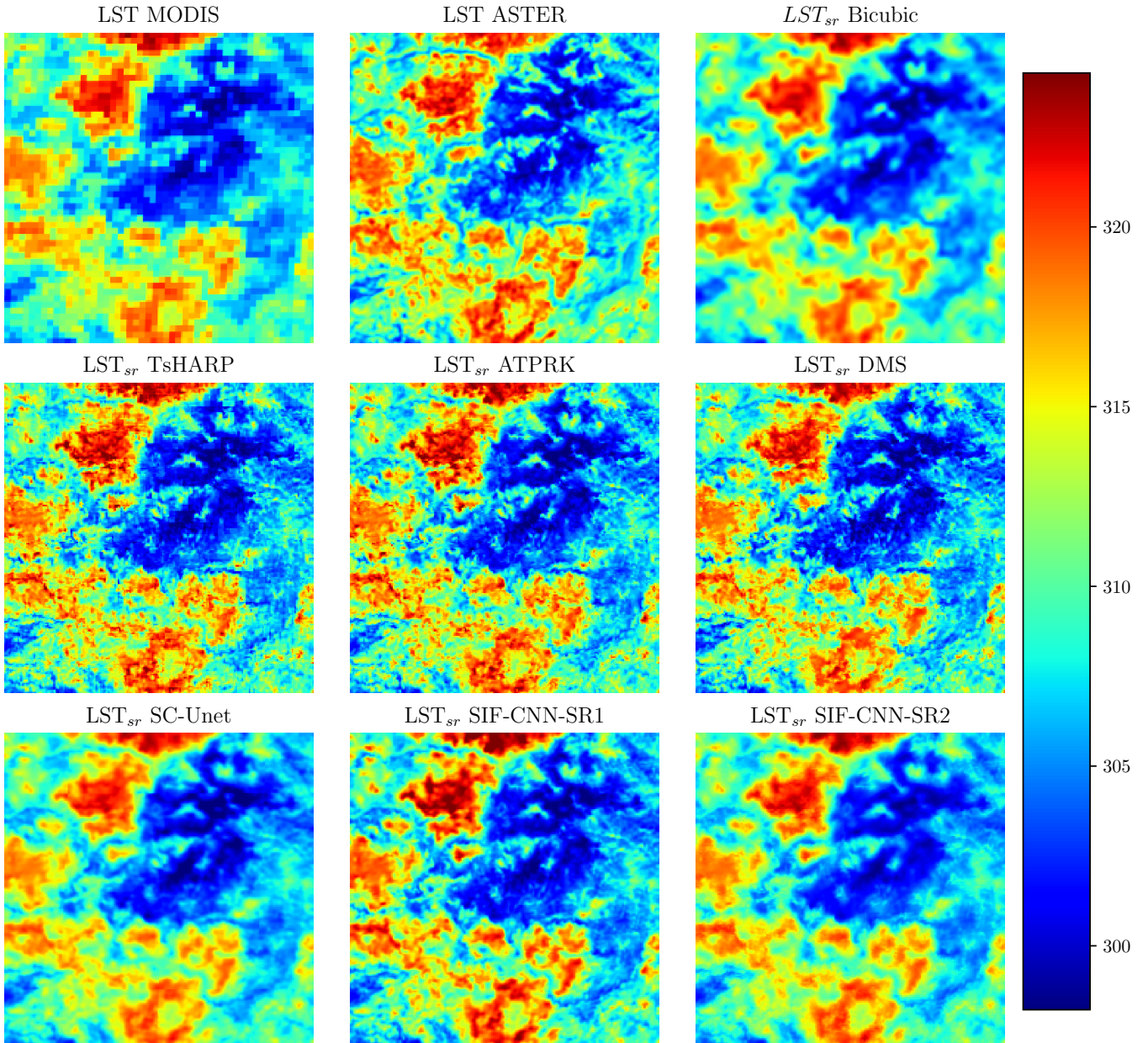


Fig. 9. Visualization of the LST of MODIS and ASTER respectively at 1km and 250m of spatial resolution alongside the super-resolution LST obtained with the different approaches.

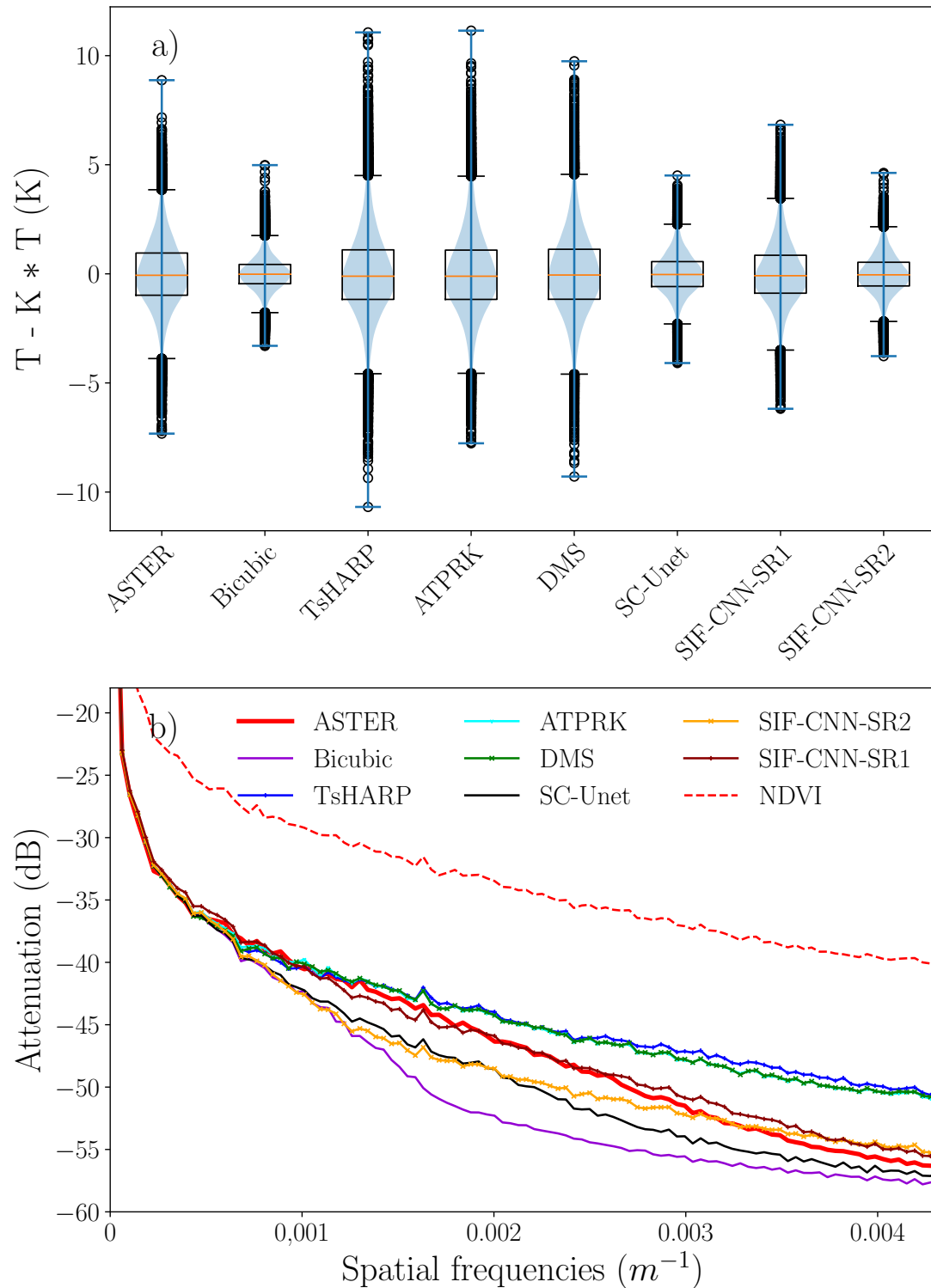


Fig. 10. Statistical analysis of the image visualized in figure 9. a) Boxplots and Violinplots representing the statistical distribution of the values of the high pass filtered LST of ASTER and obtained with the different super-resolution approaches. b) Attenuation spectra of the ASTER LST (red), LST obtained with statistical super-resolution methods TsHARP and ATPRK (blue), DMS (green), SC-Unet (black), SIF-CNN-SR1 (brown) and SIF-CNN-SR2 (orange). The attenuation spectra of the MODIS NDVI is also shown in dashed red.

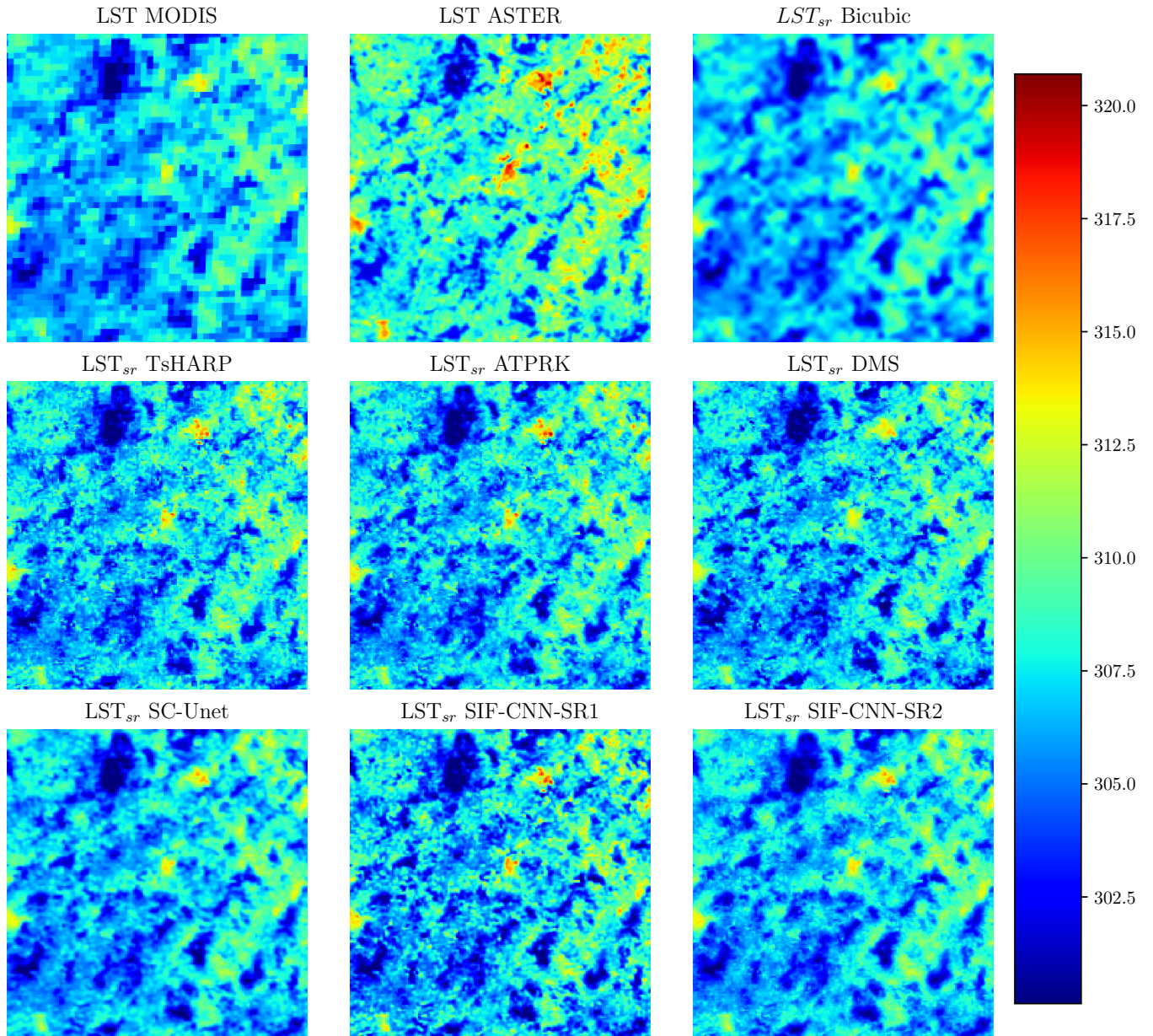


Fig. 11. Visualization of the LST of MODIS and ASTER respectively at 1km and 250m of spatial resolution alongside the super-resolution LST obtained with the different approaches.

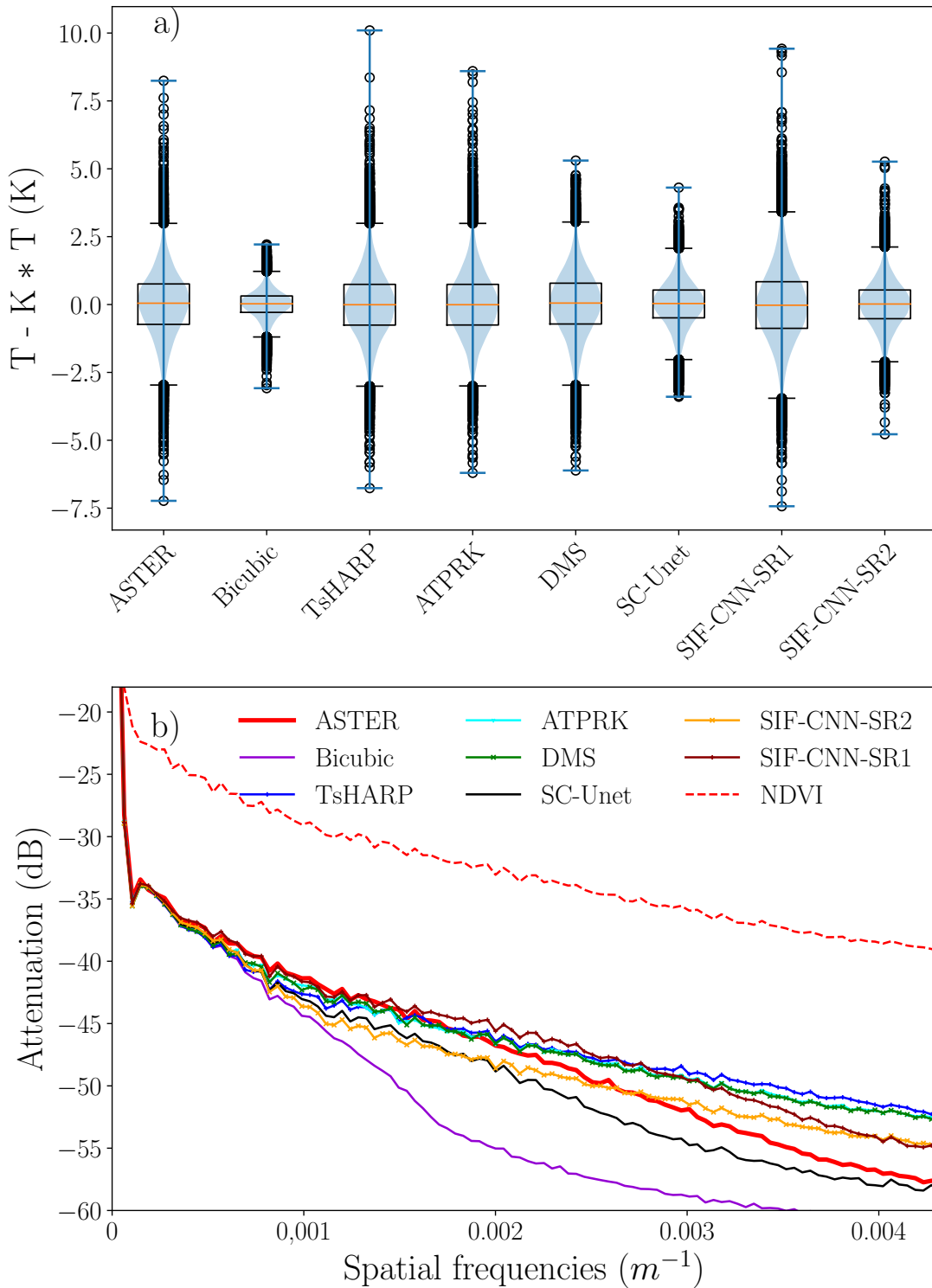


Fig. 12. Statistical analysis of the image visualized in figure 11. a) Boxplots and Violinplots representing the statistical distribution of the values of the high pass filtered LST of ASTER and obtained with the different super-resolution approaches. b) Attenuation spectra of the ASTER LST (red), LST obtained with statistical super-resolution methods TsHARP and ATPRK (blue), DMS (green), SC-Unet (black), SIF-CNN-SR1 (brown) and SIF-CNN-SR2 (orange). The attenuation spectra of the MODIS NDVI is also shown in dashed red.

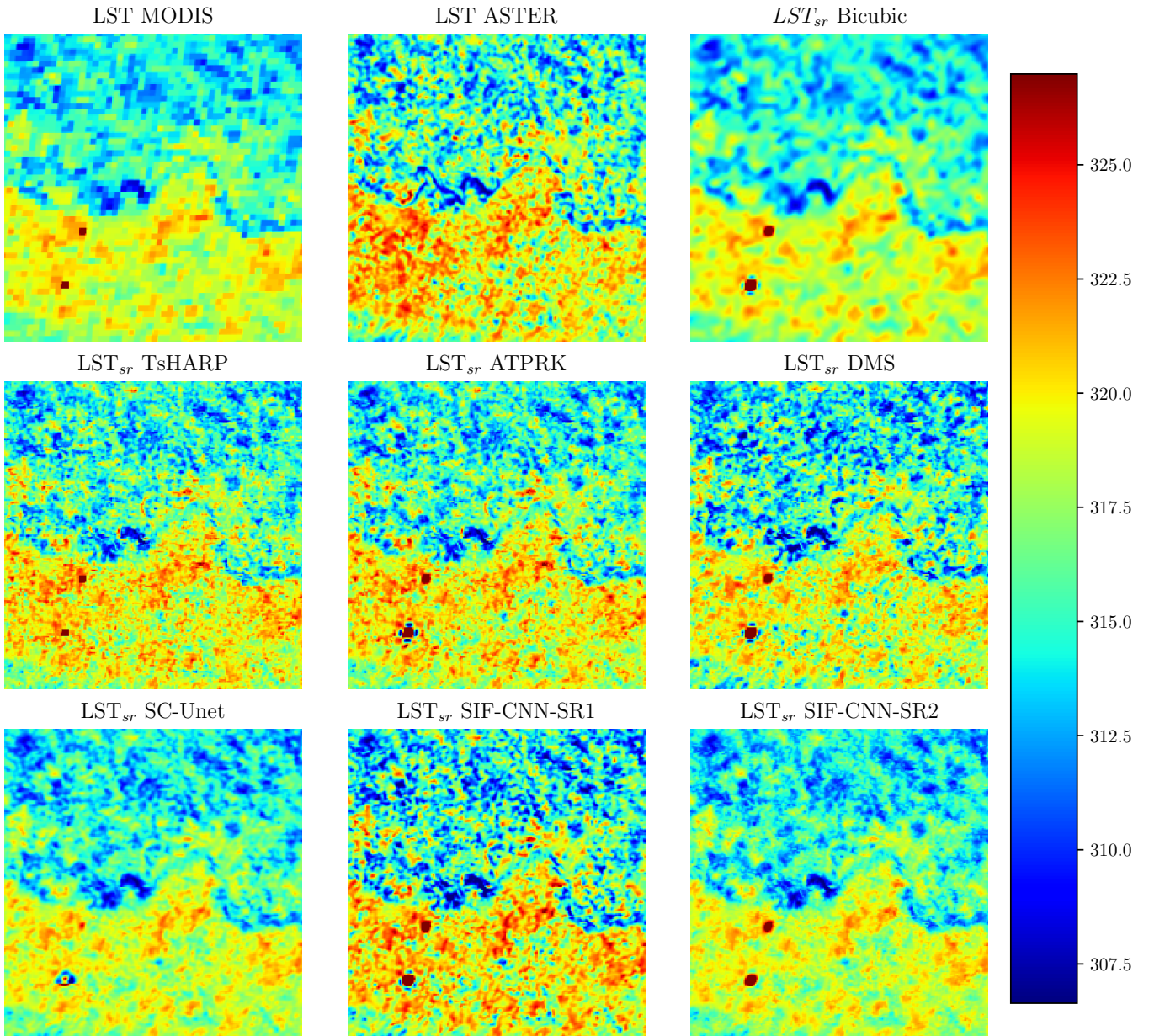


Fig. 13. Visualization of the LST of MODIS and ASTER respectively at 1km and 250m of spatial resolution alongside the super-resolution LST obtained with the different approaches.

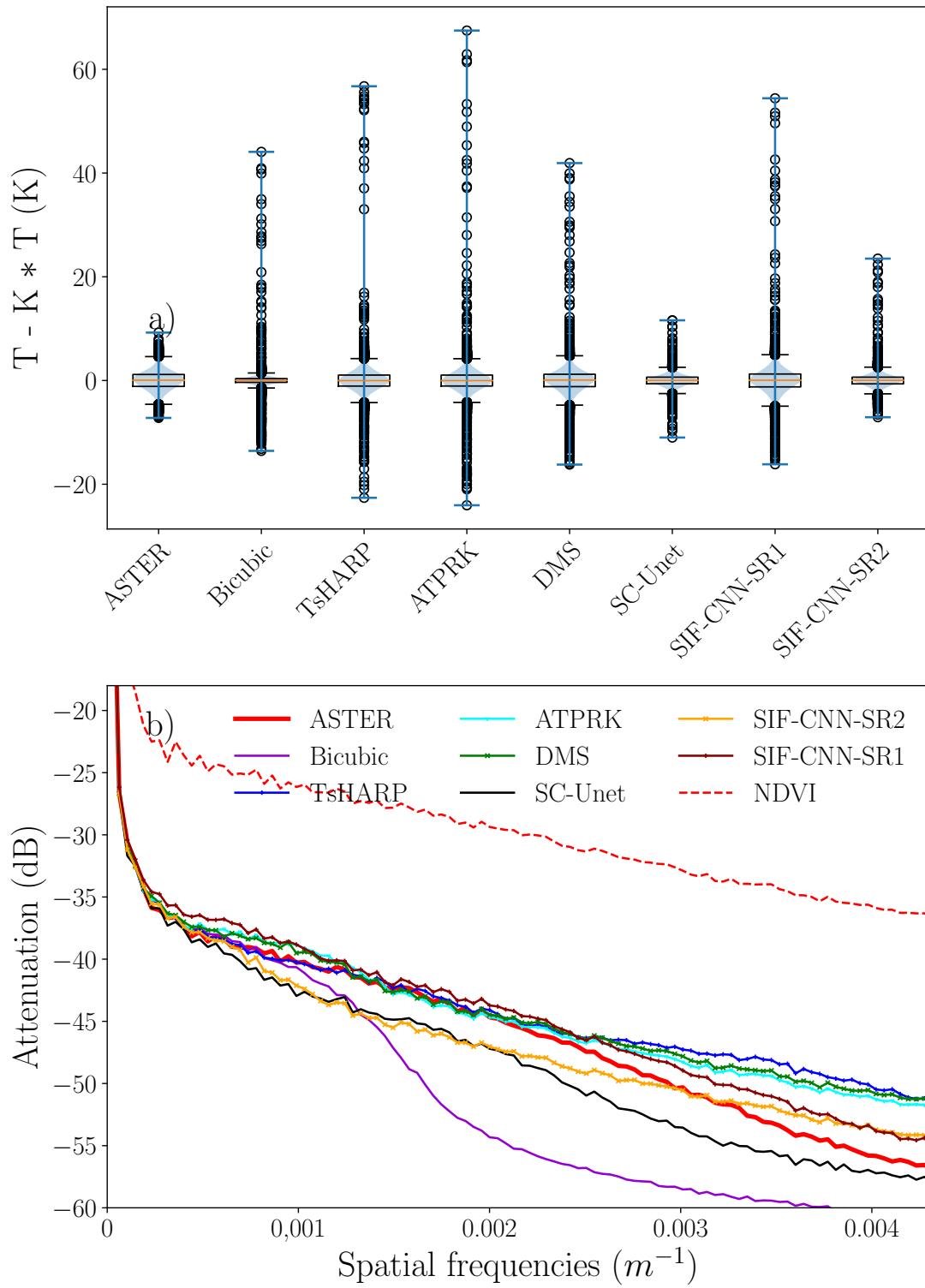


Fig. 14. Statistical analysis of the image visualized in figure 13. a) Boxplots and Violinplots representing the statistical distribution of the values of the high pass filtered LST of ASTER and obtained with the different super-resolution approaches. b) Attenuation spectra of the ASTER LST (red), LST obtained with statistical super-resolution methods TsHARP and ATPRK (blue), DMS (green), SC-Unet (black), SIF-CNN-SR1 (brown) and SIF-CNN-SR2 (orange). The attenuation spectra of the MODIS NDVI is also shown in dashed red.

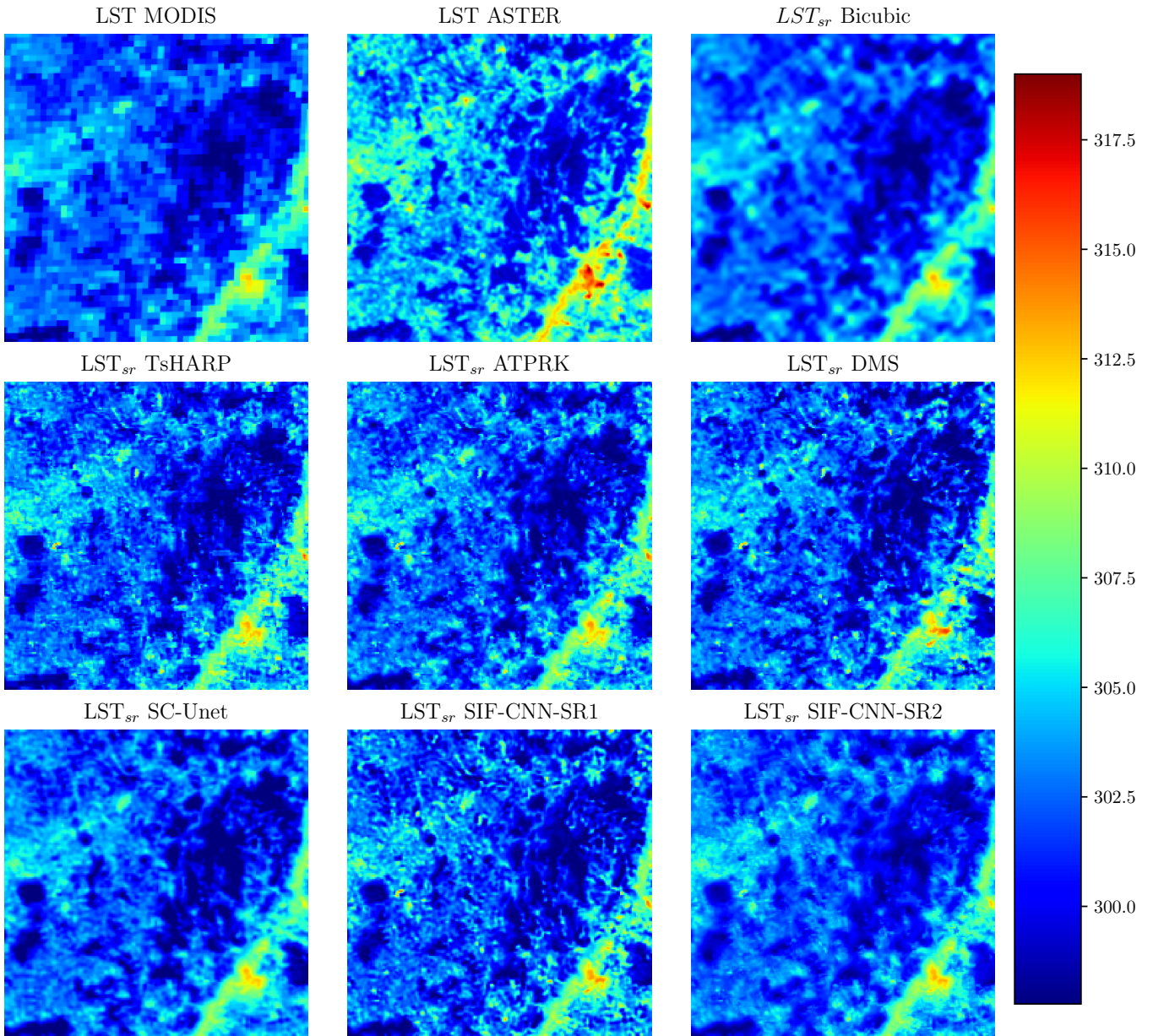


Fig. 15. Visualization of the LST of MODIS and ASTER respectively at 1km and 250m of spatial resolution alongside the super-resolution LST obtained with the different approaches.

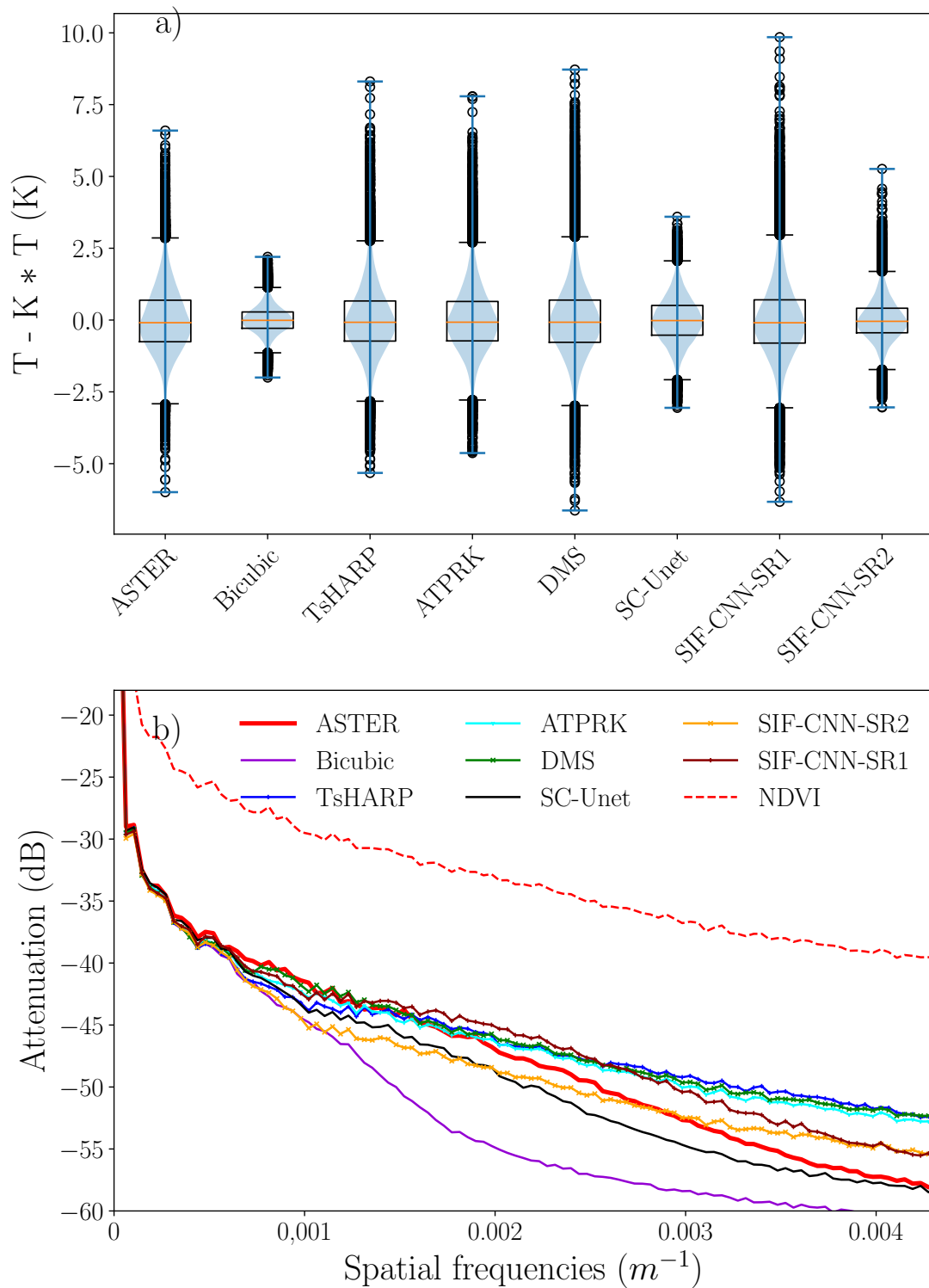


Fig. 16. Statistical analysis of the image visualized in figure 15. a) Boxplots and Violinplots representing the statistical distribution of the values of the high pass filtered LST of ASTER and obtained with the different super-resolution approaches. b) Attenuation spectra of the ASTER LST (red), LST obtained with statistical super-resolution methods TsHARP and ATPRK (blue), DMS (green), SC-Unet (black), SIF-CNN-SR1 (brown) and SIF-CNN-SR2 (orange). The attenuation spectra of the MODIS NDVI is also shown in dashed red.

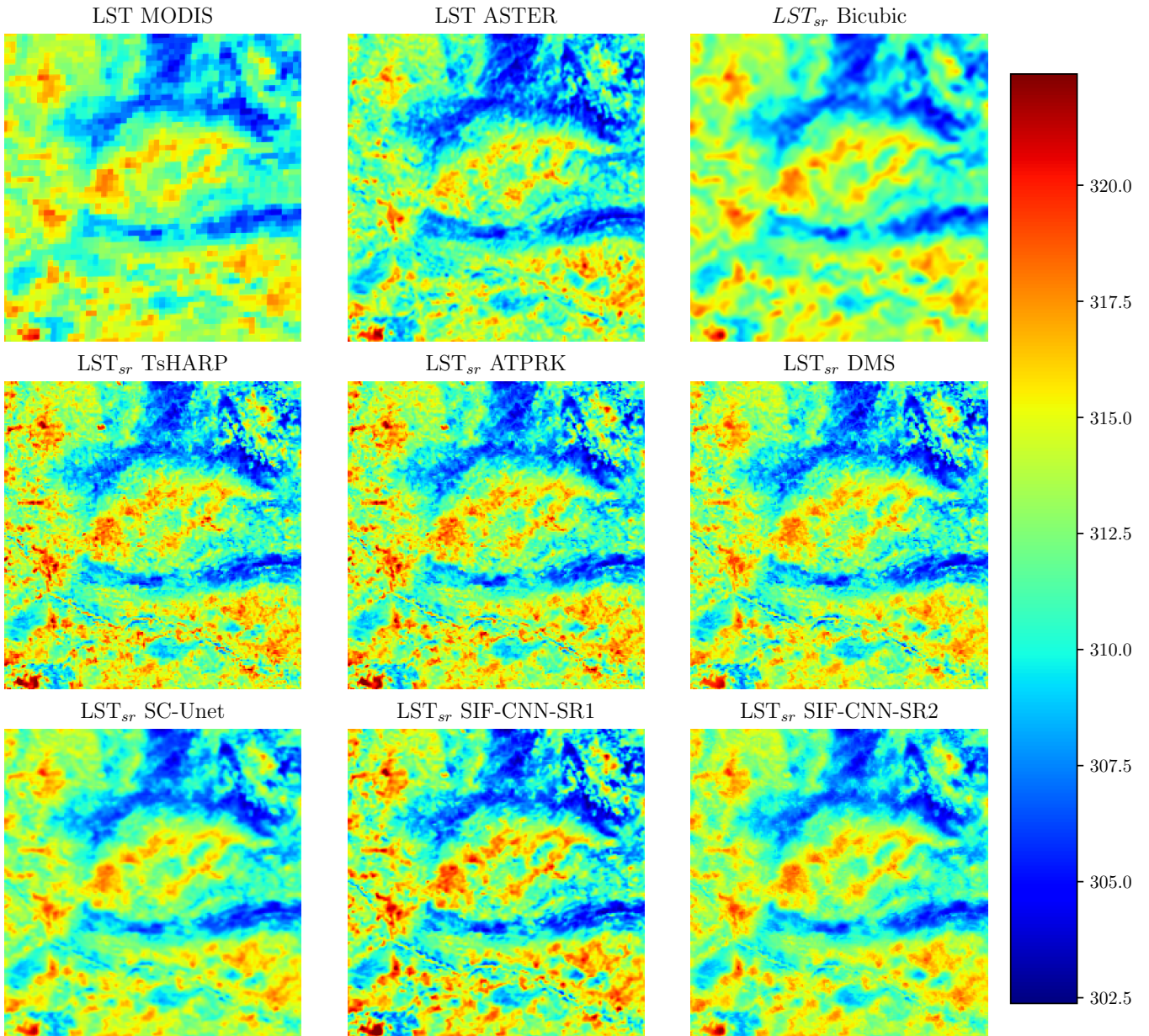


Fig. 17. Visualization of the LST of MODIS and ASTER respectively at 1km and 250m of spatial resolution alongside the super-resolution LST obtained with the different approaches.

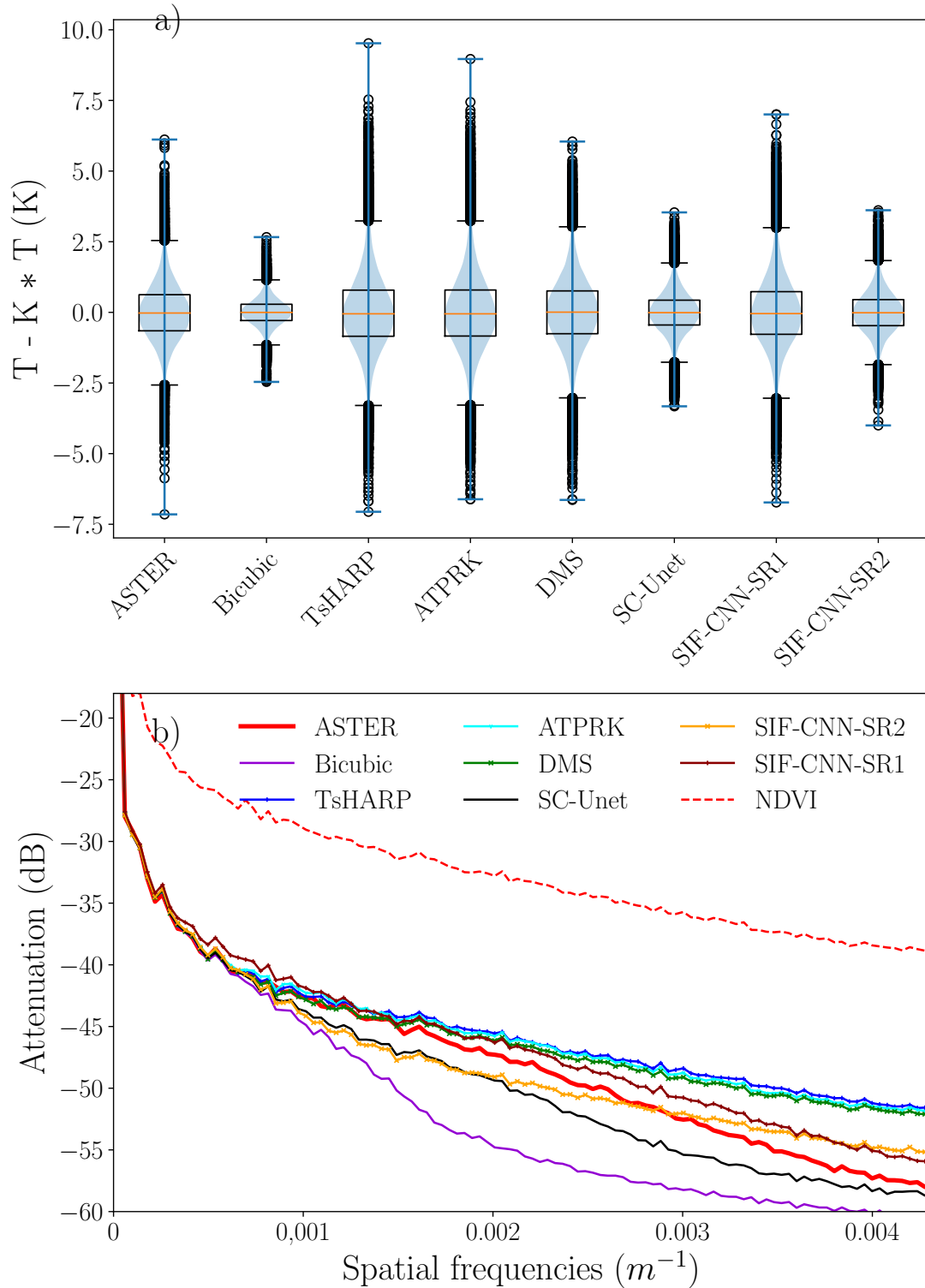


Fig. 18. Statistical analysis of the image visualized in figure 17. a) Boxplots and Violinplots representing the statistical distribution of the values of the high pass filtered LST of ASTER and obtained with the different super-resolution approaches. b) Attenuation spectra of the ASTER LST (red), LST obtained with statistical super-resolution methods TsHARP and ATPRK (blue), DMS (green), SC-Unet (black), SIF-CNN-SR1 (brown) and SIF-CNN-SR2 (orange). The attenuation spectra of the MODIS NDVI is also shown in dashed red.

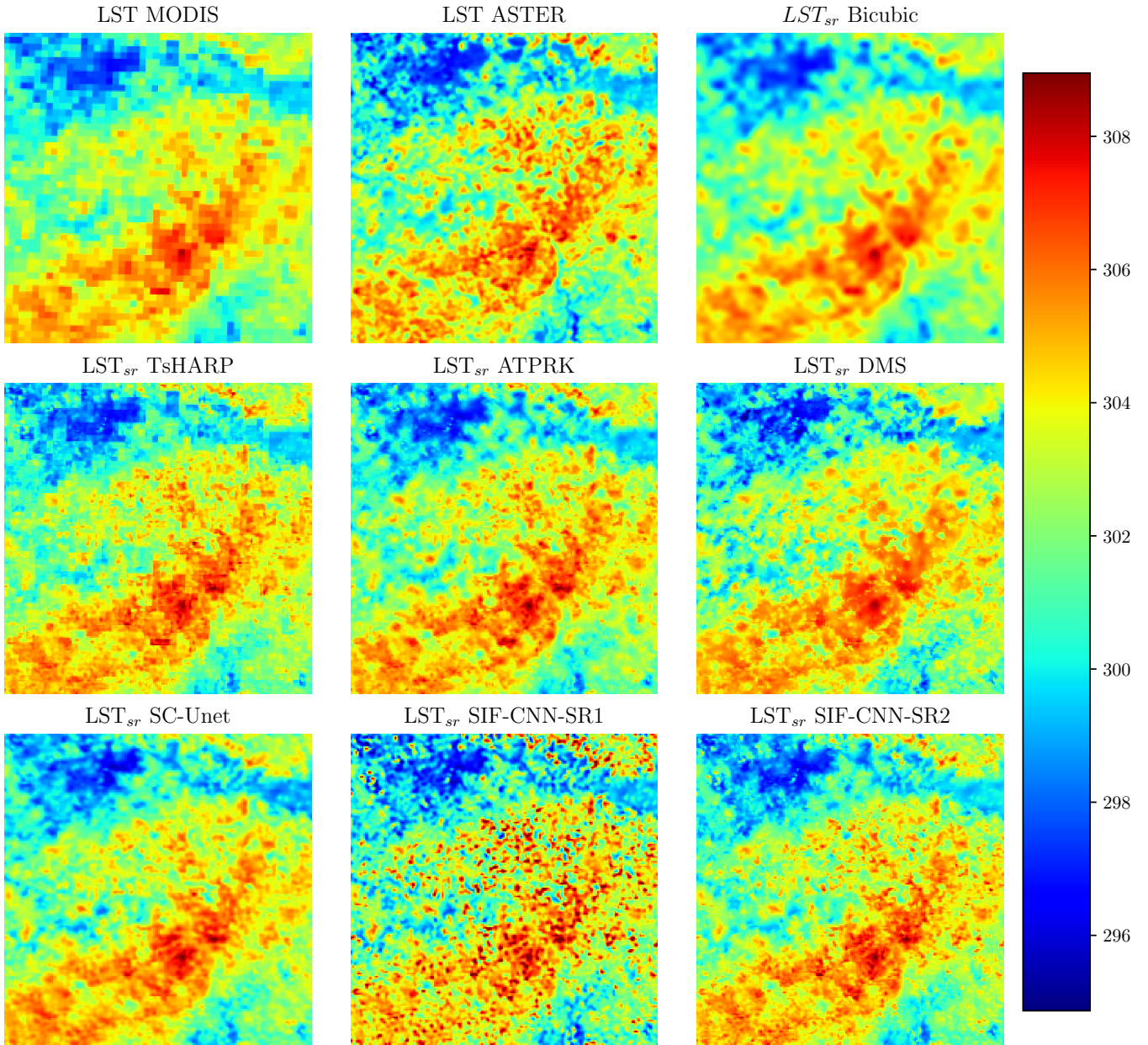


Fig. 19. Visualization of the LST of MODIS and ASTER respectively at 1km and 250m of spatial resolution alongside the super-resolution LST obtained with the different approaches.

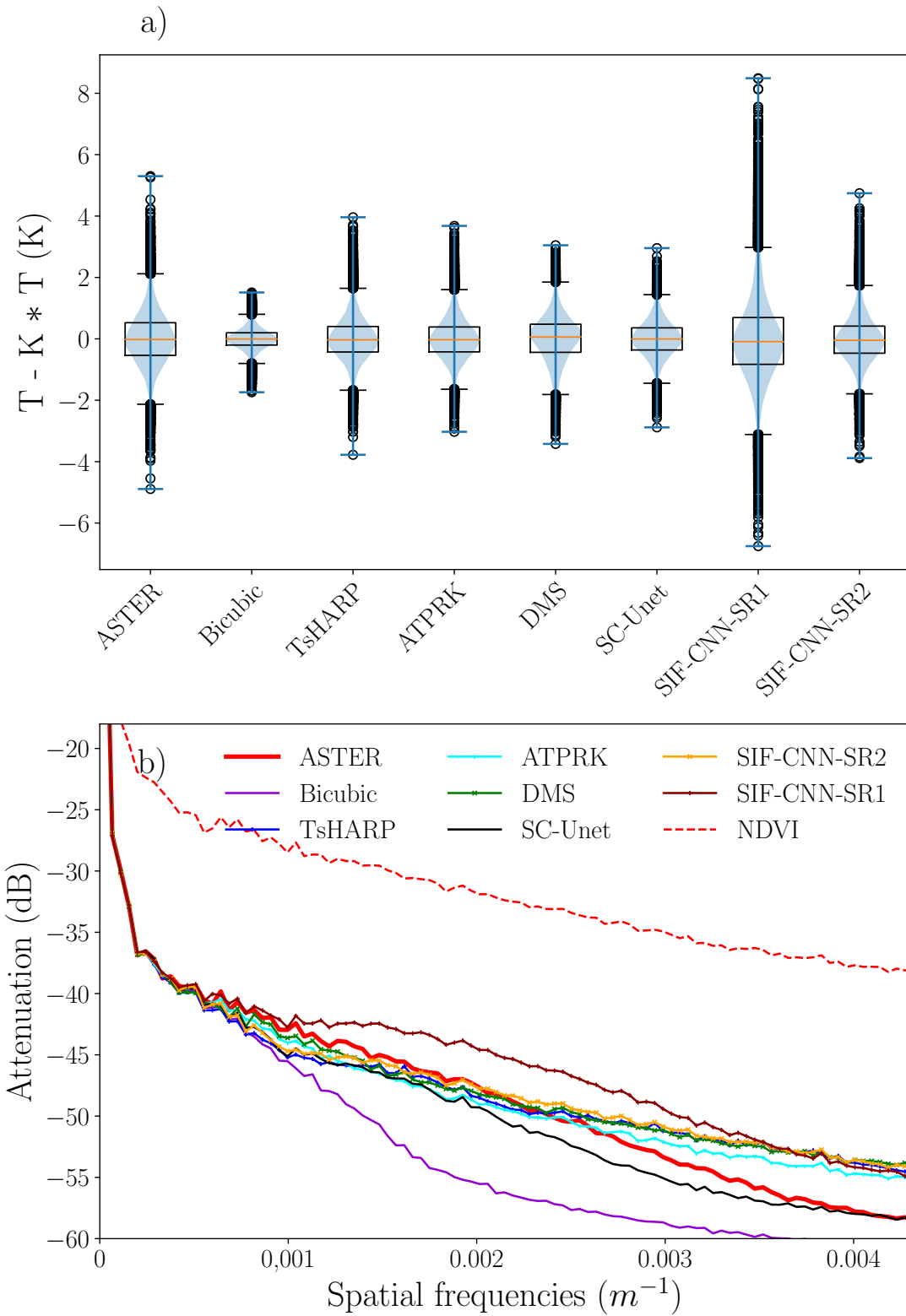


Fig. 20. Statistical analysis of the image visualized in figure 19. a) Boxplots and Violinplots representing the statistical distribution of the values of the high pass filtered LST of ASTER and obtained with the different super-resolution approaches. b) Attenuation spectra of the ASTER LST (red), LST obtained with statistical super-resolution methods TsHARP and ATPRK (blue), DMS (green), SC-Unet (black), SIF-CNN-SR1 (brown) and SIF-CNN-SR2 (orange). The attenuation spectra of the MODIS NDVI is also shown in dashed red.

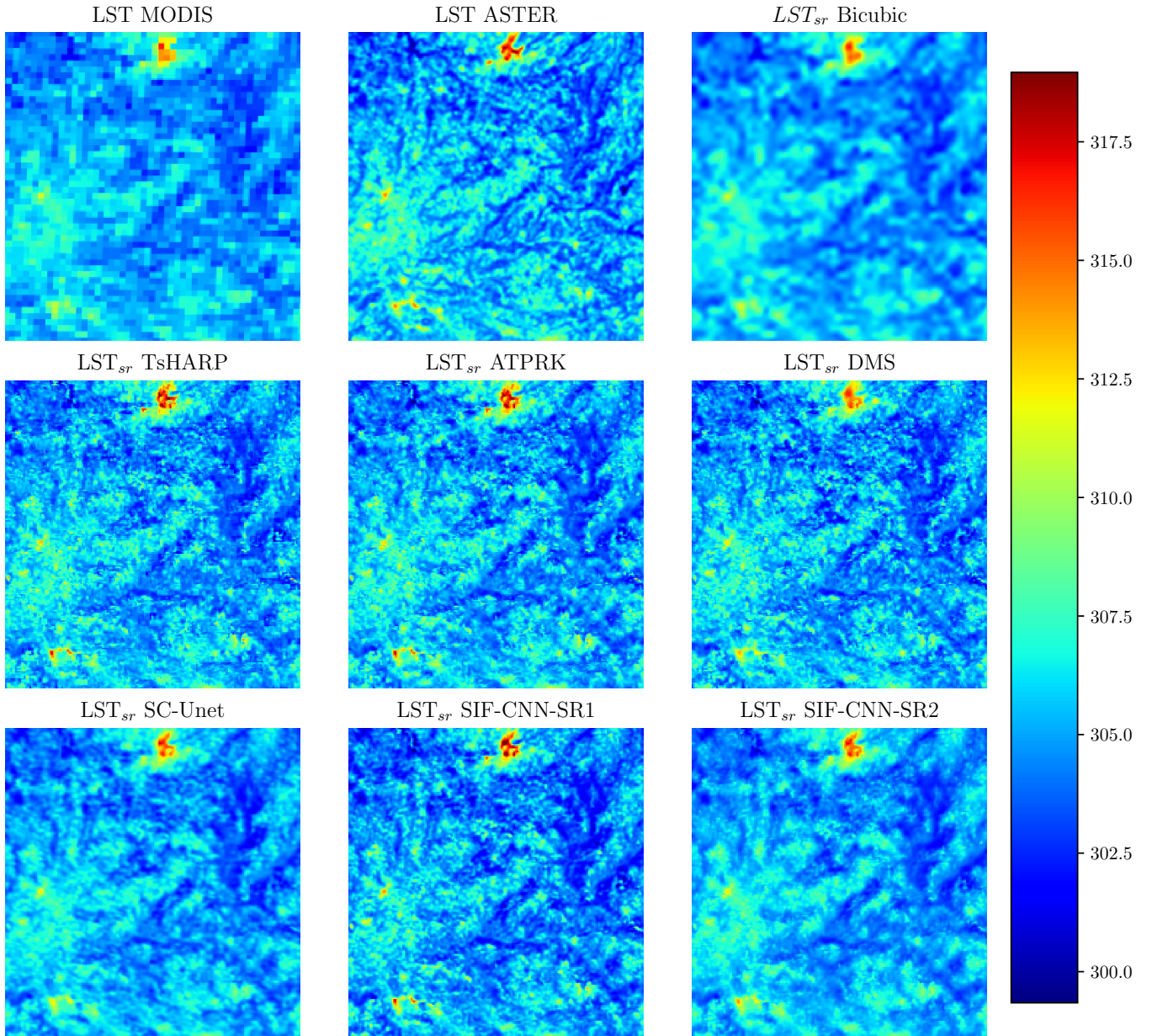


Fig. 21. Visualization of the LST of MODIS and ASTER respectively at 1km and 250m of spatial resolution alongside the super-resolution LST obtained with the different approaches.

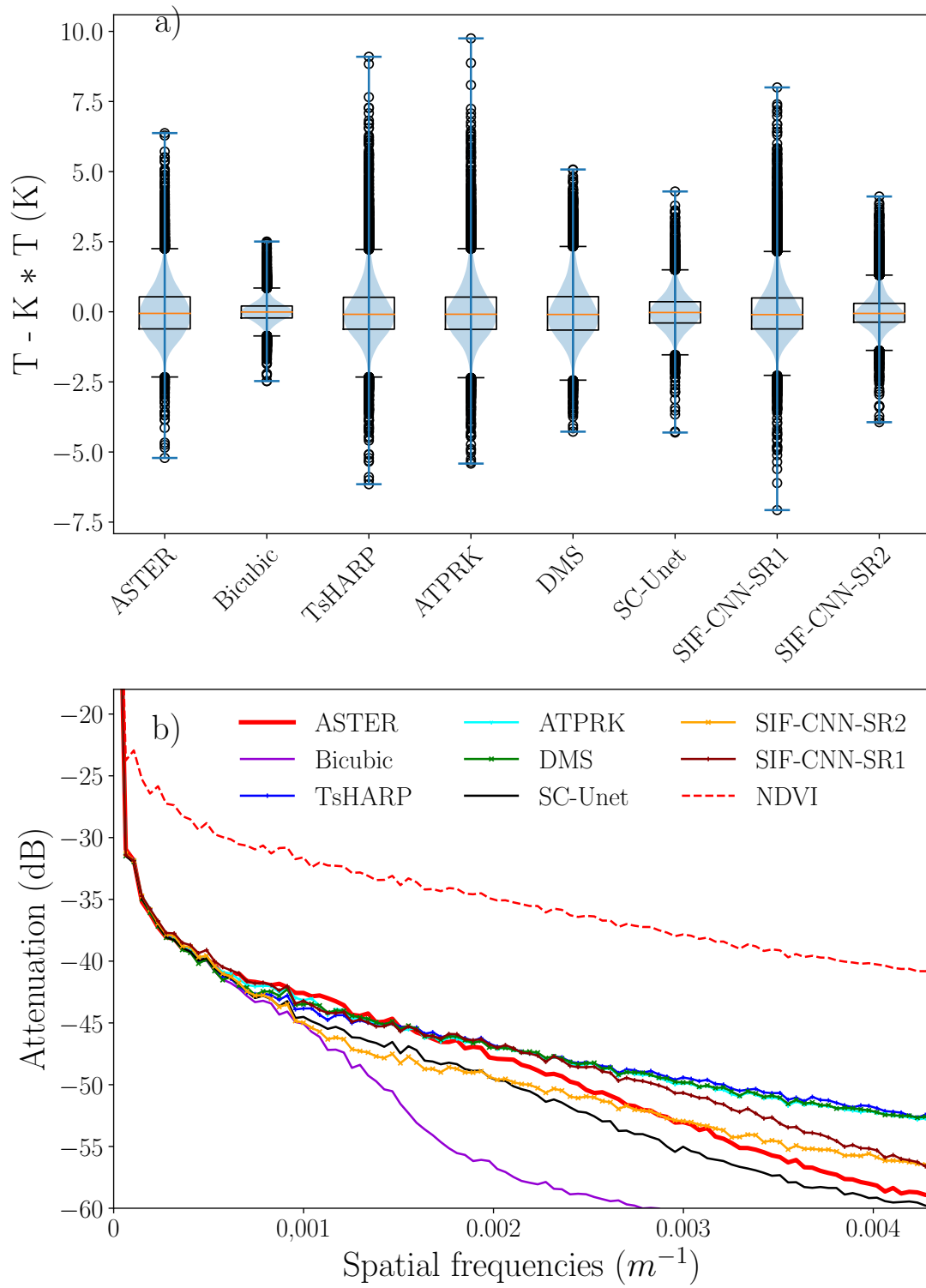


Fig. 22. Statistical analysis of the image visualized in figure 21. a) Boxplots and Violinplots representing the statistical distribution of the values of the high pass filtered LST of ASTER and obtained with the different super-resolution approaches. b) Attenuation spectra of the ASTER LST (red), LST obtained with statistical super-resolution methods TsHARP and ATPRK (blue), DMS (green), SC-Unet (black), SIF-CNN-SR1 (brown) and SIF-CNN-SR2 (orange). The attenuation spectra of the MODIS NDVI is also shown in dashed red.

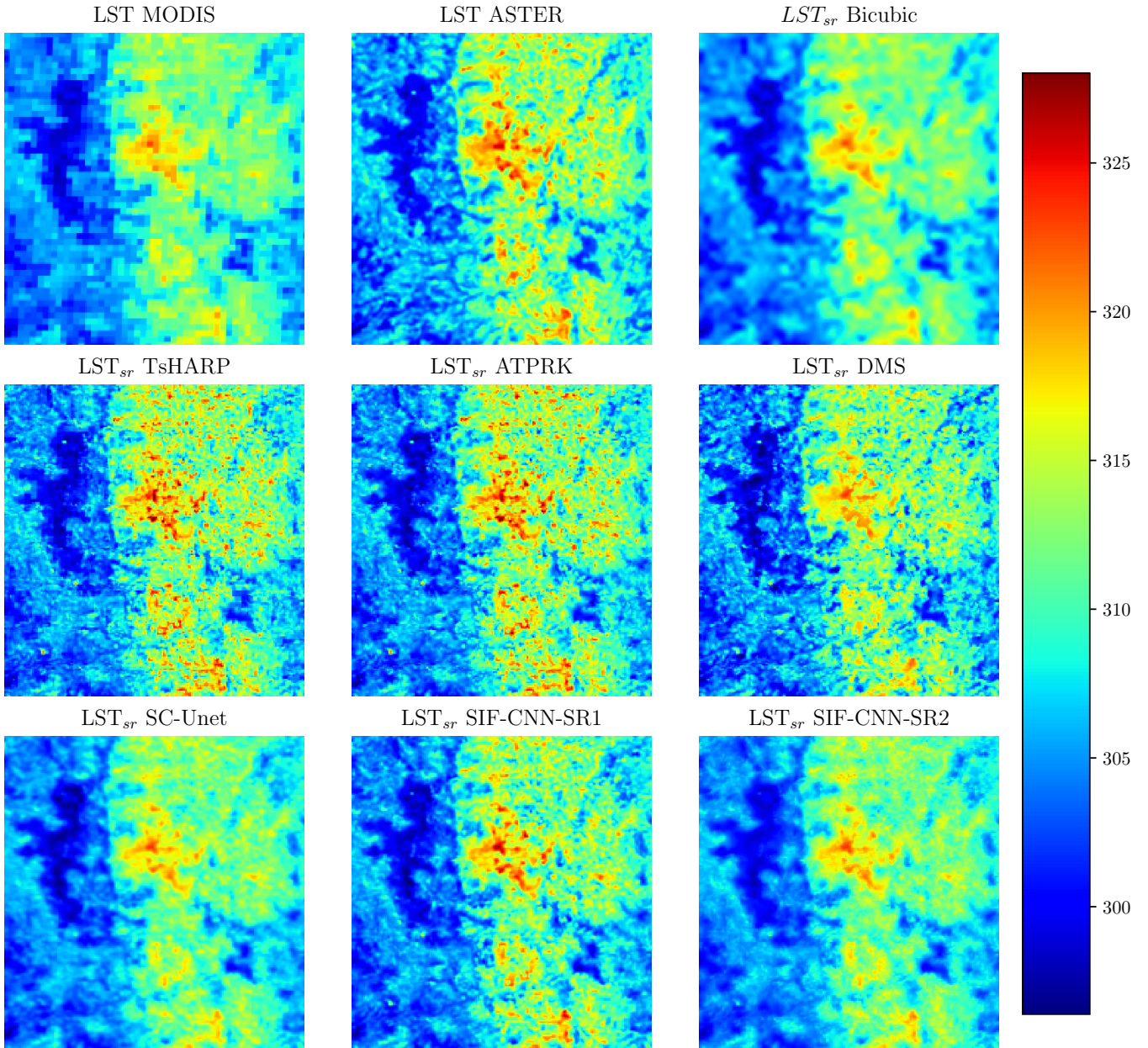


Fig. 23. Visualization of the LST of MODIS and ASTER respectively at 1km and 250m of spatial resolution alongside the super-resolution LST obtained with the different approaches.

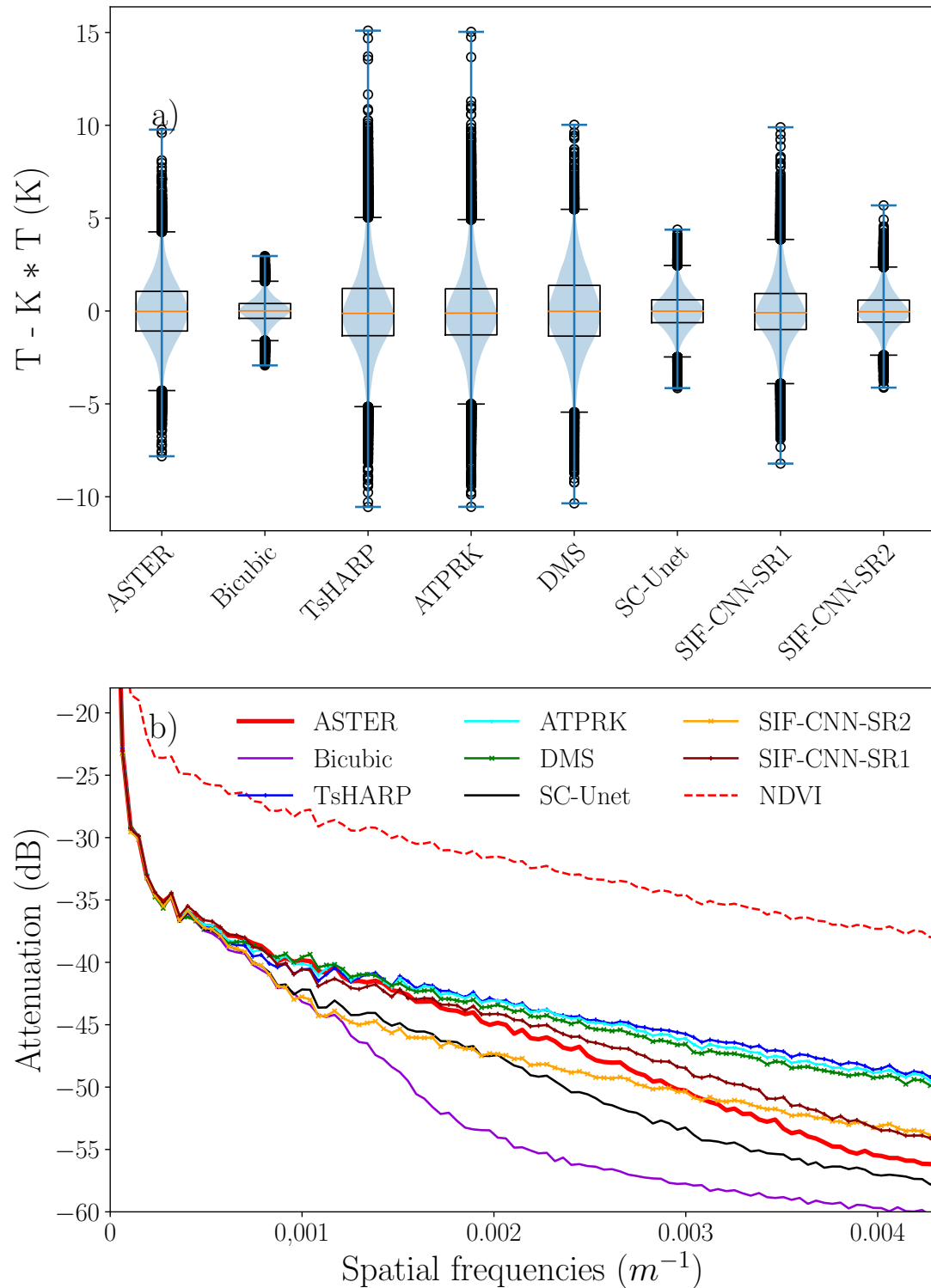


Fig. 24. Statistical analysis of the image visualized in figure 23. a) Boxplots and Violinplots representing the statistical distribution of the values of the high pass filtered LST of ASTER and obtained with the different super-resolution approaches. b) Attenuation spectra of the ASTER LST (red), LST obtained with statistical super-resolution methods TsHARP and ATPRK (blue), DMS (green), SC-Unet (black), SIF-CNN-SR1 (brown) and SIF-CNN-SR2 (orange). The attenuation spectra of the MODIS NDVI is also shown in dashed red.

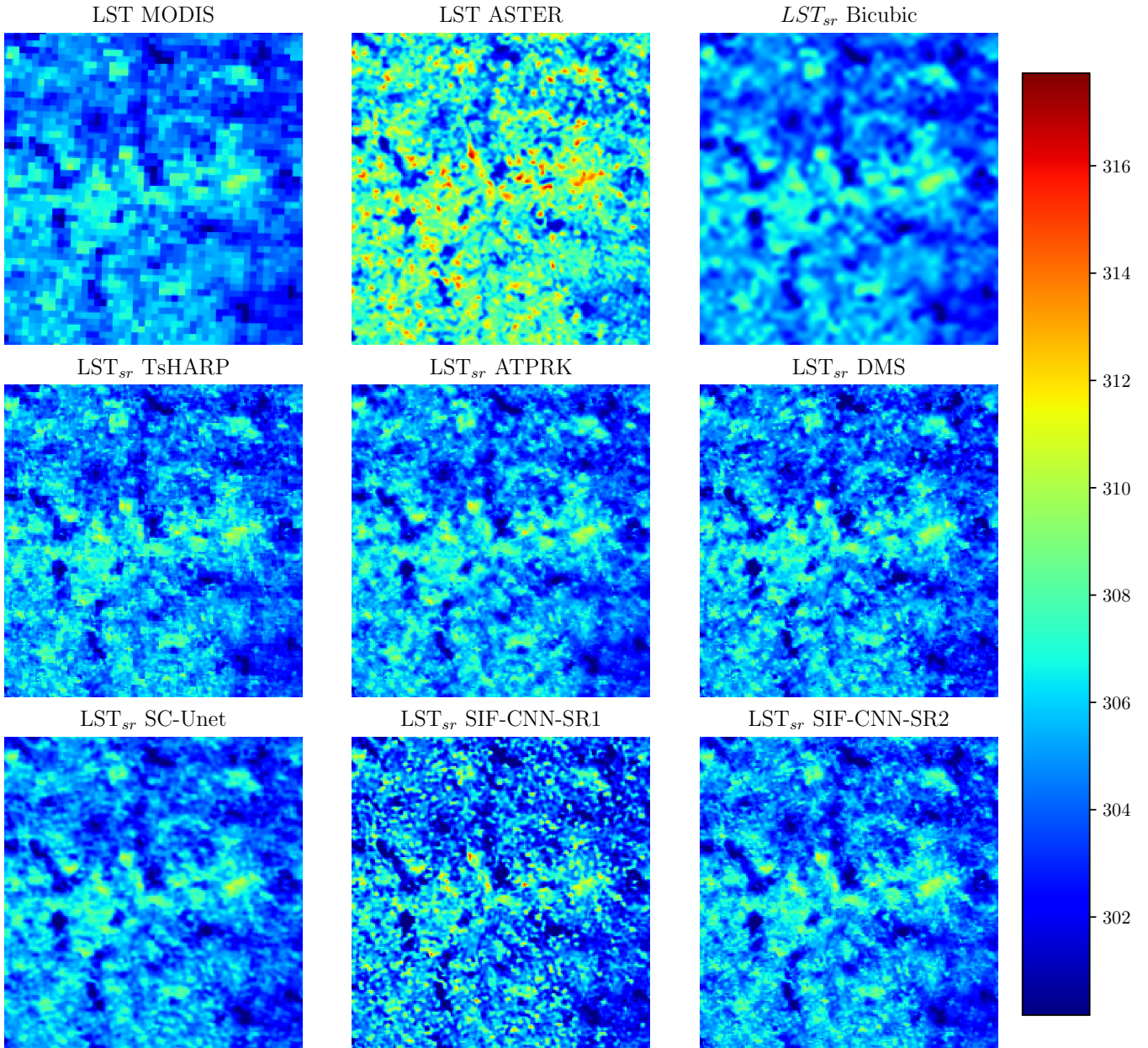


Fig. 25. Visualization of the LST of MODIS and ASTER respectively at 1km and 250m of spatial resolution alongside the super-resolution LST obtained with the different approaches.

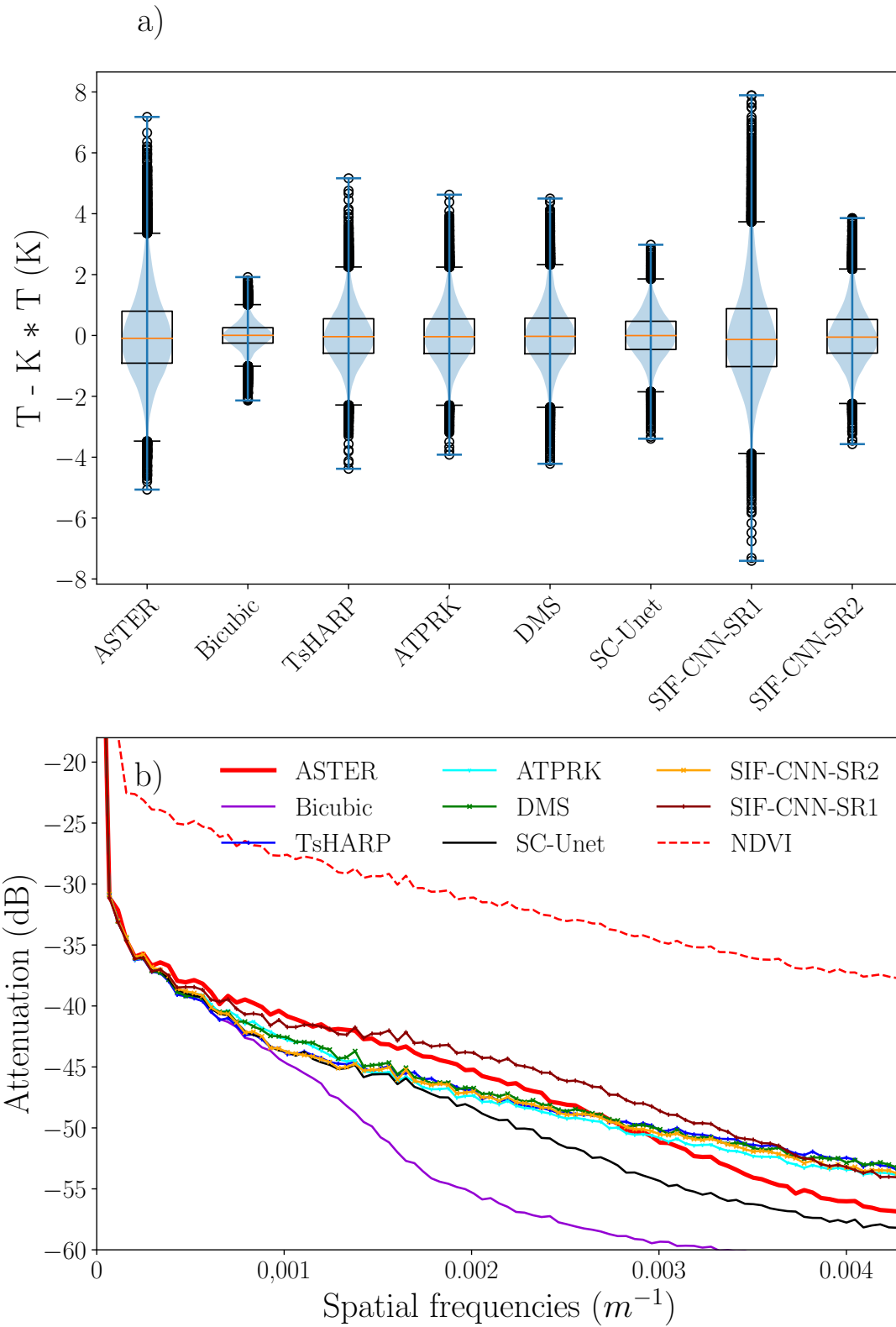


Fig. 26. Statistical analysis of the image visualized in figure 25. a) Boxplots and Violinplots representing the statistical distribution of the values of the high pass filtered LST of ASTER and obtained with the different super-resolution approaches. b) Attenuation spectra of the ASTER LST (red), LST obtained with statistical super-resolution methods TsHARP and ATPRK (blue), DMS (green), SC-Unet (black), SIF-CNN-SR1 (brown) and SIF-CNN-SR2 (orange). The attenuation spectra of the MODIS NDVI is also shown in dashed red.

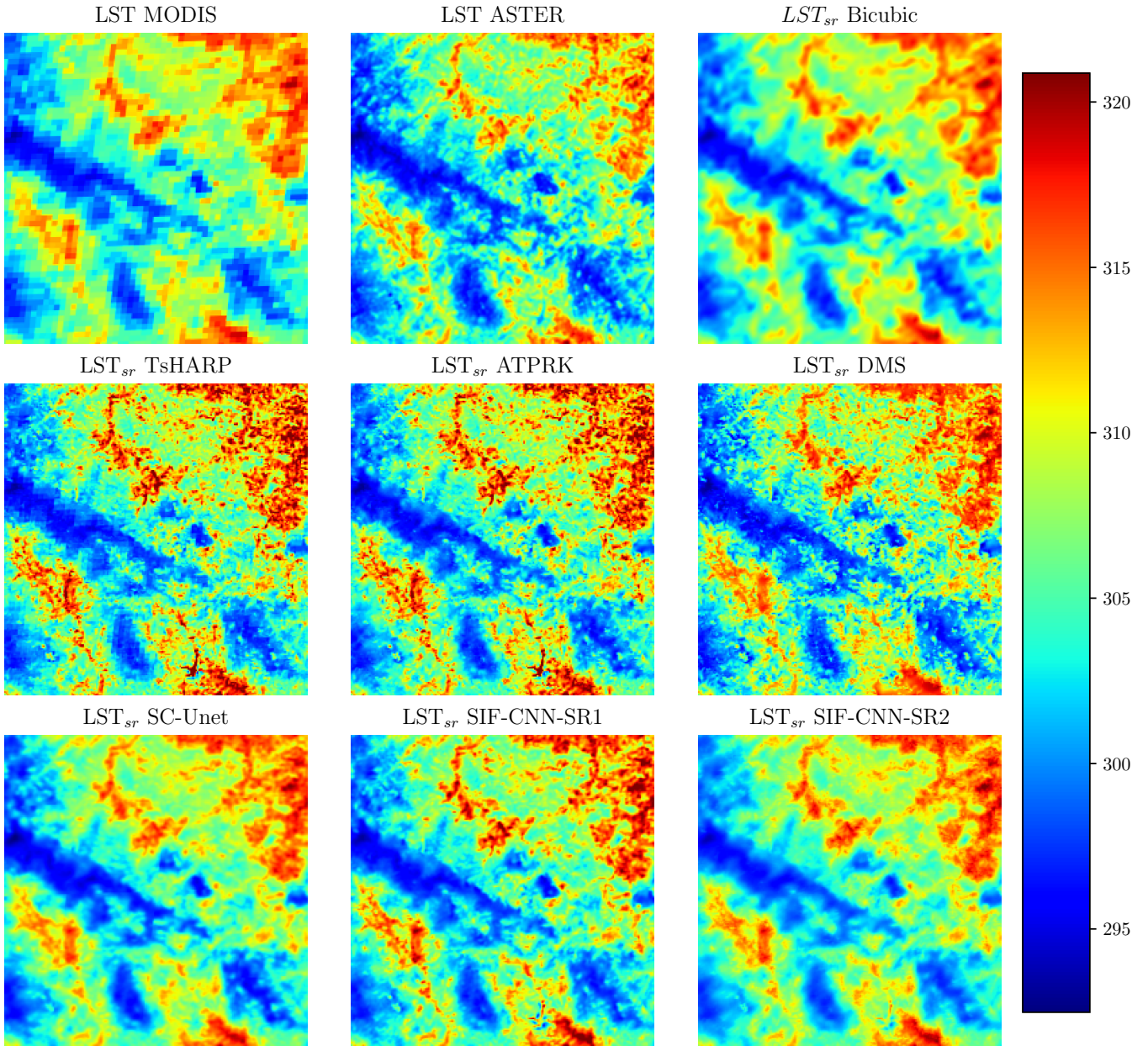


Fig. 27. Visualization of the LST of MODIS and ASTER respectively at 1km and 250m of spatial resolution alongside the super-resolution LST obtained with the different approaches.

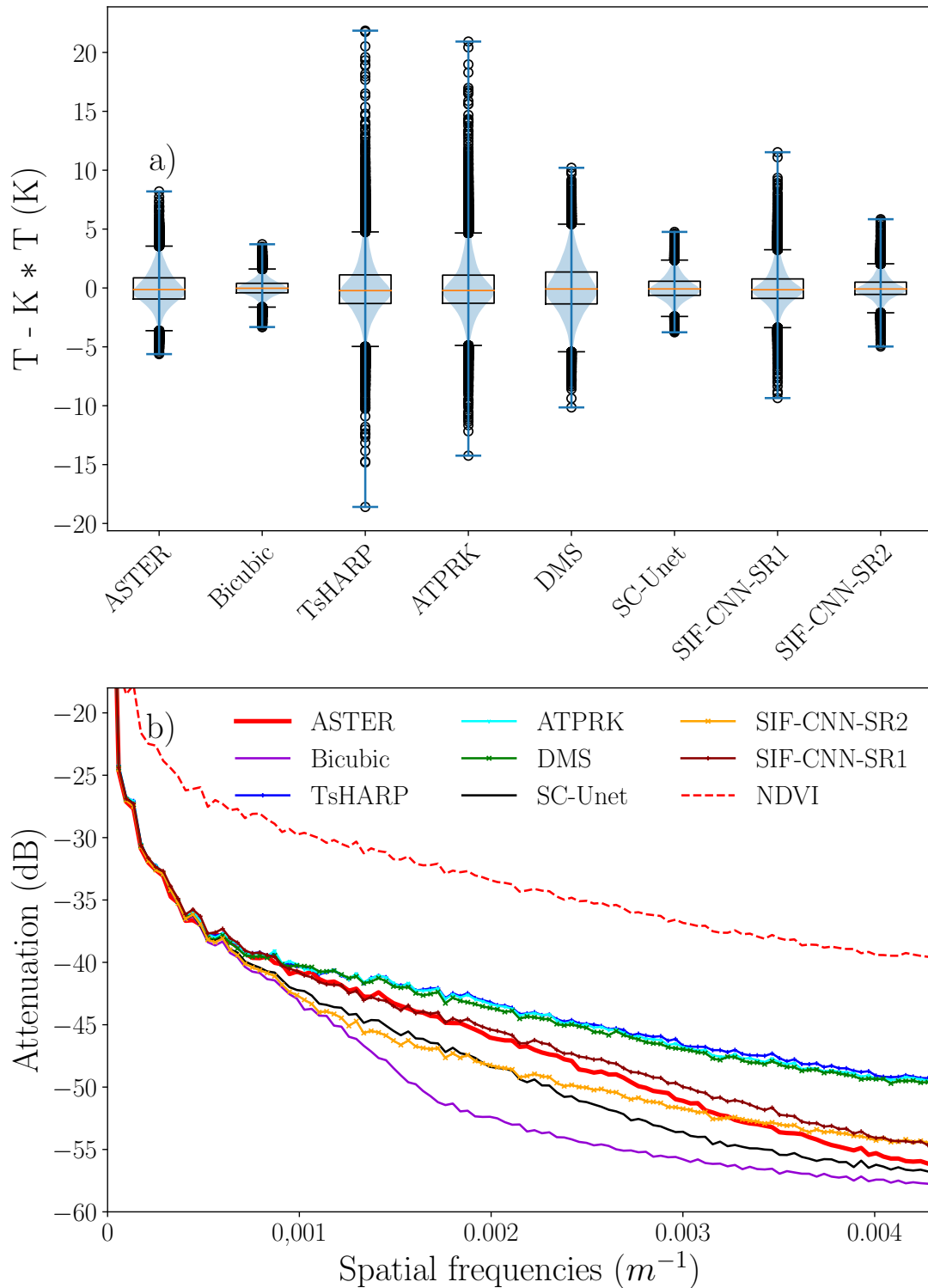


Fig. 28. Statistical analysis of the image visualized in figure 27. a) Boxplots and Violinplots representing the statistical distribution of the values of the high pass filtered LST of ASTER and obtained with the different super-resolution approaches. b) Attenuation spectra of the ASTER LST (red), LST obtained with statistical super-resolution methods TsHARP and ATPRK (blue), DMS (green), SC-Unet (black), SIF-CNN-SR1 (brown) and SIF-CNN-SR2 (orange). The attenuation spectra of the MODIS NDVI is also shown in dashed red.

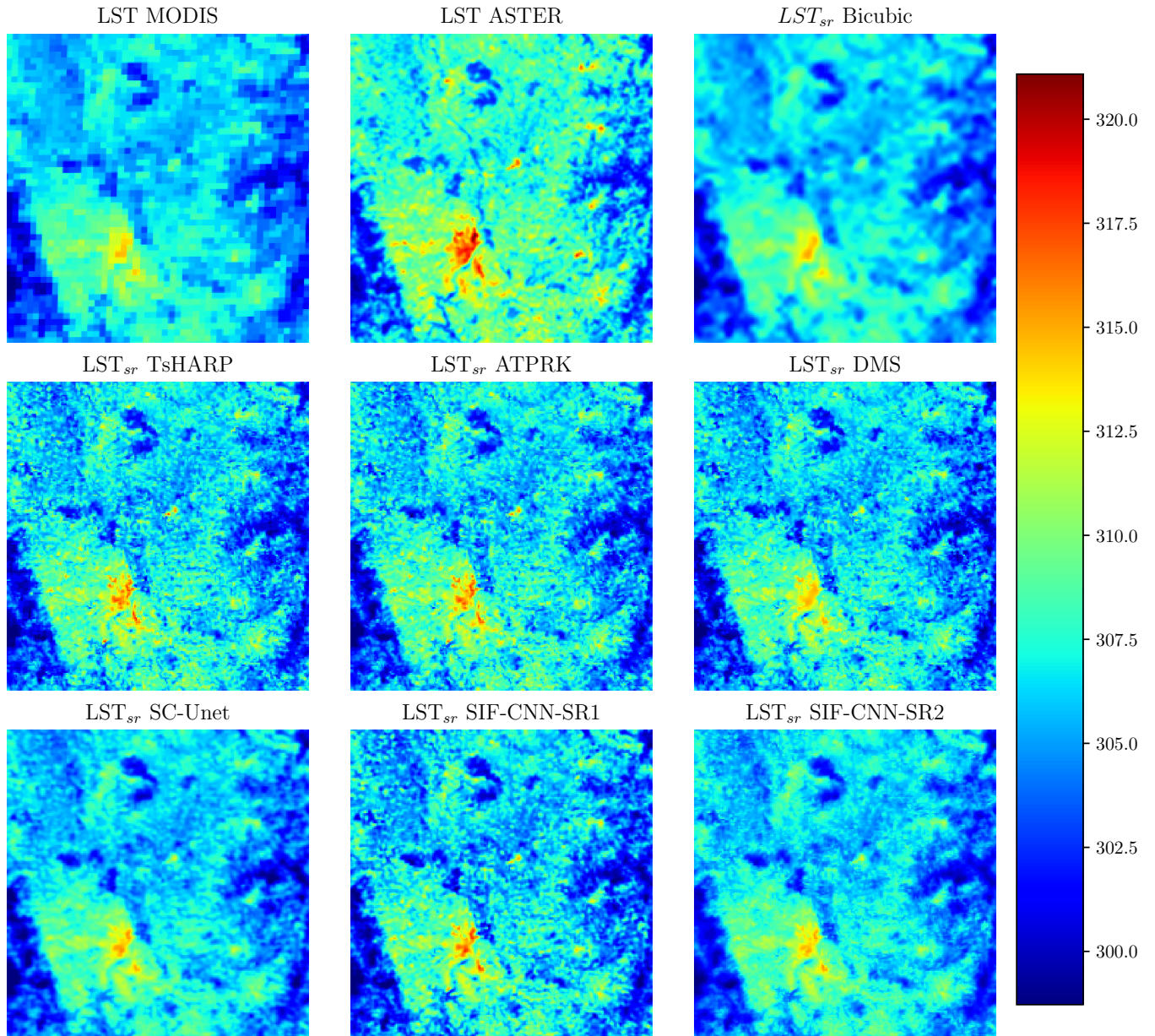


Fig. 29. Visualization of the LST of MODIS and ASTER respectively at 1km and 250m of spatial resolution alongside the super-resolution LST obtained with the different approaches.

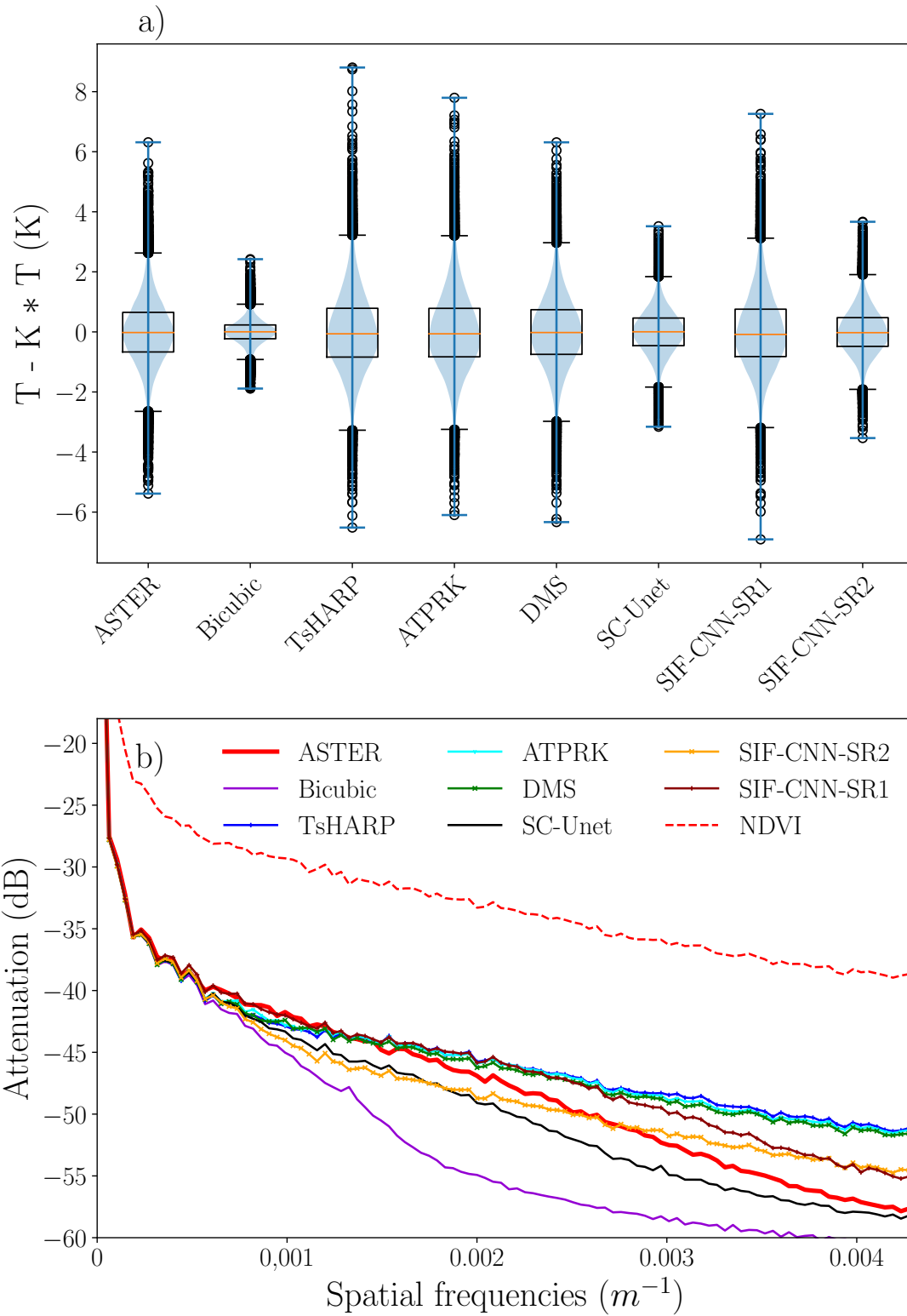


Fig. 30. Statistical analysis of the image visualized in figure 29. a) Boxplots and Violinplots representing the statistical distribution of the values of the high pass filtered LST of ASTER and obtained with the different super-resolution approaches. b) Attenuation spectra of the ASTER LST (red), LST obtained with statistical super-resolution methods TsHARP and ATPRK (blue), DMS (green), SC-Unet (black), SIF-CNN-SR1 (brown) and SIF-CNN-SR2 (orange). The attenuation spectra of the MODIS NDVI is also shown in dashed red.

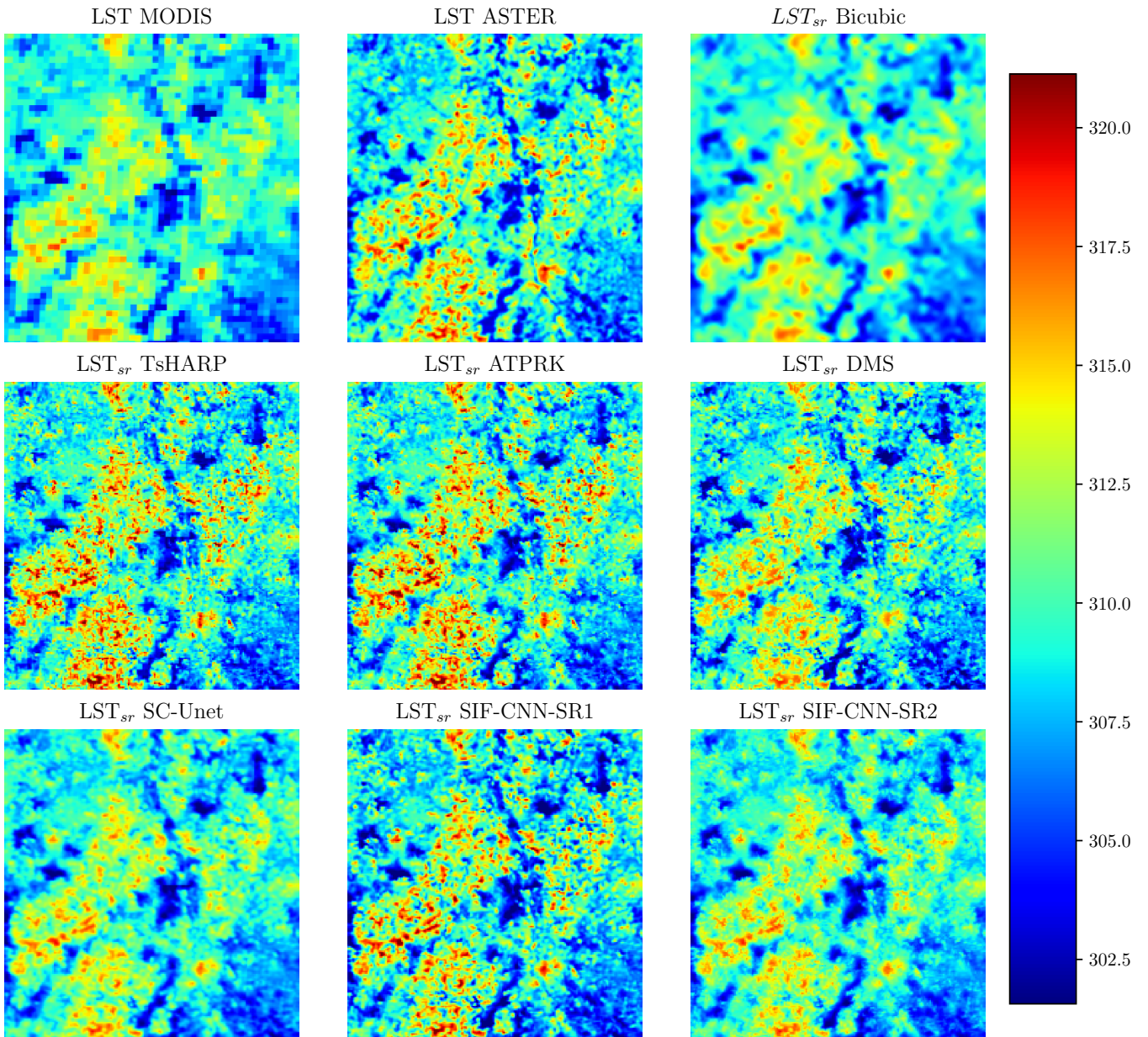


Fig. 31. Visualization of the LST of MODIS and ASTER respectively at 1km and 250m of spatial resolution alongside the super-resolution LST obtained with the different approaches.

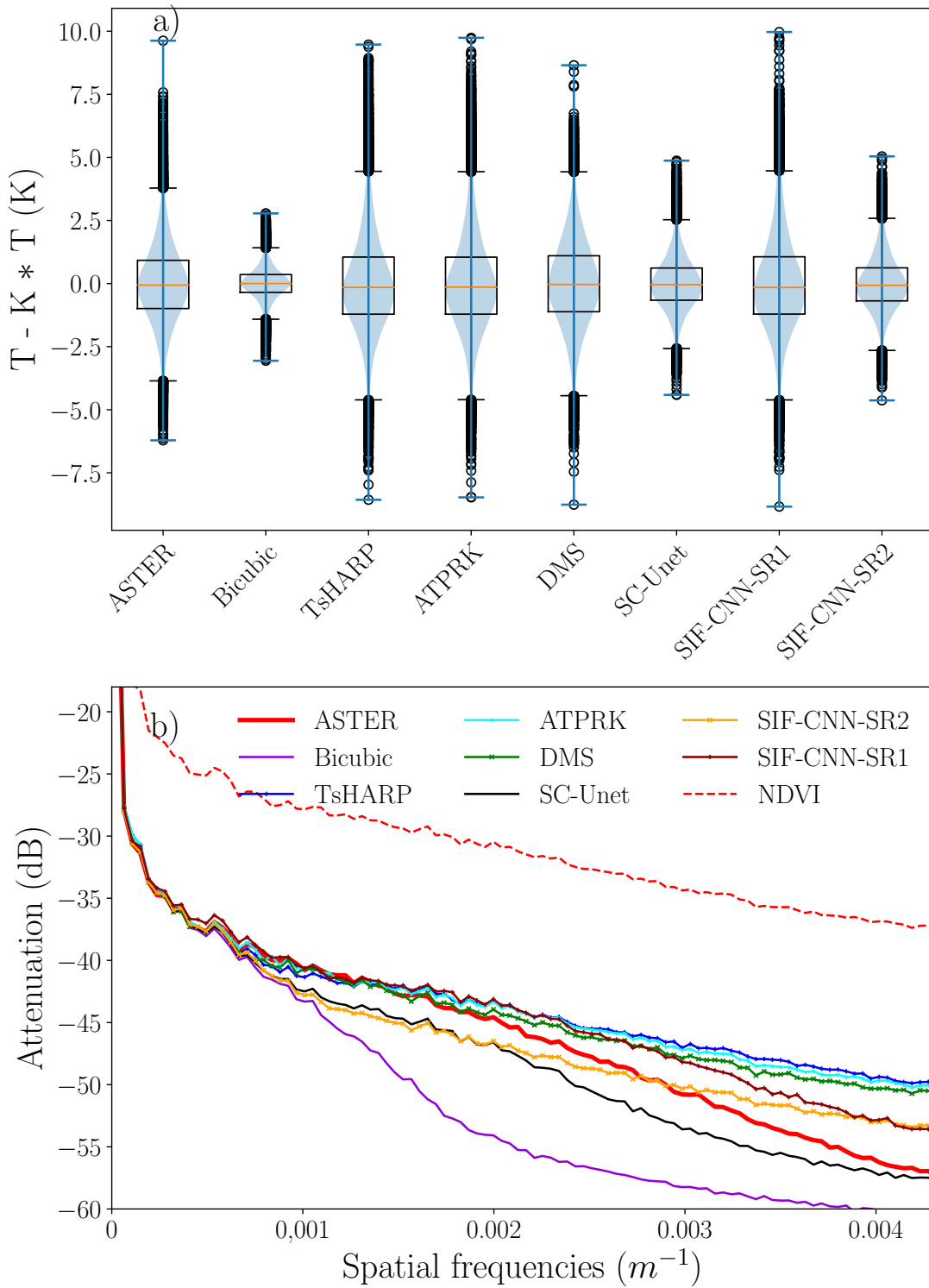


Fig. 32. Statistical analysis of the image visualized in figure 31. a) Boxplots and Violinplots representing the statistical distribution of the values of the high pass filtered LST of ASTER and obtained with the different super-resolution approaches. b) Attenuation spectra of the ASTER LST (red), LST obtained with statistical super-resolution methods TsHARP and ATPRK (blue), DMS (green), SC-Unet (black), SIF-CNN-SR1 (brown) and SIF-CNN-SR2 (orange). The attenuation spectra of the MODIS NDVI is also shown in dashed red.

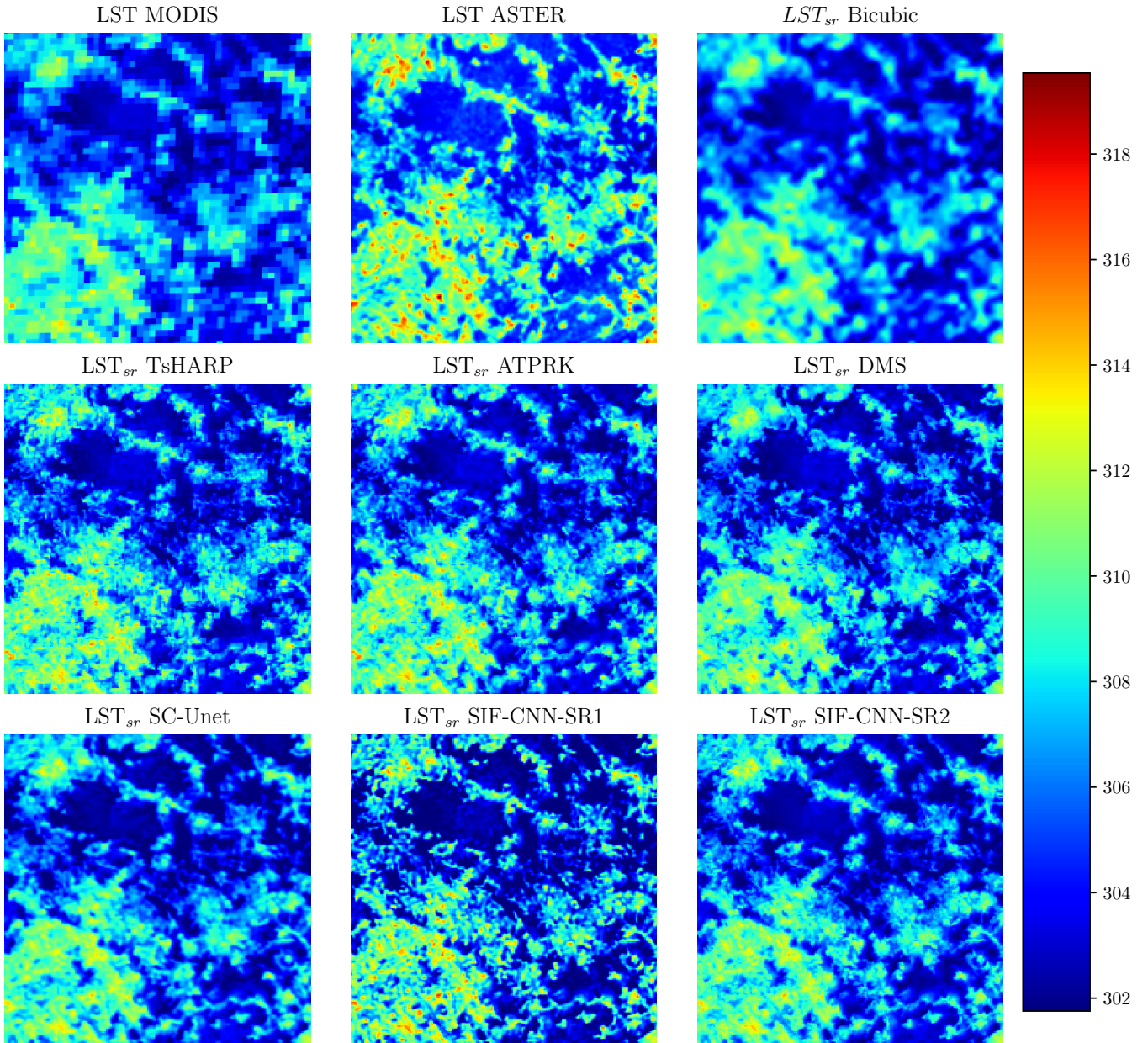


Fig. 33. Visualization of the LST of MODIS and ASTER respectively at 1km and 250m of spatial resolution alongside the super-resolution LST obtained with the different approaches.

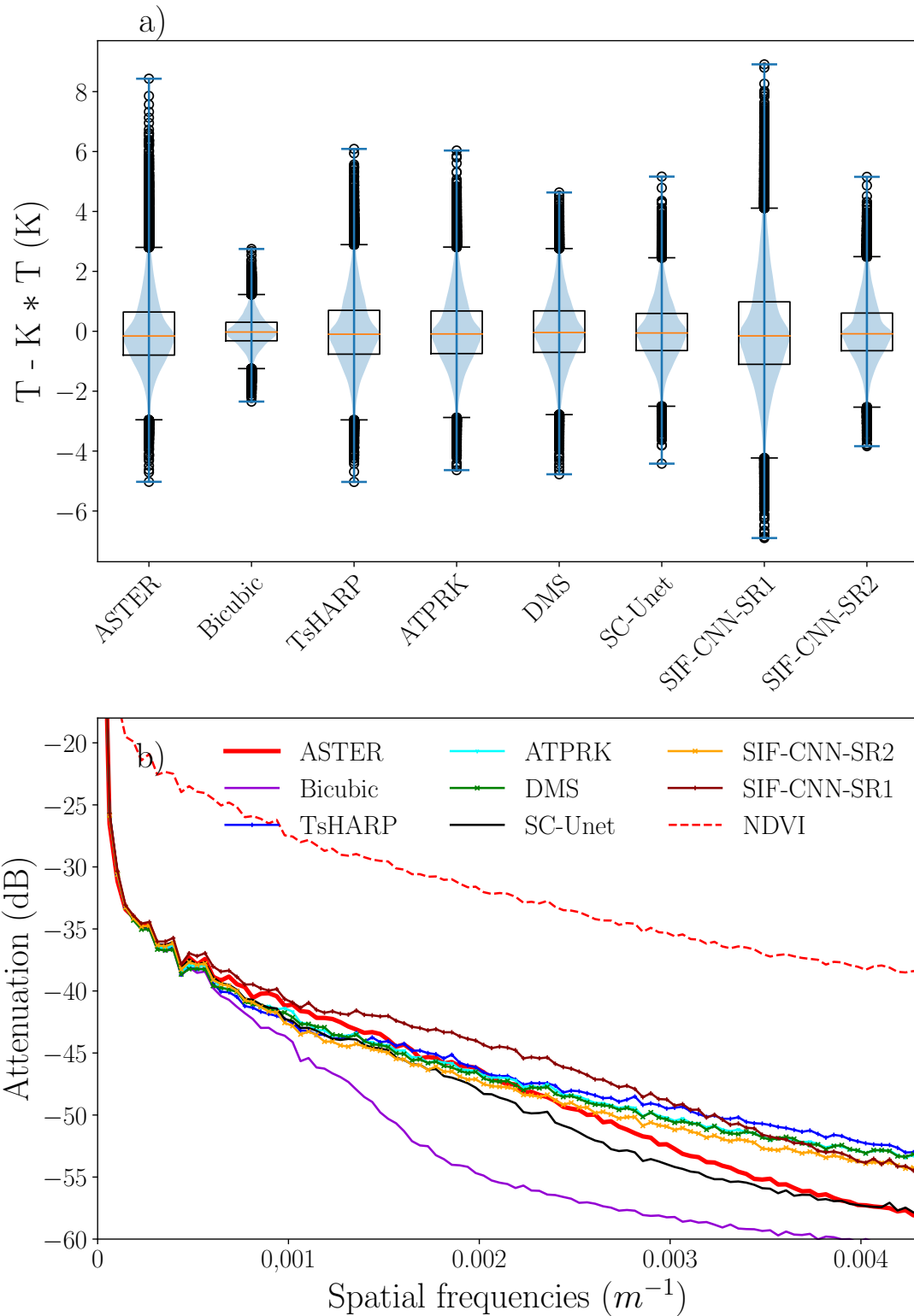


Fig. 34. Statistical analysis of the image visualized in figure 33. a) Boxplots and Violinplots representing the statistical distribution of the values of the high pass filtered LST of ASTER and obtained with the different super-resolution approaches. b) Attenuation spectra of the ASTER LST (red), LST obtained with statistical super-resolution methods TsHARP and ATPRK (blue), DMS (green), SC-Unet (black), SIF-CNN-SR1 (brown) and SIF-CNN-SR2 (orange). The attenuation spectra of the MODIS NDVI is also shown in dashed red.

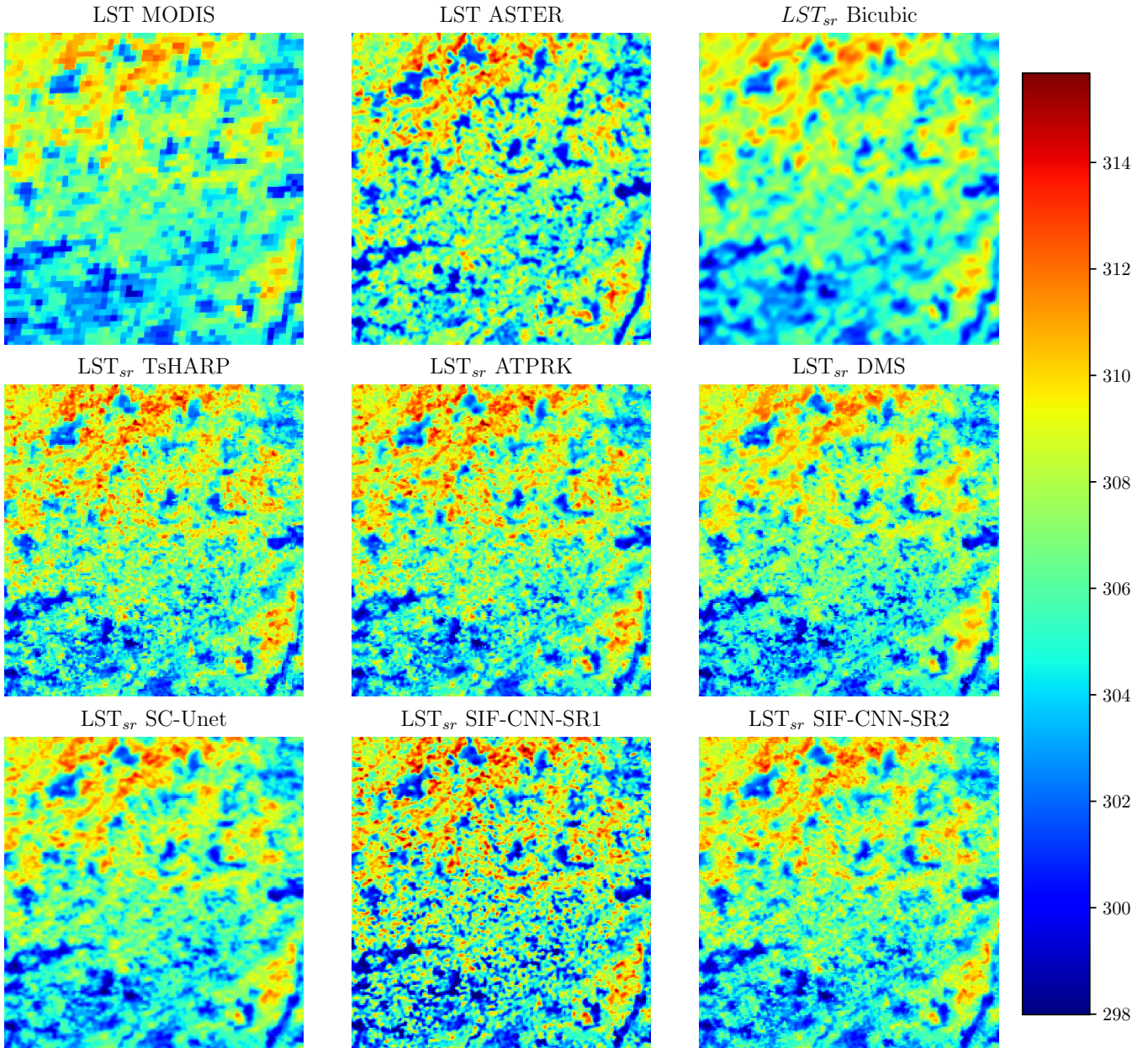


Fig. 35. Visualization of the LST of MODIS and ASTER respectively at 1km and 250m of spatial resolution alongside the super-resolution LST obtained with the different approaches.

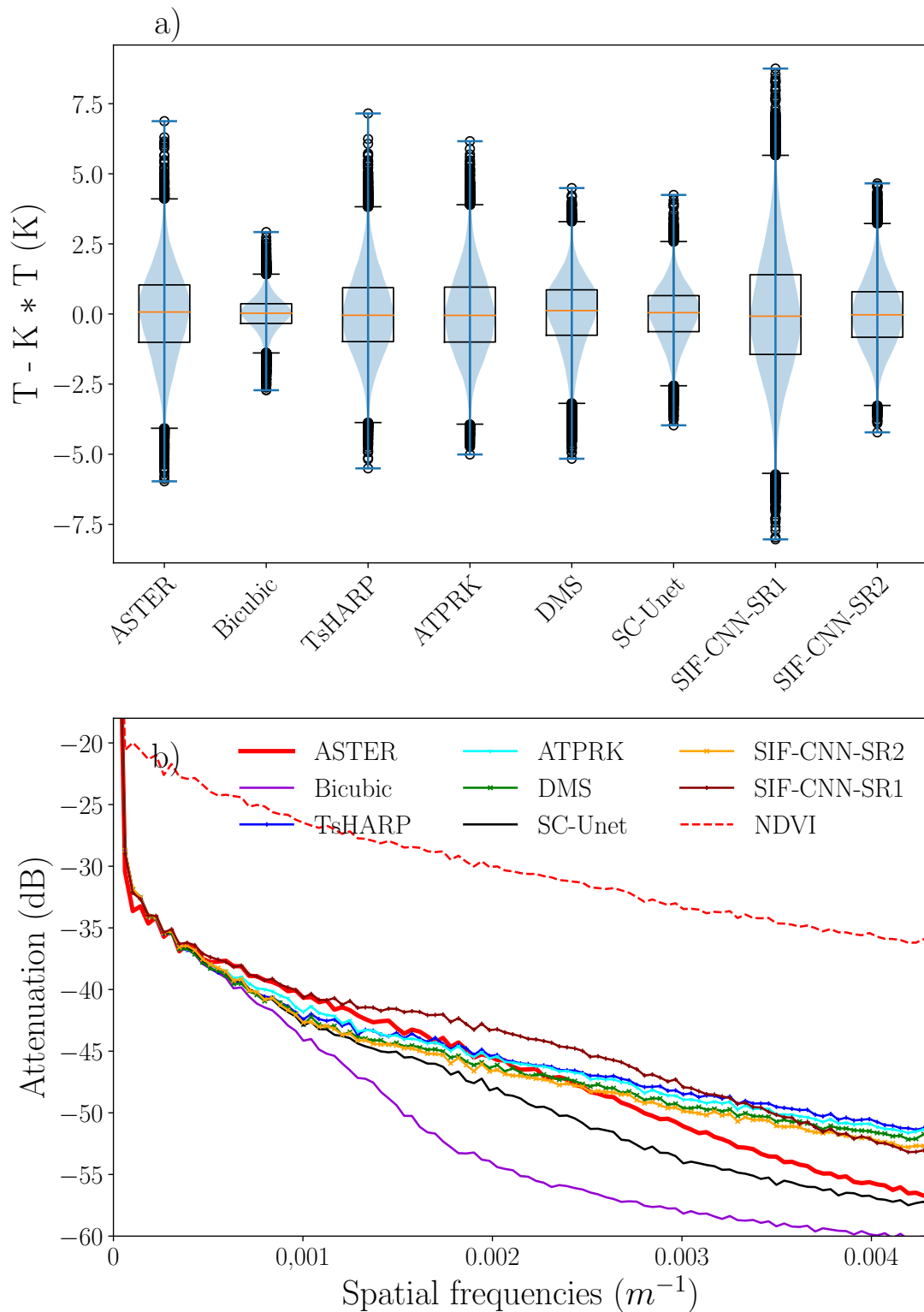


Fig. 36. Statistical analysis of the image visualized in figure 35. a) Boxplots and Violinplots representing the statistical distribution of the values of the high pass filtered LST of ASTER and obtained with the different super-resolution approaches. b) Attenuation spectra of the ASTER LST (red), LST obtained with statistical super-resolution methods TsHARP and ATPRK (blue), DMS (green), SC-Unet (black), SIF-CNN-SR1 (brown) and SIF-CNN-SR2 (orange). The attenuation spectra of the MODIS NDVI is also shown in dashed red.

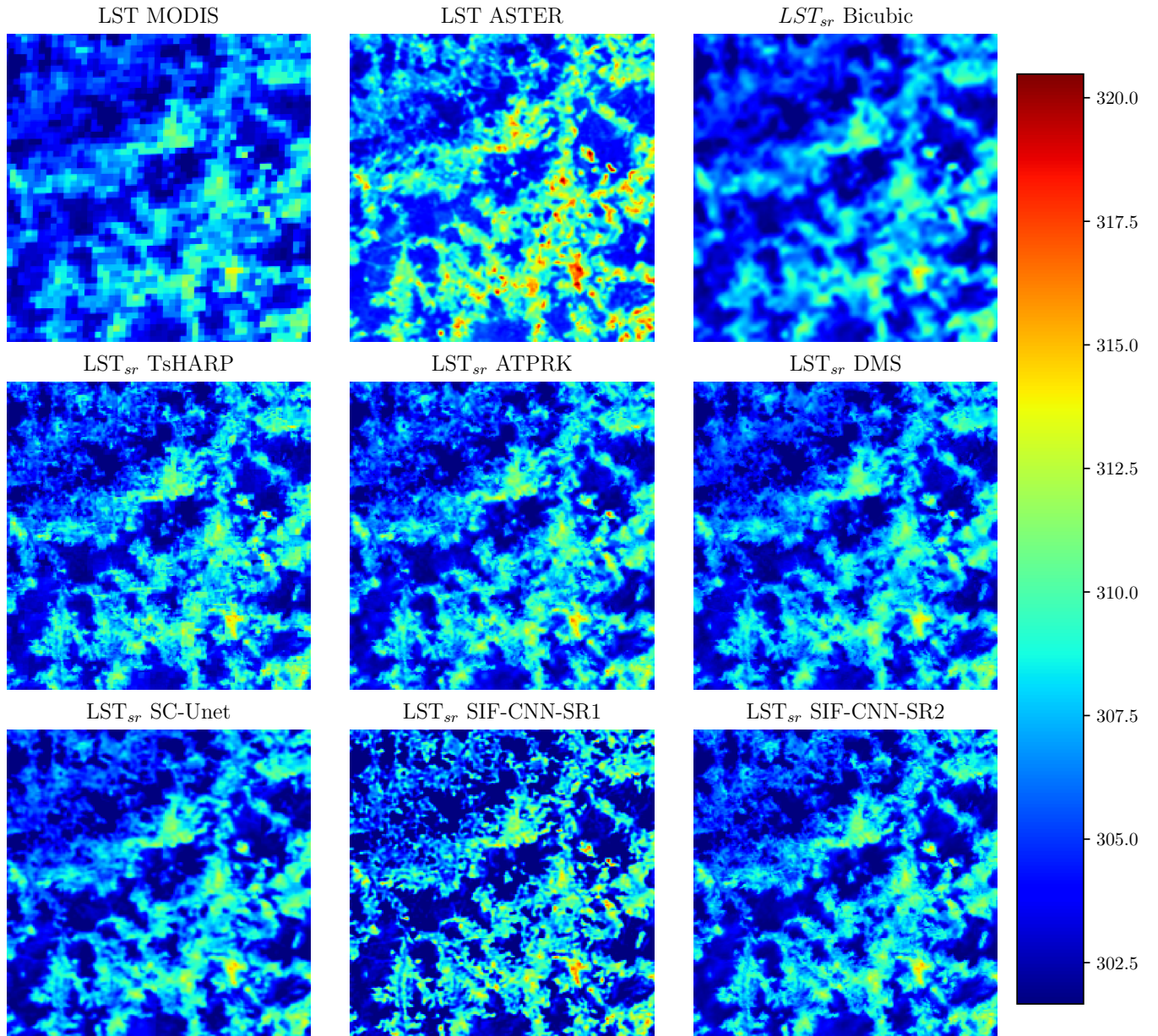


Fig. 37. Visualization of the LST of MODIS and ASTER respectively at 1km and 250m of spatial resolution alongside the super-resolution LST obtained with the different approaches.

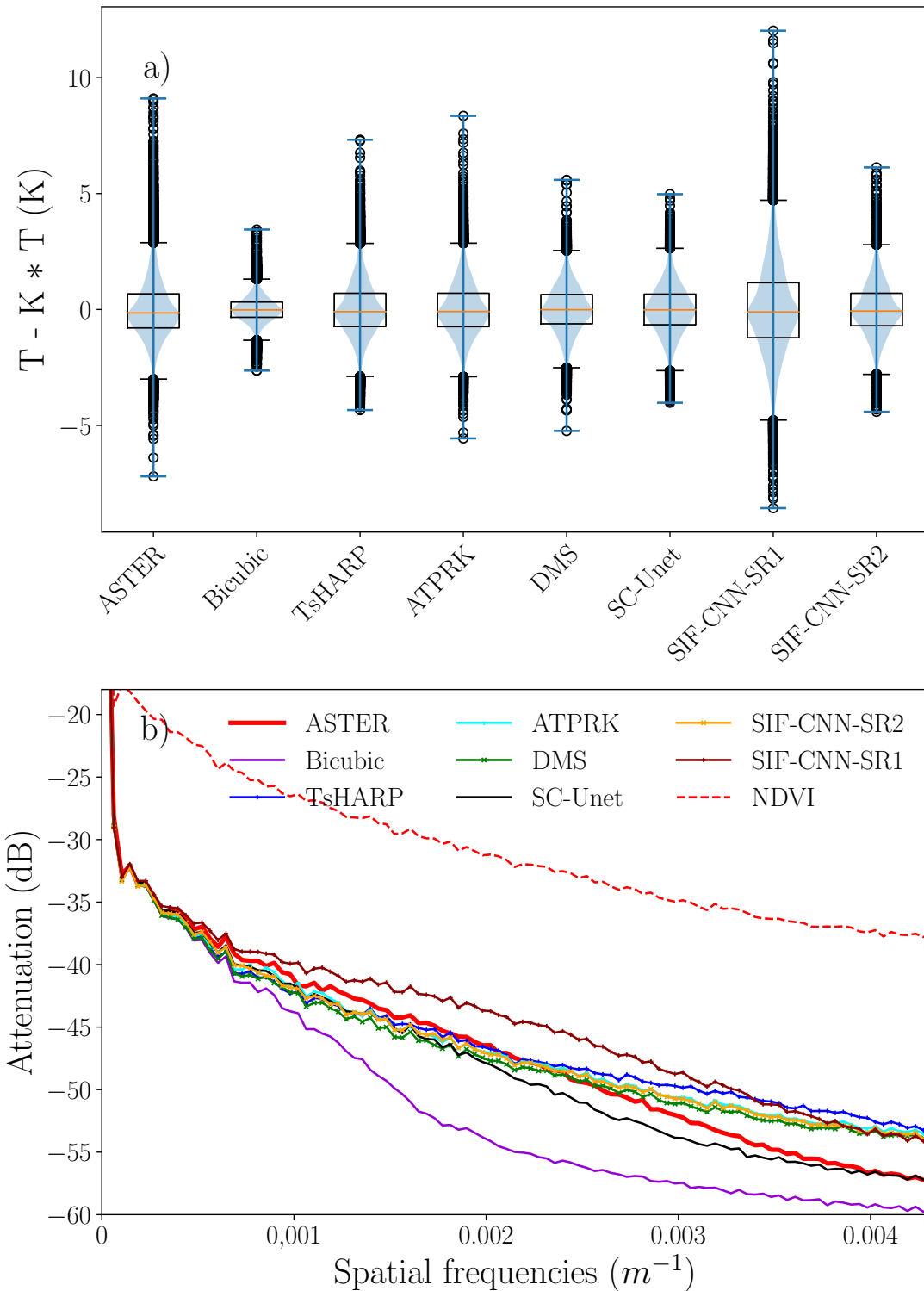


Fig. 38. Statistical analysis of the image visualized in figure 37. a) Boxplots and Violinplots representing the statistical distribution of the values of the high pass filtered LST of ASTER and obtained with the different super-resolution approaches. b) Attenuation spectra of the ASTER LST (red), LST obtained with statistical super-resolution methods TsHARP and ATPRK (blue), DMS (green), SC-Unet (black), SIF-CNN-SR1 (brown) and SIF-CNN-SR2 (orange). The attenuation spectra of the MODIS NDVI is also shown in dashed red.

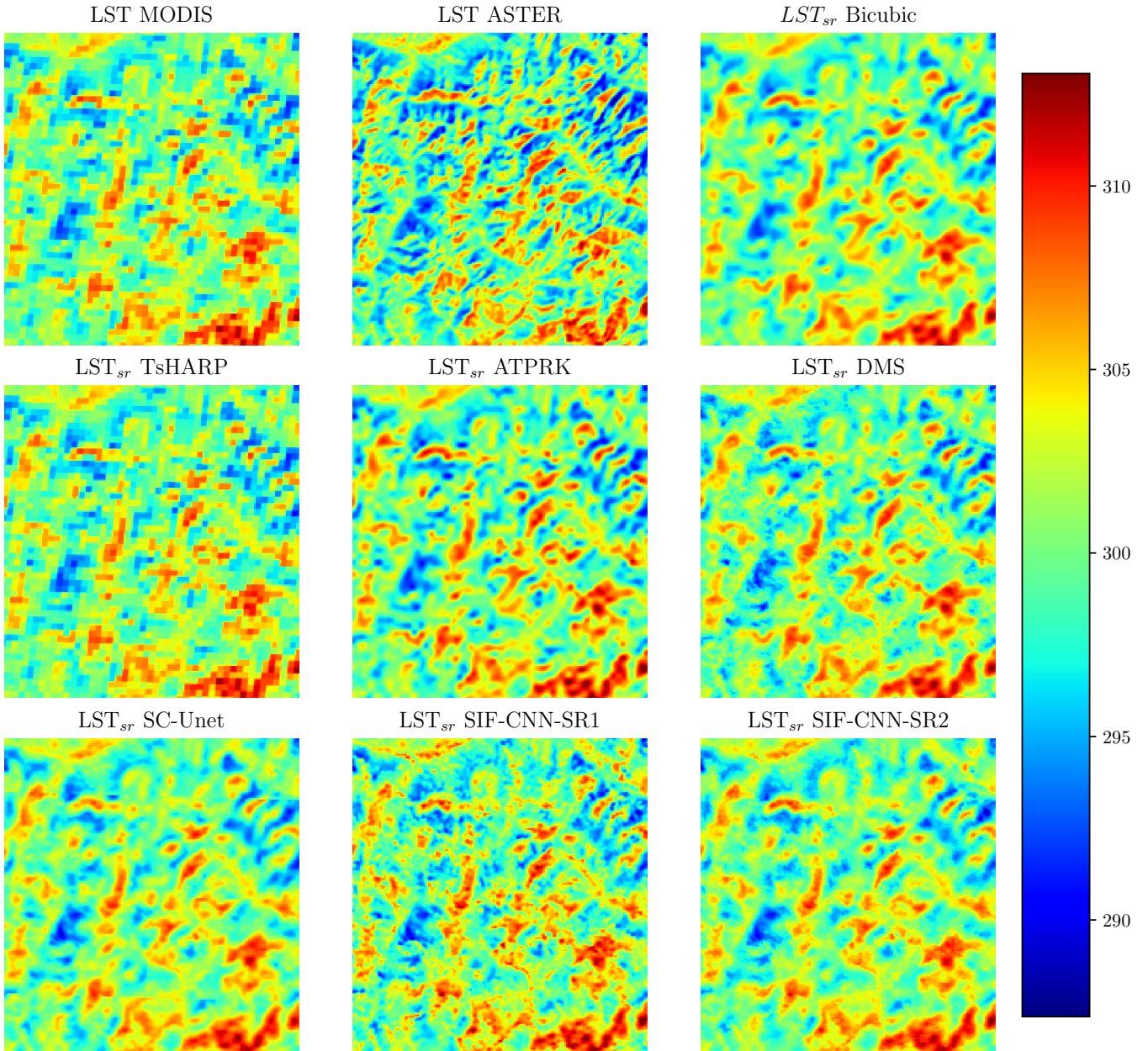


Fig. 39. Visualization of the LST of MODIS and ASTER respectively at 1km and 250m of spatial resolution alongside the super-resolution LST obtained with the different approaches.

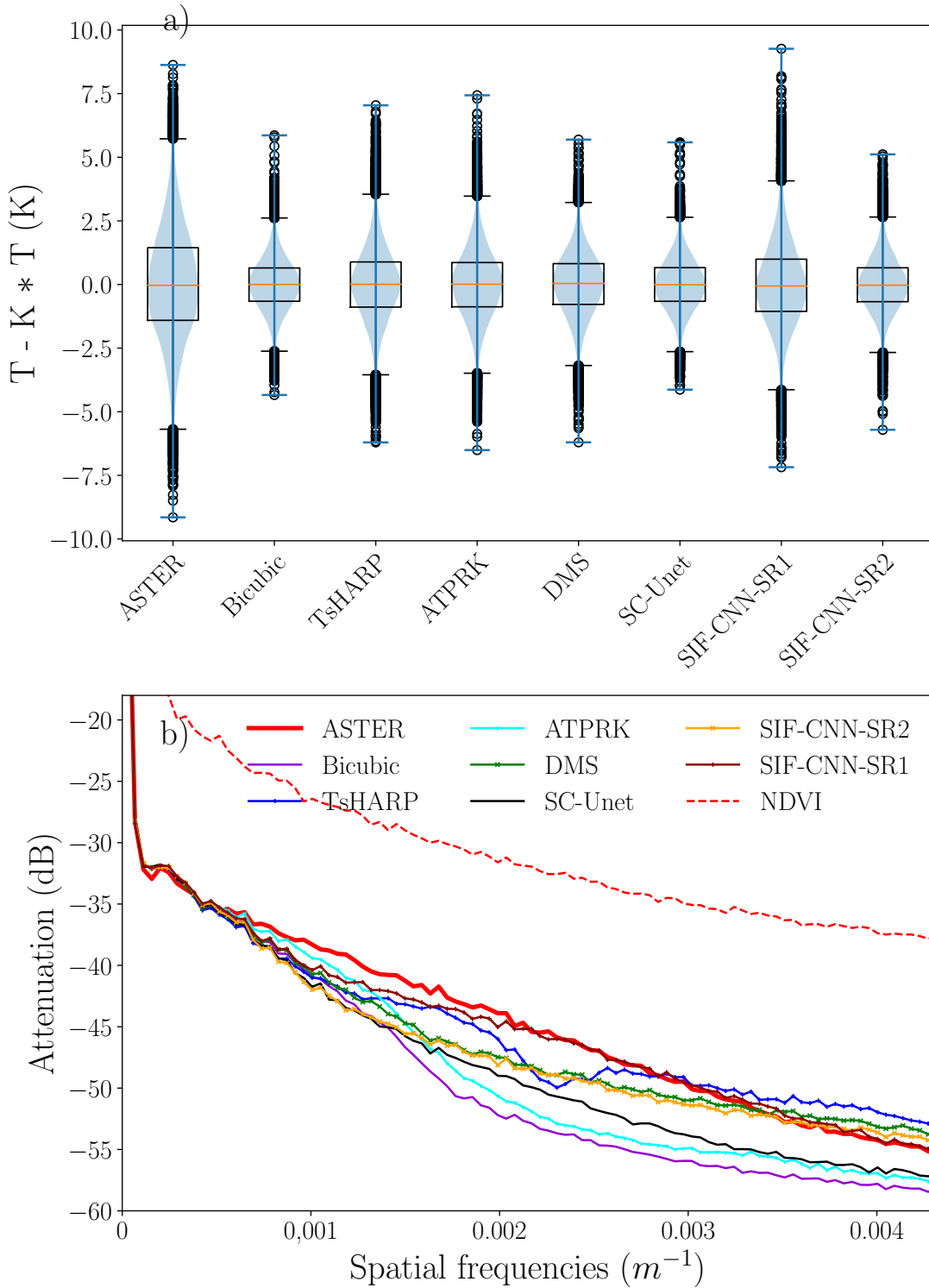


Fig. 40. Statistical analysis of the image visualized in figure 39. a) Boxplots and Violinplots representing the statistical distribution of the values of the high pass filtered LST of ASTER and obtained with the different super-resolution approaches. b) Attenuation spectra of the ASTER LST (red), LST obtained with statistical super-resolution methods TsHARP and ATPRK (blue), DMS (green), SC-Unet (black), SIF-CNN-SR1 (brown) and SIF-CNN-SR2 (orange). The attenuation spectra of the MODIS NDVI is also shown in dashed red.

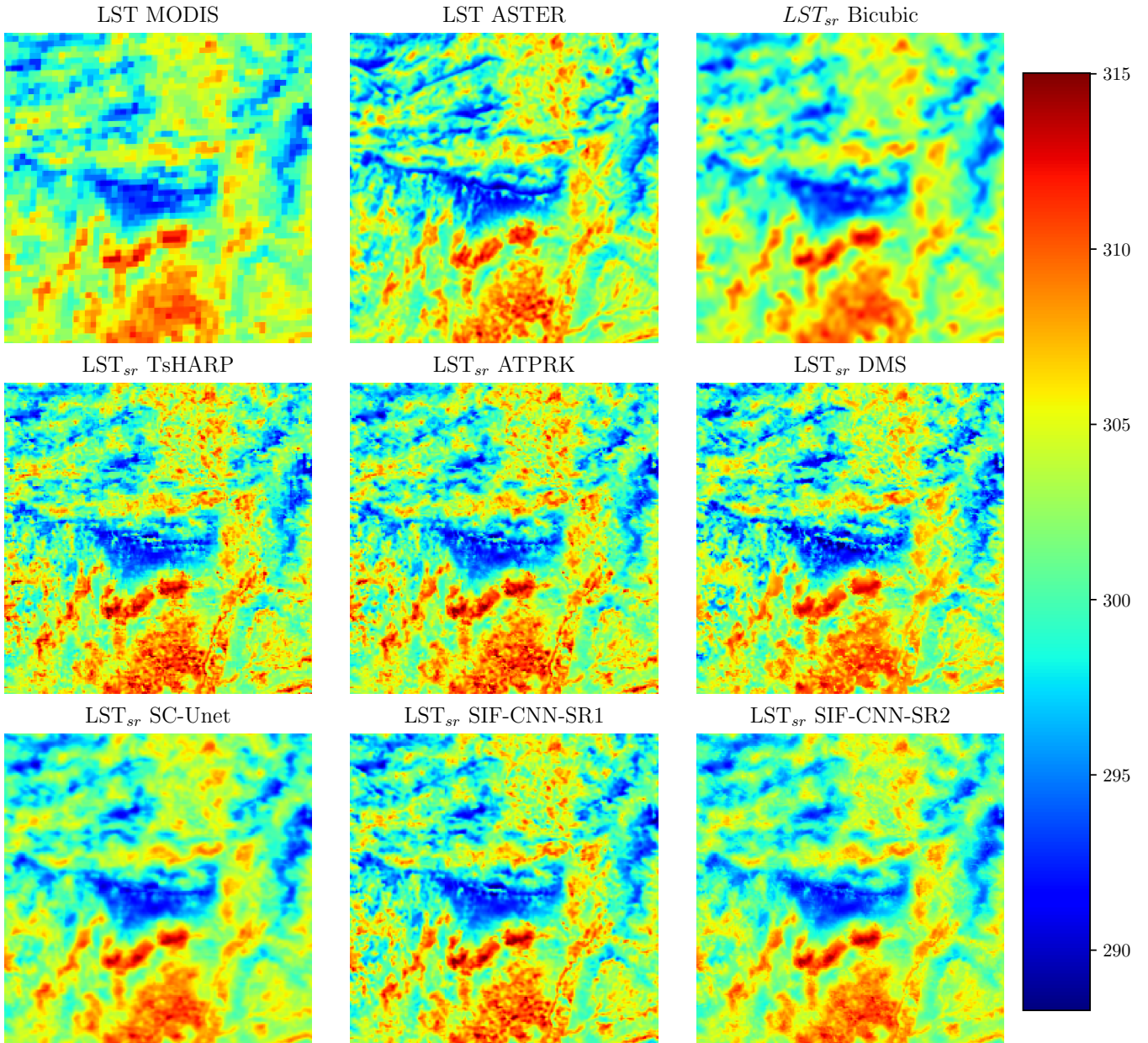


Fig. 41. Visualization of the LST of MODIS and ASTER respectively at 1km and 250m of spatial resolution alongside the super-resolution LST obtained with the different approaches.

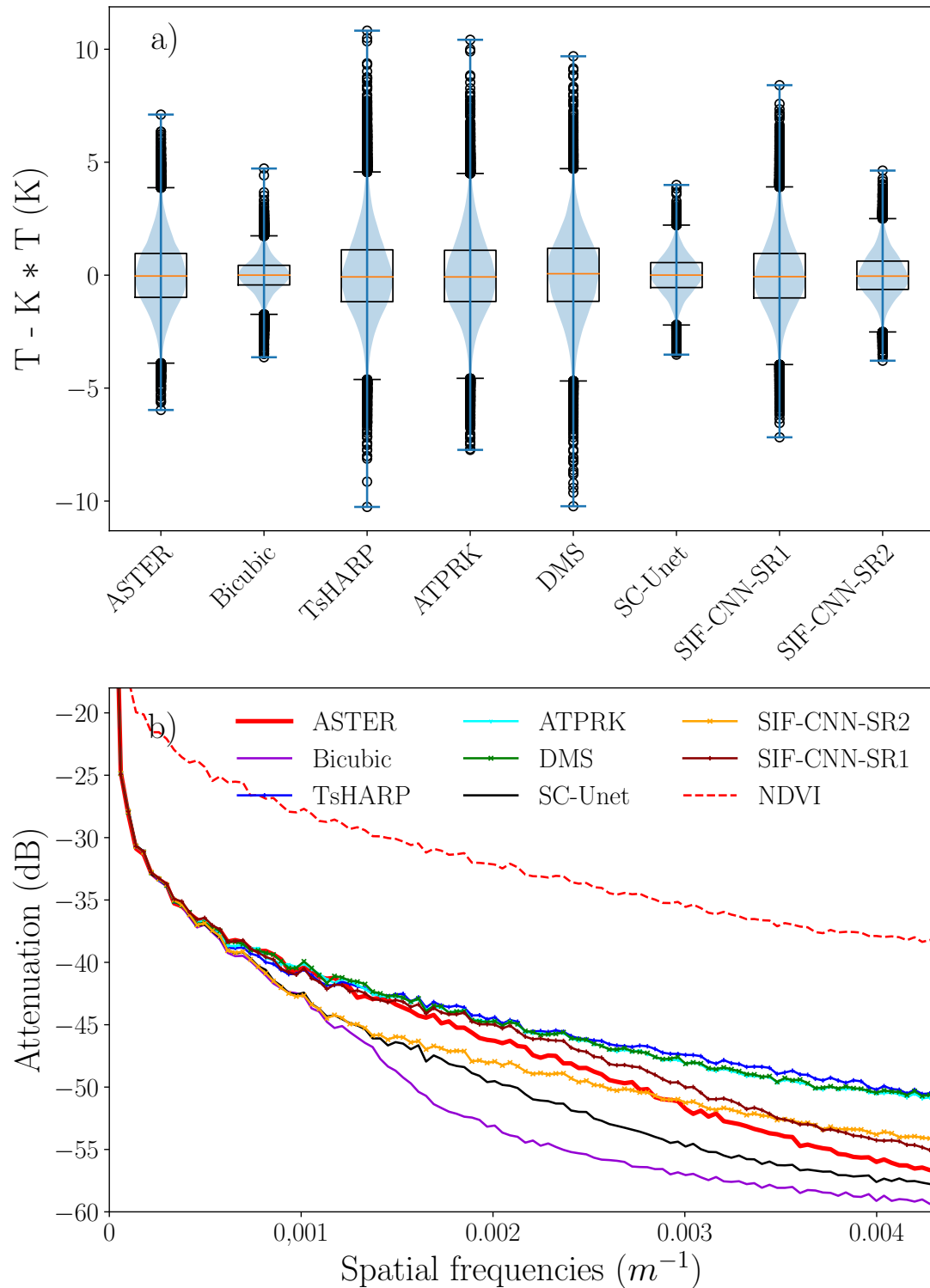


Fig. 42. Statistical analysis of the image visualized in figure 41. a) Boxplots and Violinplots representing the statistical distribution of the values of the high pass filtered LST of ASTER and obtained with the different super-resolution approaches. b) Attenuation spectra of the ASTER LST (red), LST obtained with statistical super-resolution methods TsHARP and ATPRK (blue), DMS (green), SC-Unet (black), SIF-CNN-SR1 (brown) and SIF-CNN-SR2 (orange). The attenuation spectra of the MODIS NDVI is also shown in dashed red.

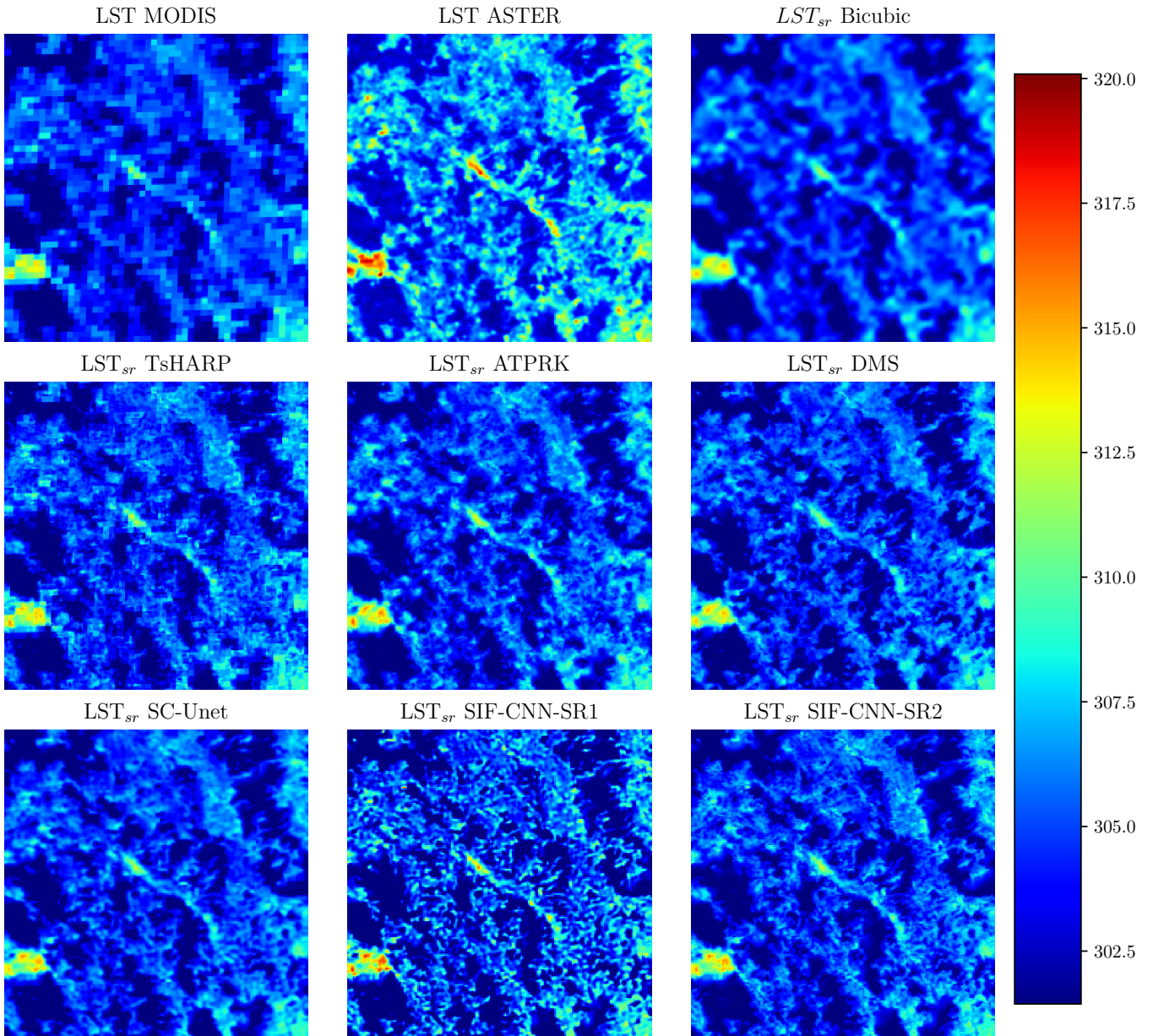


Fig. 43. Visualization of the LST of MODIS and ASTER respectively at 1km and 250m of spatial resolution alongside the super-resolution LST obtained with the different approaches.

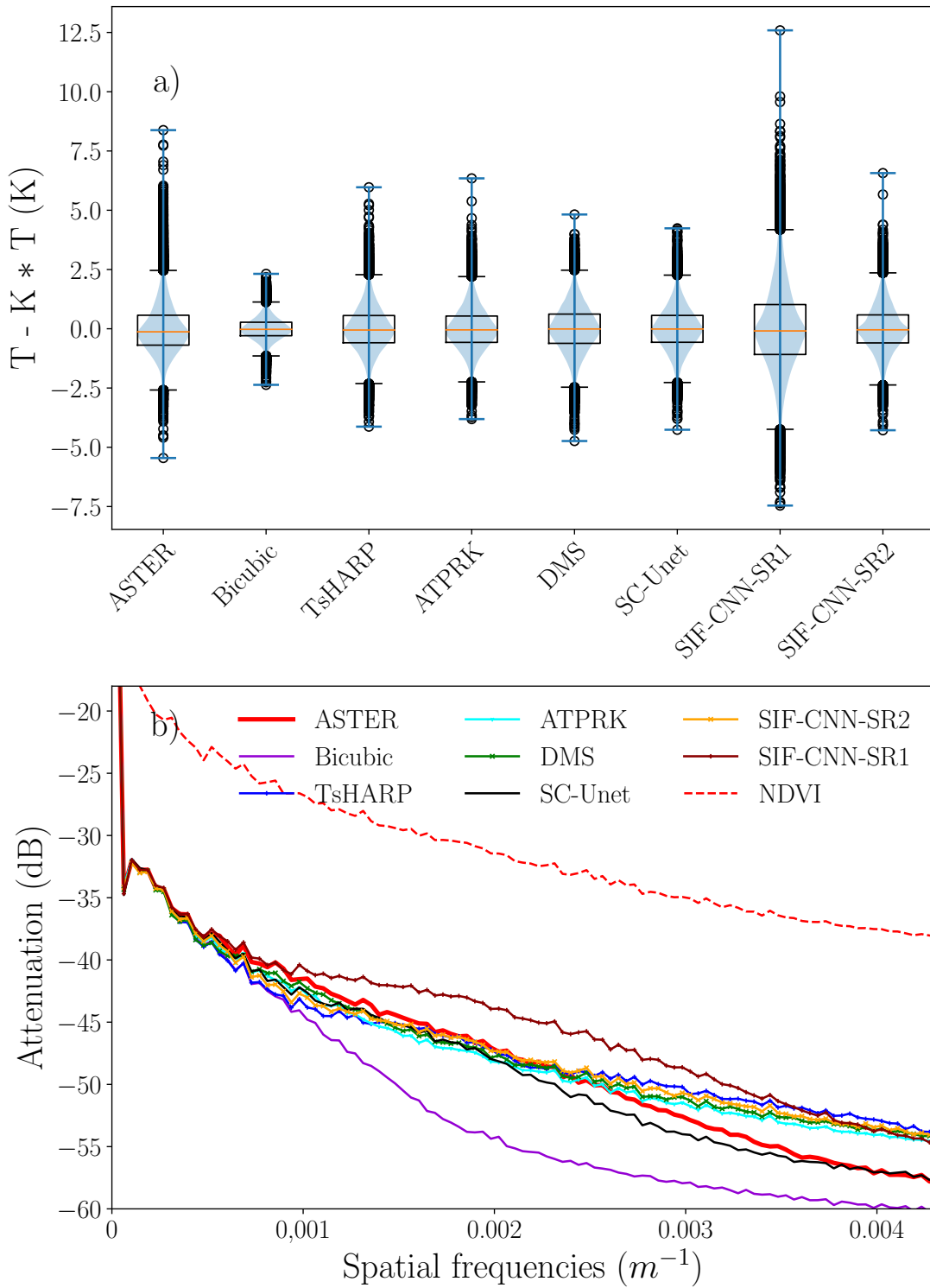


Fig. 44. Statistical analysis of the image visualized in figure 43. a) Boxplots and Violinplots representing the statistical distribution of the values of the high pass filtered LST of ASTER and obtained with the different super-resolution approaches. b) Attenuation spectra of the ASTER LST (red), LST obtained with statistical super-resolution methods TsHARP and ATPRK (blue), DMS (green), SC-Unet (black), SIF-CNN-SR1 (brown) and SIF-CNN-SR2 (orange). The attenuation spectra of the MODIS NDVI is also shown in dashed red.

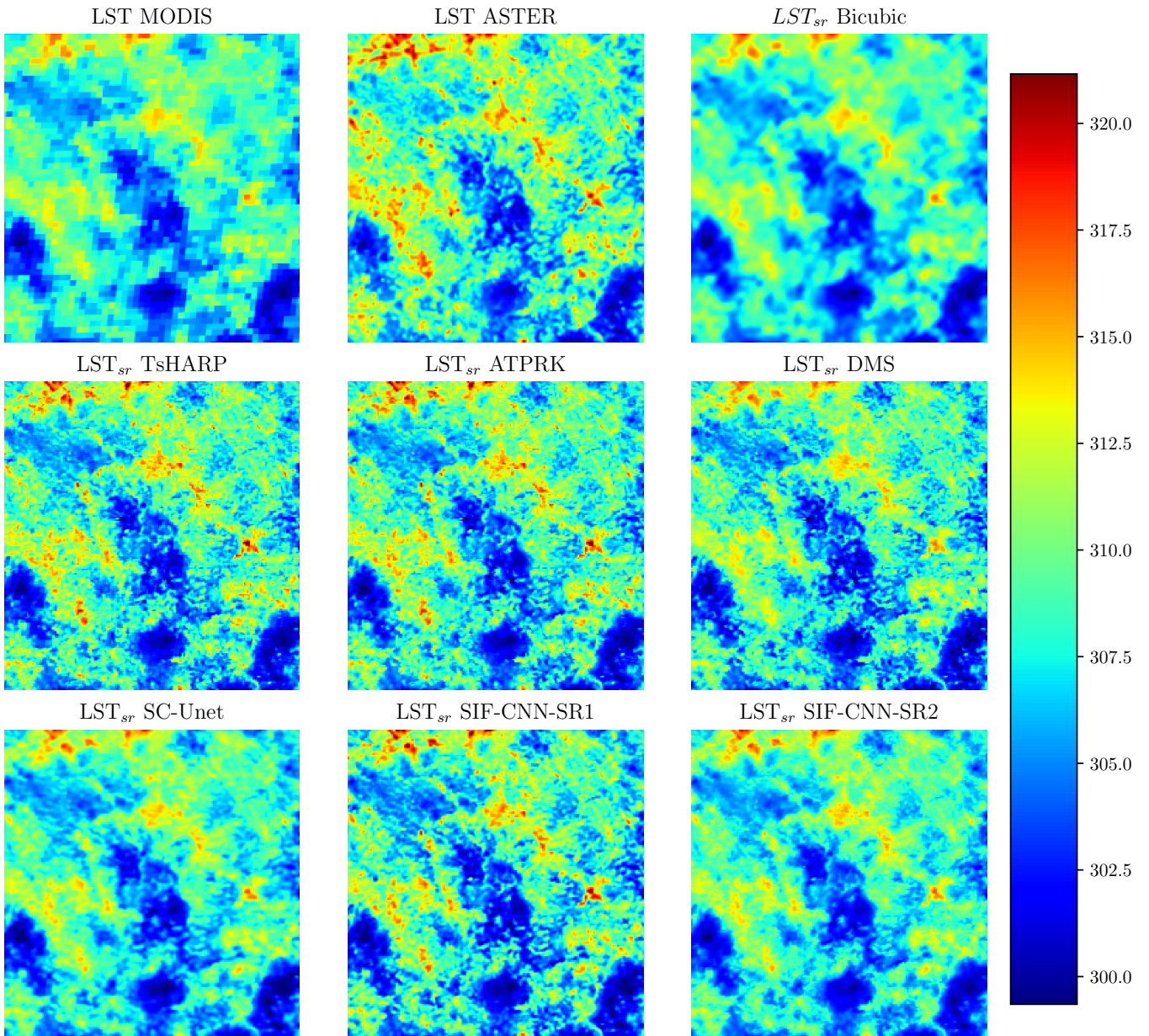


Fig. 45. Visualization of the LST of MODIS and ASTER respectively at 1km and 250m of spatial resolution alongside the super-resolution LST obtained with the different approaches.

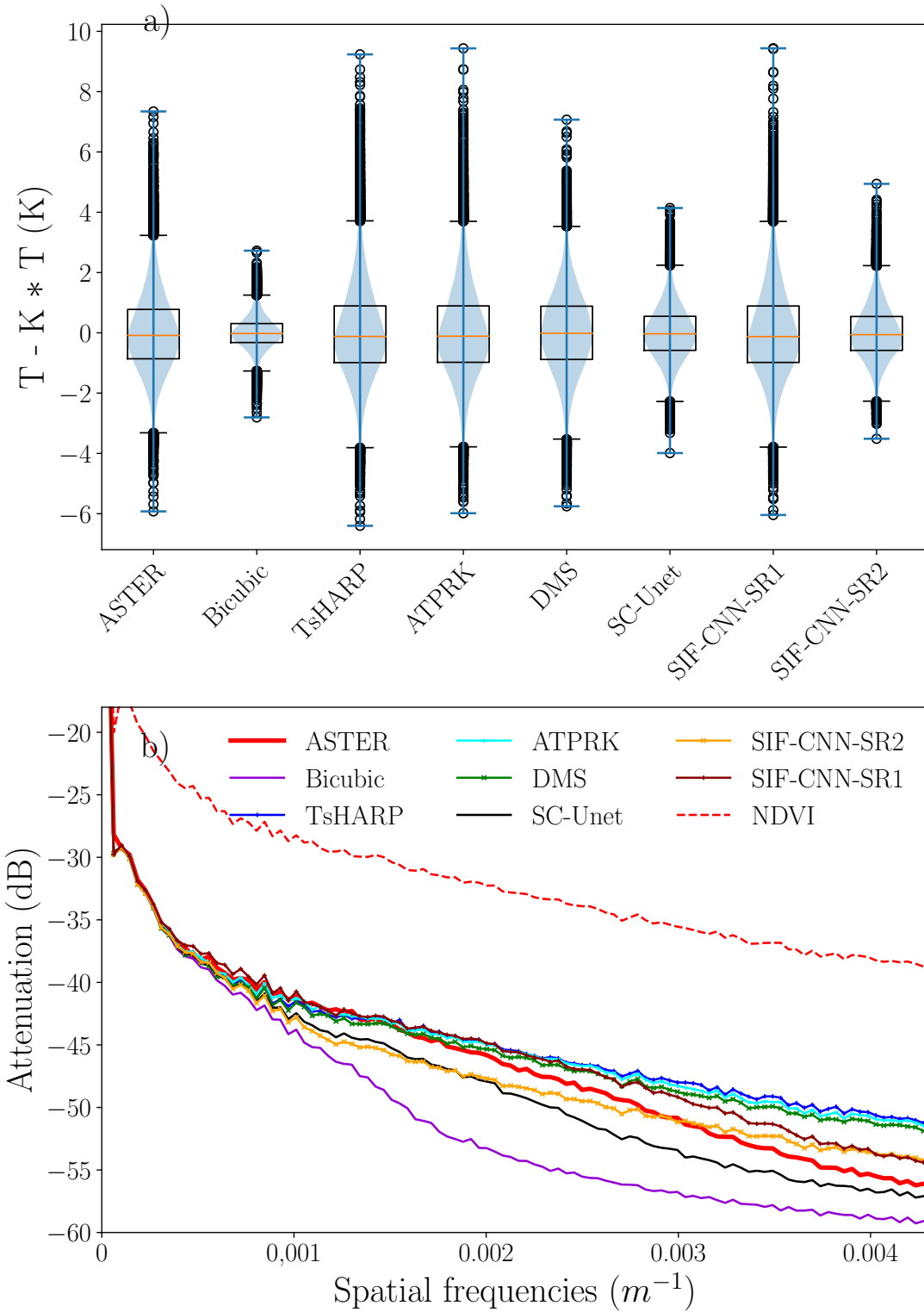


Fig. 46. Statistical analysis of the image visualized in figure 45. a) Boxplots and Violinplots representing the statistical distribution of the values of the high pass filtered LST of ASTER and obtained with the different super-resolution approaches. b) Attenuation spectra of the ASTER LST (red), LST obtained with statistical super-resolution methods TsHARP and ATPRK (blue), DMS (green), SC-Unet (black), SIF-CNN-SR1 (brown) and SIF-CNN-SR2 (orange). The attenuation spectra of the MODIS NDVI is also shown in dashed red.

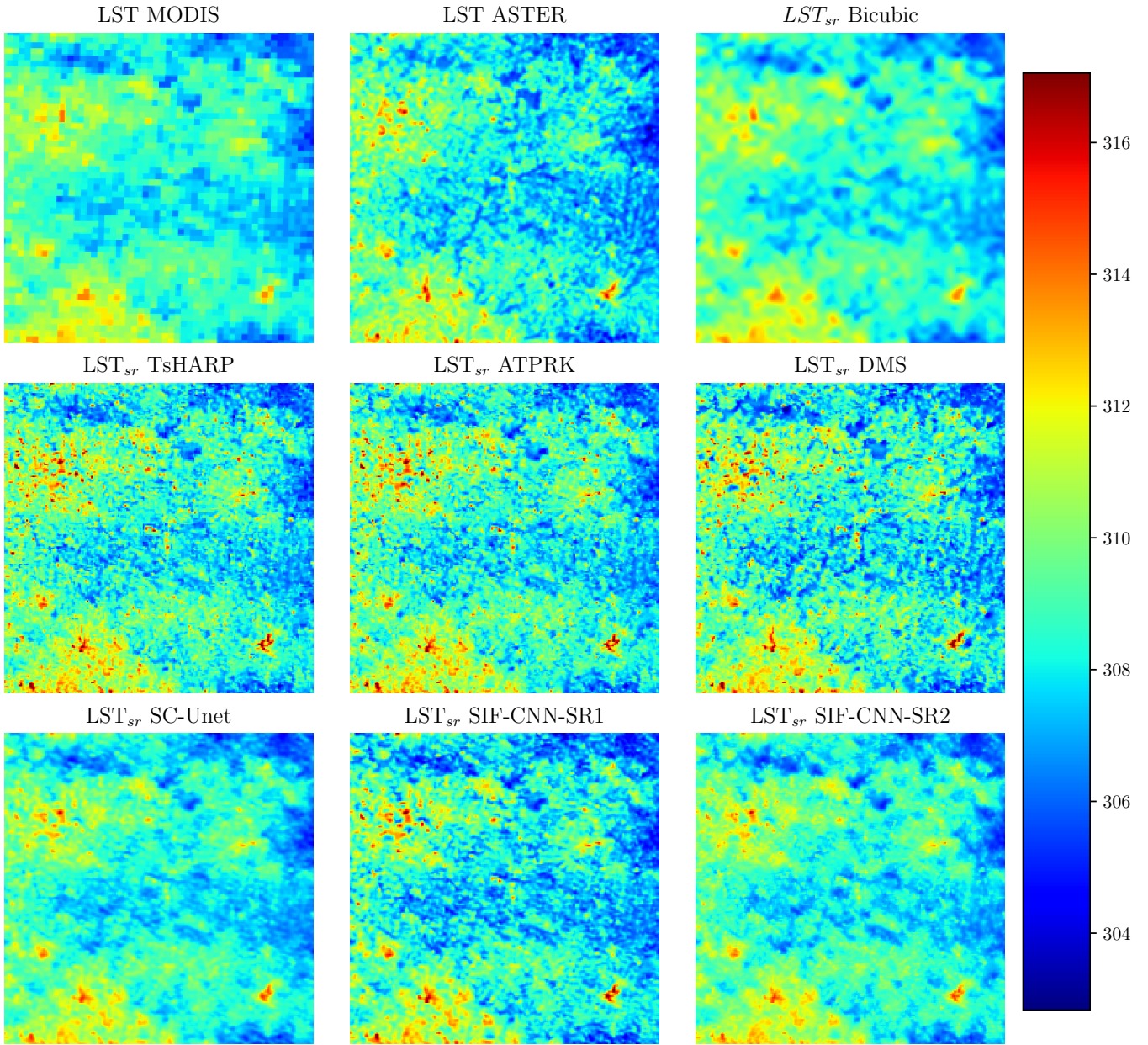


Fig. 47. Visualization of the LST of MODIS and ASTER respectively at 1km and 250m of spatial resolution alongside the super-resolution LST obtained with the different approaches.

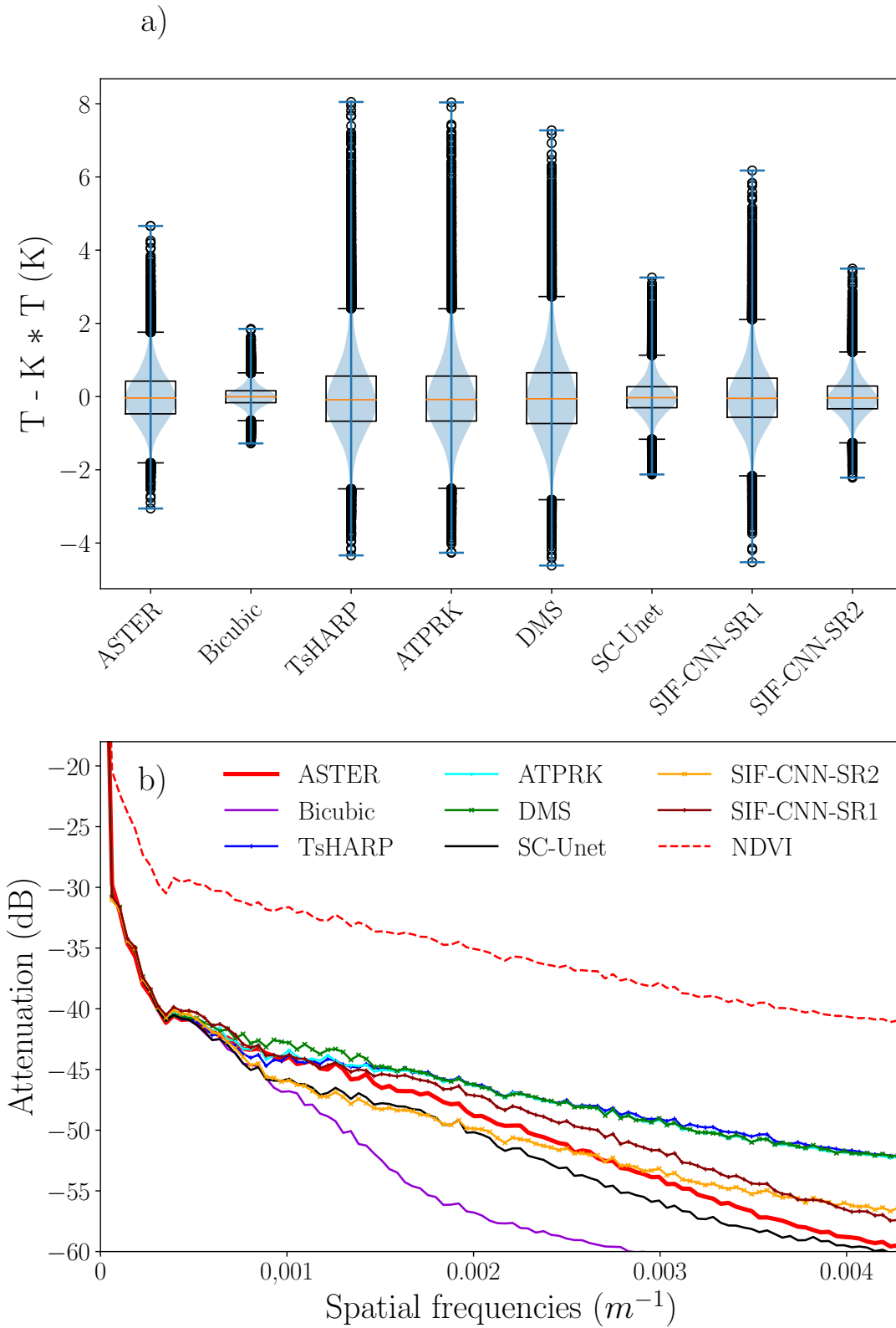


Fig. 48. Statistical analysis of the image visualized in figure 47. a) Boxplots and Violinplots representing the statistical distribution of the values of the high pass filtered LST of ASTER and obtained with the different super-resolution approaches. b) Attenuation spectra of the ASTER LST (red), LST obtained with statistical super-resolution methods TsHARP and ATPRK (blue), DMS (green), SC-Unet (black), SIF-CNN-SR1 (brown) and SIF-CNN-SR2 (orange). The attenuation spectra of the MODIS NDVI is also shown in dashed red.

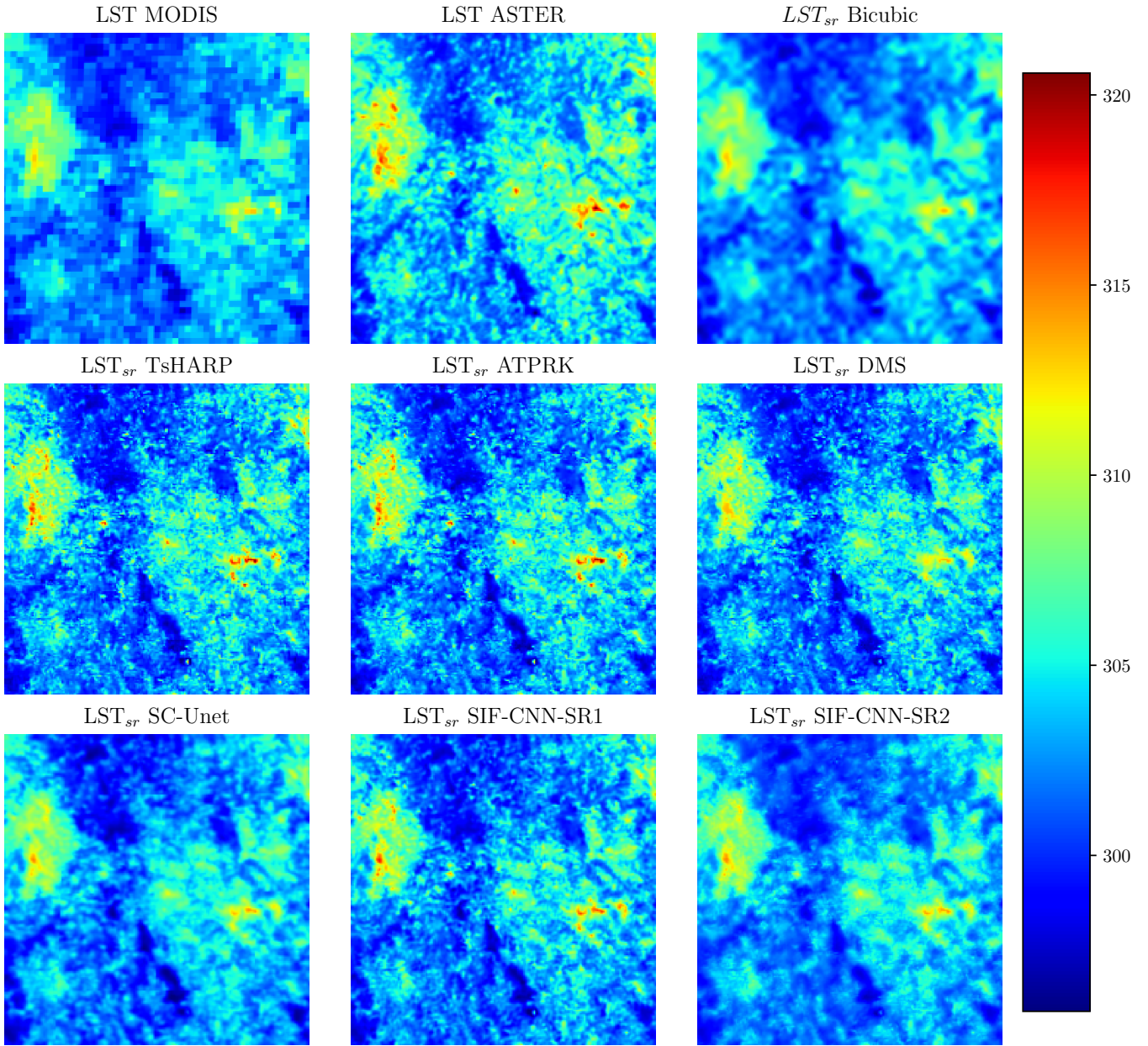


Fig. 49. Visualization of the LST of MODIS and ASTER respectively at 1km and 250m of spatial resolution alongside the super-resolution LST obtained with the different approaches.

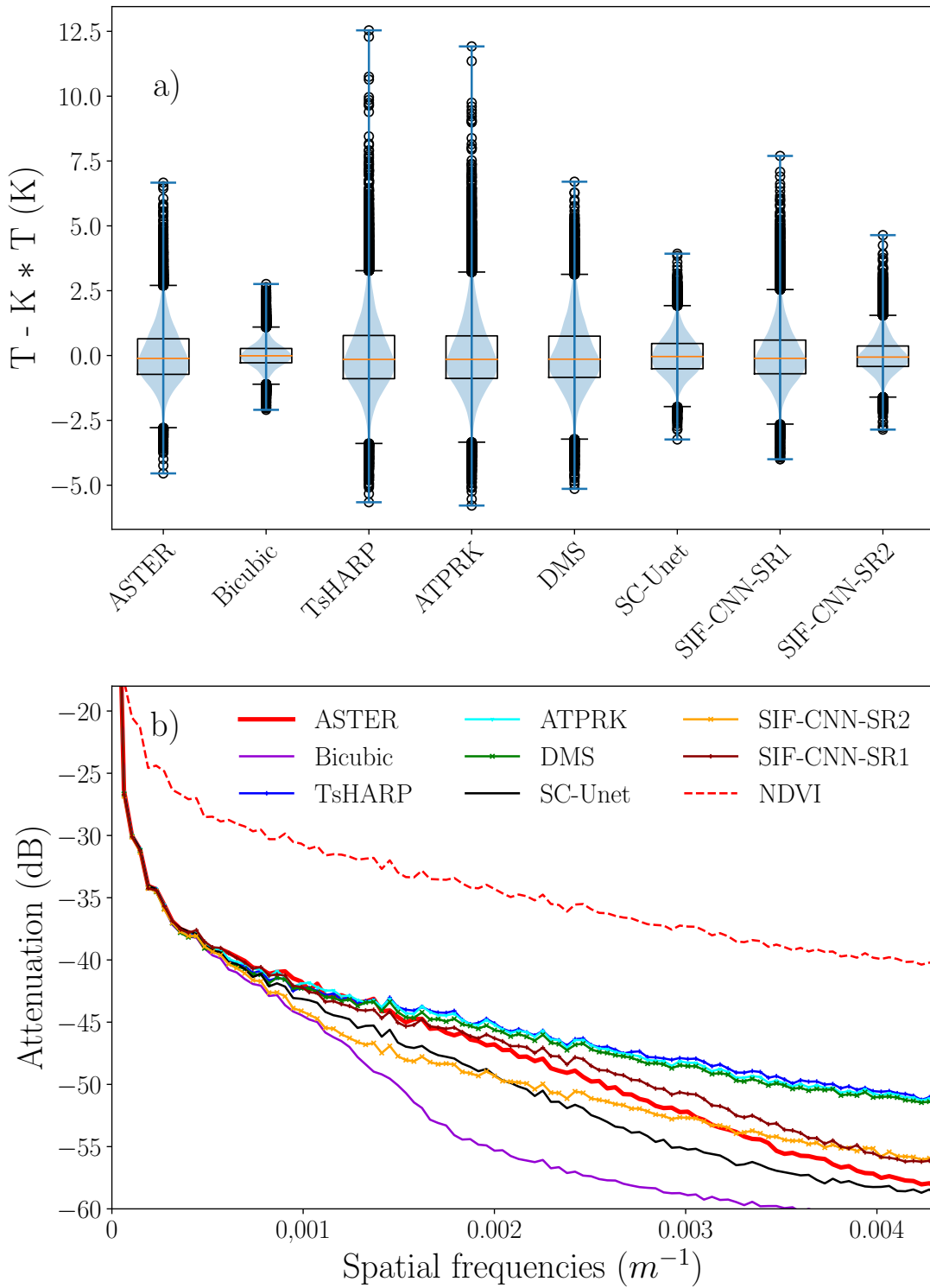


Fig. 50. Statistical analysis of the image visualized in figure 49. a) Boxplots and Violinplots representing the statistical distribution of the values of the high pass filtered LST of ASTER and obtained with the different super-resolution approaches. b) Attenuation spectra of the ASTER LST (red), LST obtained with statistical super-resolution methods TsHARP and ATPRK (blue), DMS (green), SC-Unet (black), SIF-CNN-SR1 (brown) and SIF-CNN-SR2 (orange). The attenuation spectra of the MODIS NDVI is also shown in dashed red.

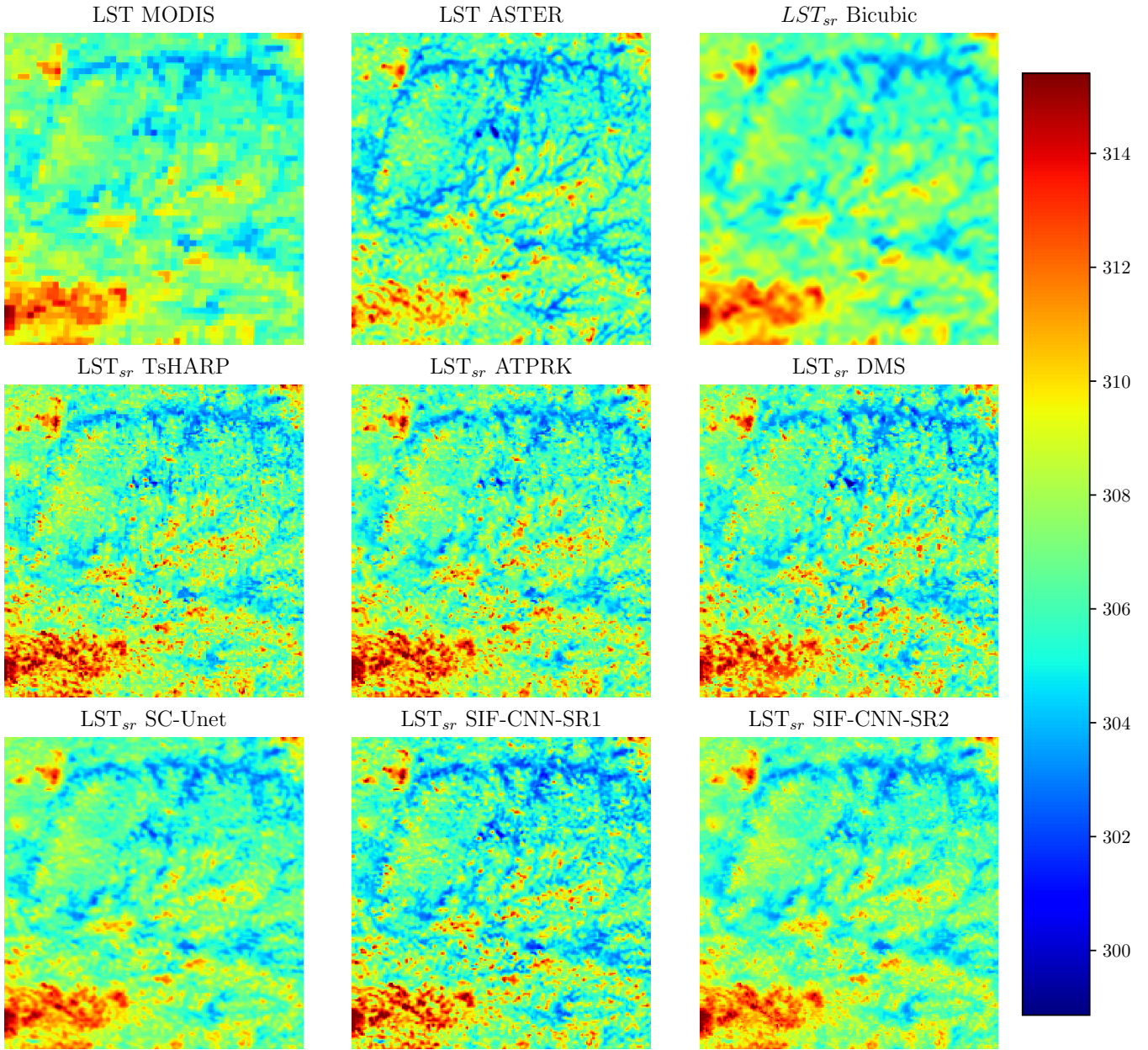


Fig. 51. Visualization of the LST of MODIS and ASTER respectively at 1km and 250m of spatial resolution alongside the super-resolution LST obtained with the different approaches.

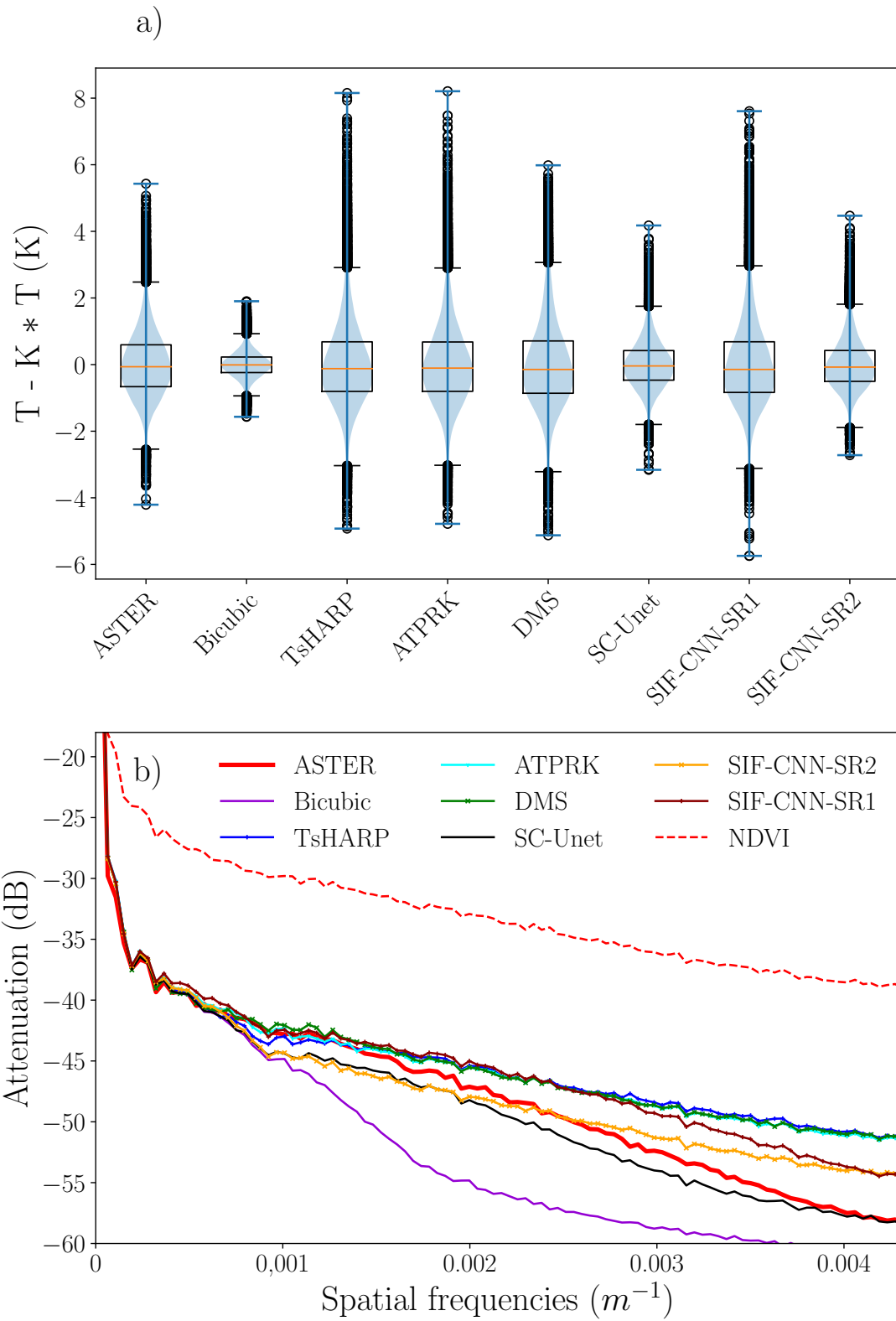


Fig. 52. Statistical analysis of the image visualized in figure 51. a) Boxplots and Violinplots representing the statistical distribution of the values of the high pass filtered LST of ASTER and obtained with the different super-resolution approaches. b) Attenuation spectra of the ASTER LST (red), LST obtained with statistical super-resolution methods TsHARP and ATPRK (blue), DMS (green), SC-Unet (black), SIF-CNN-SR1 (brown) and SIF-CNN-SR2 (orange). The attenuation spectra of the MODIS NDVI is also shown in dashed red.

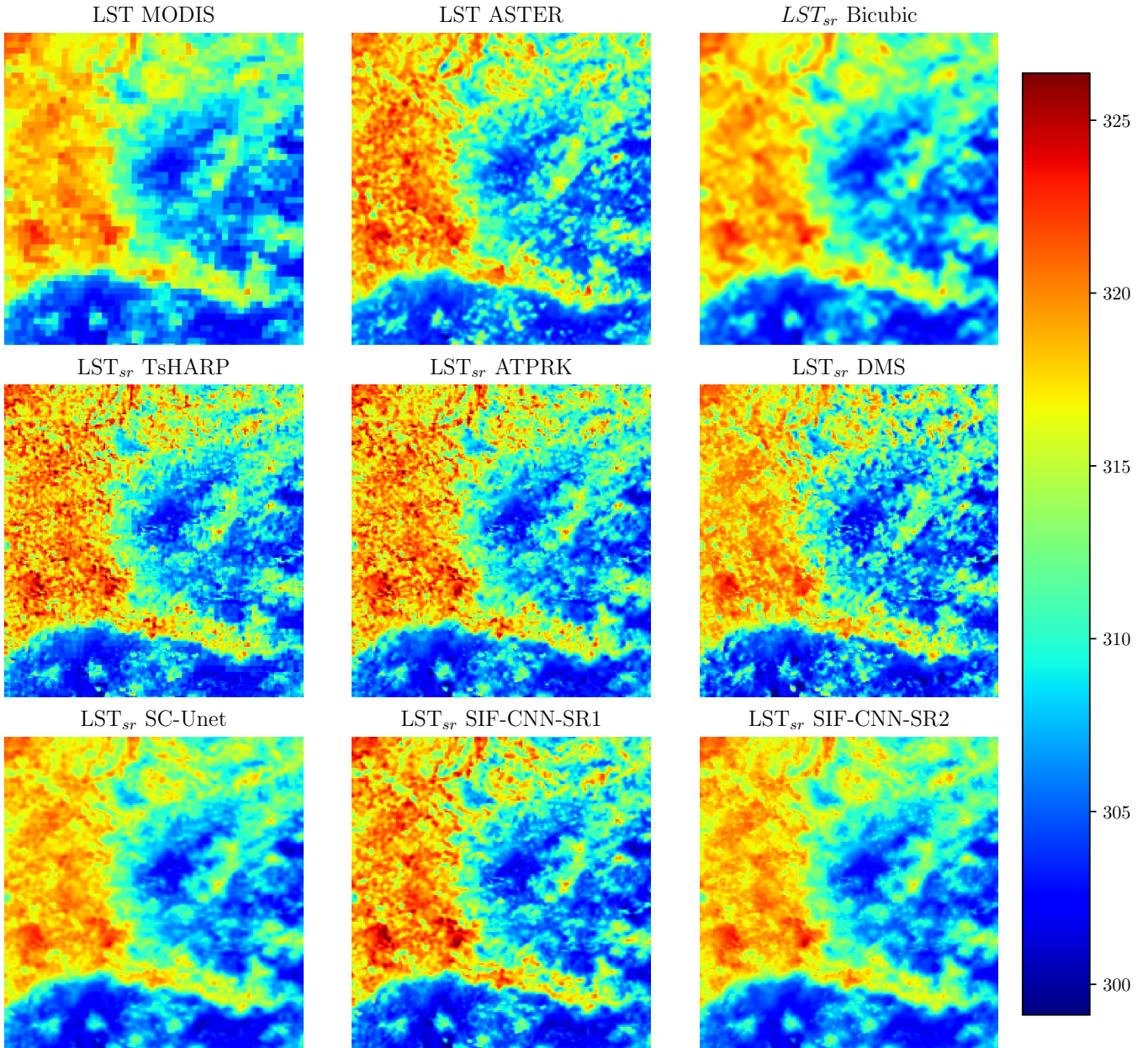


Fig. 53. Visualization of the LST of MODIS and ASTER respectively at 1km and 250m of spatial resolution alongside the super-resolution LST obtained with the different approaches.

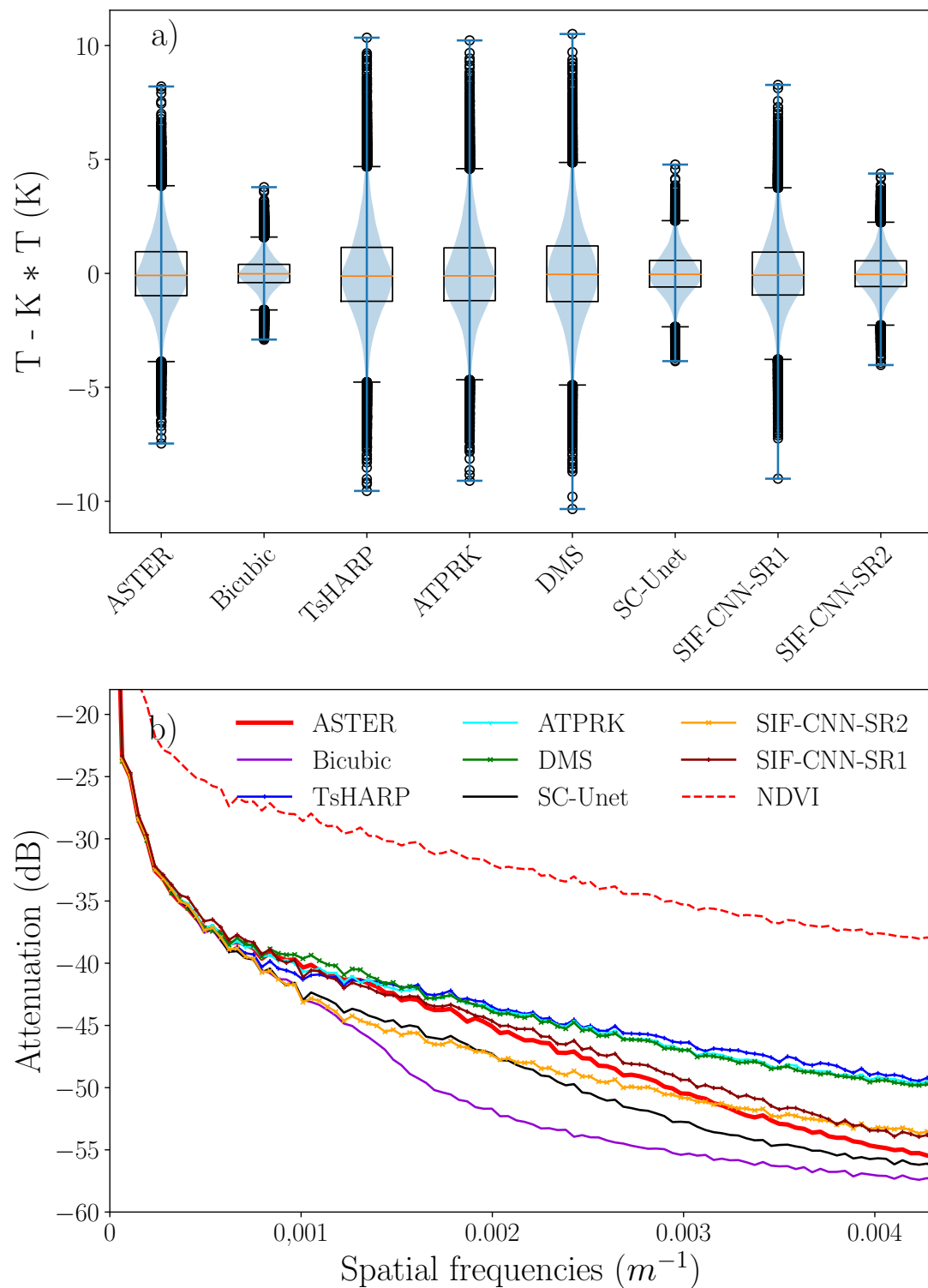


Fig. 54. Statistical analysis of the image visualized in figure 53. a) Boxplots and Violinplots representing the statistical distribution of the values of the high pass filtered LST of ASTER and obtained with the different super-resolution approaches. b) Attenuation spectra of the ASTER LST (red), LST obtained with statistical super-resolution methods TsHARP and ATPRK (blue), DMS (green), SC-Unet (black), SIF-CNN-SR1 (brown) and SIF-CNN-SR2 (orange). The attenuation spectra of the MODIS NDVI is also shown in dashed red.

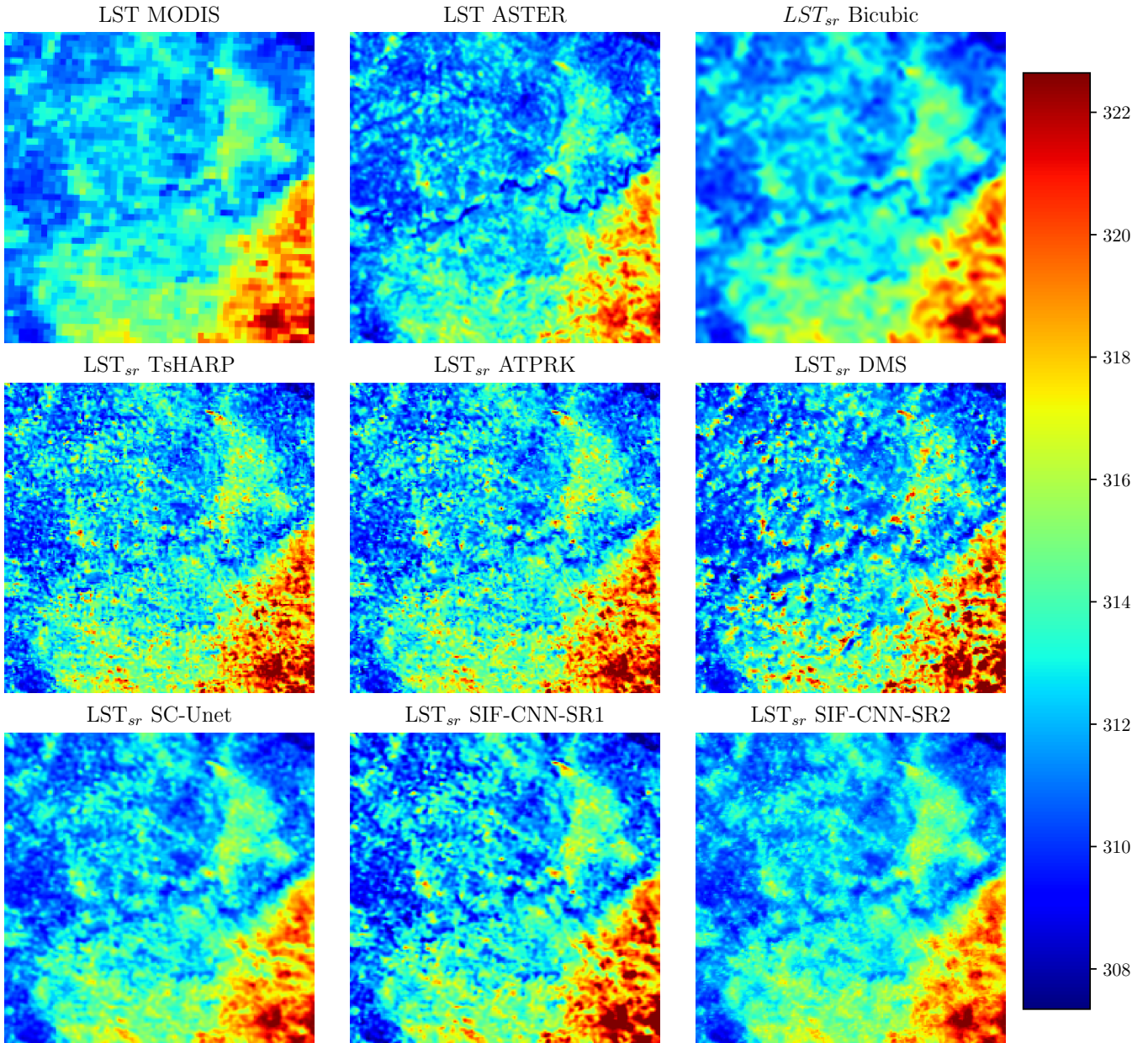


Fig. 55. Visualization of the LST of MODIS and ASTER respectively at 1km and 250m of spatial resolution alongside the super-resolution LST obtained with the different approaches.

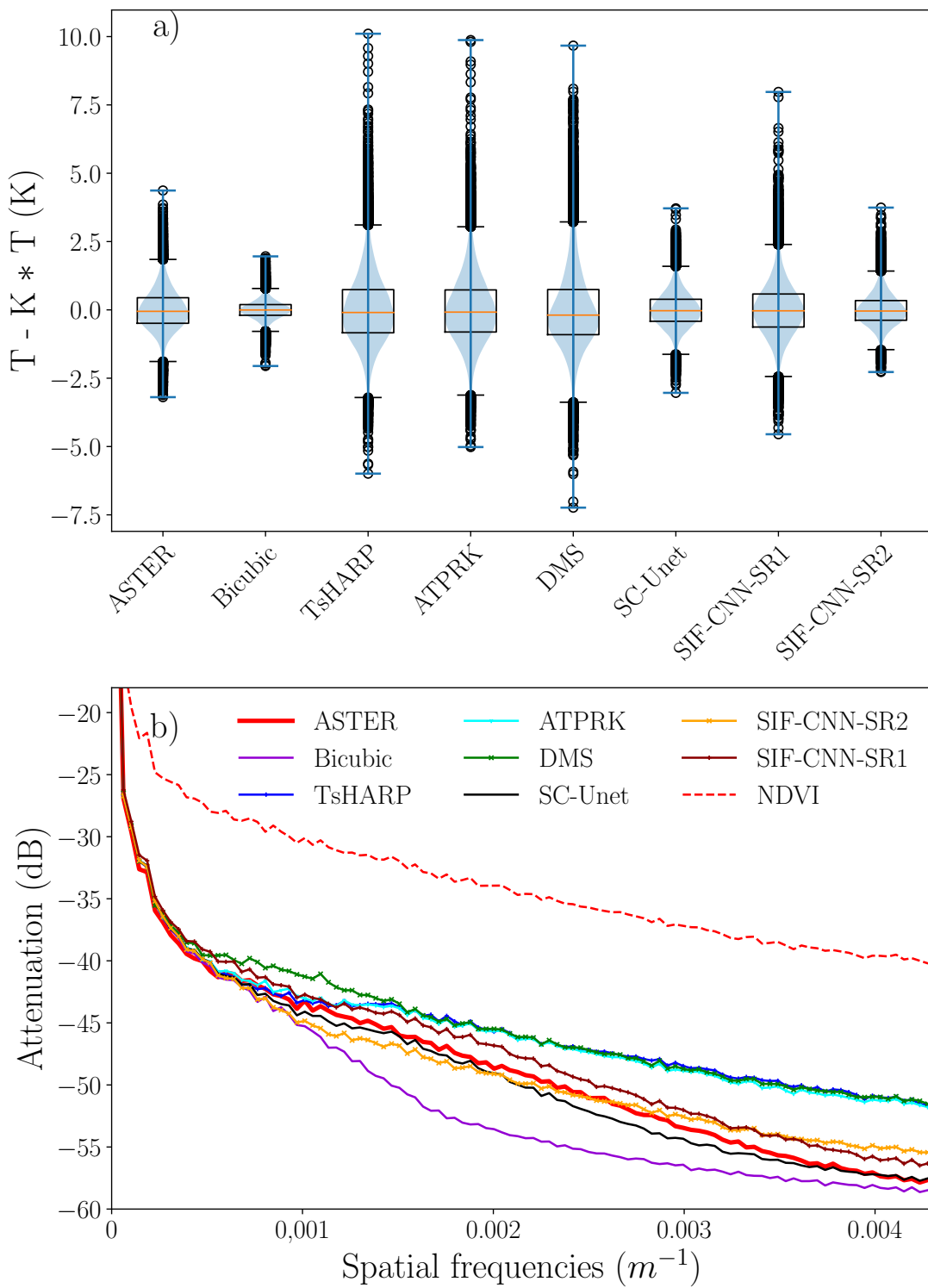


Fig. 56. Statistical analysis of the image visualized in figure 55. a) Boxplots and Violinplots representing the statistical distribution of the values of the high pass filtered LST of ASTER and obtained with the different super-resolution approaches. b) Attenuation spectra of the ASTER LST (red), LST obtained with statistical super-resolution methods TsHARP and ATPRK (blue), DMS (green), SC-Unet (black), SIF-CNN-SR1 (brown) and SIF-CNN-SR2 (orange). The attenuation spectra of the MODIS NDVI is also shown in dashed red.